Self-Consistent Field Theory and Its Applications by M. W. Matsen

in Soft Matter, Volume 1: Polymer Melts and Mixtures
edited by G. Gompper and M. Schick

Wiley-VCH, Weinheim, 2006

Contents

1 Self-consistent field theory and its applications

M. W. Matsen [1]

Department of Physics,
University of Reading,
Reading, RG6 6AF,
United Kingdom

Polymers refer to a spectacularly diverse class of macromolecules formed by covalently linking together small molecules, *monomers*, to form long chains. Figure 1.1 sketches an assortment of typical architectures, the simplest of which is the linear homopolymer formed from a single strand of identical monomers. There are also copolymer molecules consisting of two or more chemically distinct monomer units; the most common example being the random copolymer, where there is no particular pattern to the monomer sequence. In other cases, the different monomers are grouped together in long intervals to form block copolymer molecules; Fig. 1.1 shows the simplest, a diblock copolymer, formed from one block of A-type units attached to another of B-type units. Although linear chains are the most typical, an almost endless variety of other more elaborate architectures, such as combs, stars and rings, are possible. The monomers themselves also come in a rich variety, some of the more standard of which are listed in Fig. 1.2. The difference in chemistries can have a profound effect on the molecular interactions and chain flexibility. Some monomers produce rigid rod-like polymers, others produce molecules with liquid-crystalline behavior, a few become ionic in solution, and some are even electrically conducting. The monomer type also has a strong effect on the liquid to solid transition temperature, and influences whether the polymeric material solidifies into a glassy or semi-crystalline state.

As a result of their economical production coupled with their rich and varied properties, polymers have become a vital class of materials for the industrial sector. In addition, some of their exotic behaviors are now being realized for more sophisticated applications in, for example, the emerging field of nanotechnology. Consequently, research on polymeric macromolecules has flourished over the past several decades, and now stands as one of the dominant areas in soft condensed matter physics. Through the years of experimental and theoretical investigation, a number of elegant theories have been developed to describe their behavior, and this Chapter is devoted to one of the most successful, self-consistent field theory (SCFT) (Edwards 1965).

Considering the difficulty in modeling systems containing relatively simple molecules such as water, one might expect that large polymer molecules would pose an intractable task. However, the opposite is true. The sheer size of these macromolecules (each typically containing something like 10^3 to 10^5 atoms) actually simplifies the problem. As a result of their

[1] e-mail address: m.w.matsen@reading.ac.uk

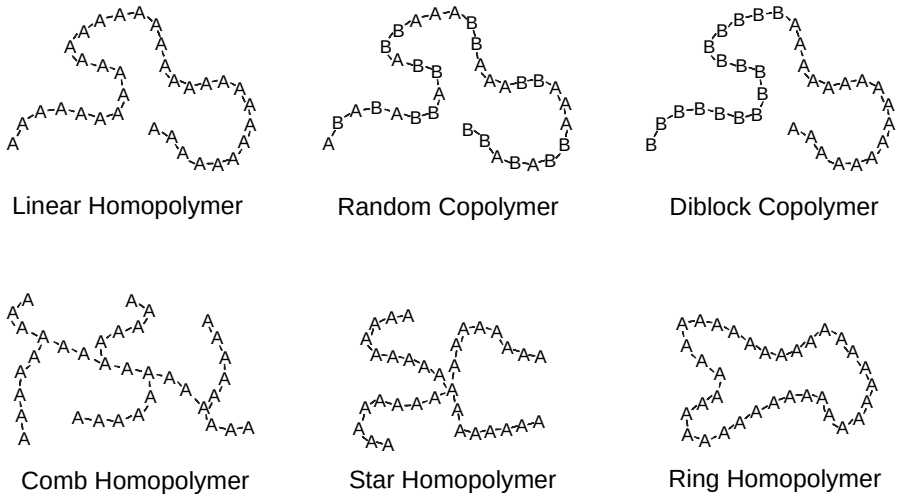

Figure 1.1: Selection of polymer architectures. Molecules consisting of a single monomer type (i.e., A) are referred to as homopolymer, and those with two or more types (i.e., A and B) are called copolymers.

tremendous molecular weight, the atomic details play a relative small part in their overall behavior, leading to universal properties among the vast array of different polymer types. For example, the characteristic size of a high-molecular-weight polymer in a homogeneous environment scales with the degree of polymerization (i.e., the total number of monomers) to an exponent that is independent of the monomer type. The chemical details of the monomer only affect the proportionality constant. A further advantage of modeling polymers is that their configurations tend to be very open, resulting in a huge degree of interdigitation among the polymers, such that any given molecule is typically in contact with hundreds of others. This has a damping effect on the molecular correlations, which in turn causes mean-field techniques to become highly effective, something that is unfortunately not true of small-molecule systems.

With the advantages favoring mean-field theory, it becomes possible to provide accurate predictions for the equilibrium behavior of polymeric systems. However, polymers are renowned for their slow dynamics and can remain out of equilibrium for long periods of time. In fact, this is effectively a rule for the solid state, where both glassy and semi-crystalline polymers become forever trapped in non-equilibrium configurations. This restricts the application of statistical mechanics to the melt (or liquid) state, where the dynamics can be reasonably fast. Even though there are relatively few applications of polymers in their melt state, this is the phase in which materials are processed and so a thorough understanding of equilibrium melts is paramount.

This Chapter provides a basic introduction to SCFT for modeling polymeric melts; for further reading, see Whitmore and Vavasour (1995), Schmid (1998), Fredrickson et al. (2002), and Matsen (2002a). SCFT is a theory with a remarkable track-record for versatility and reliability, undoubtedly because of its prudent choice of well-grounded assumptions and ap-

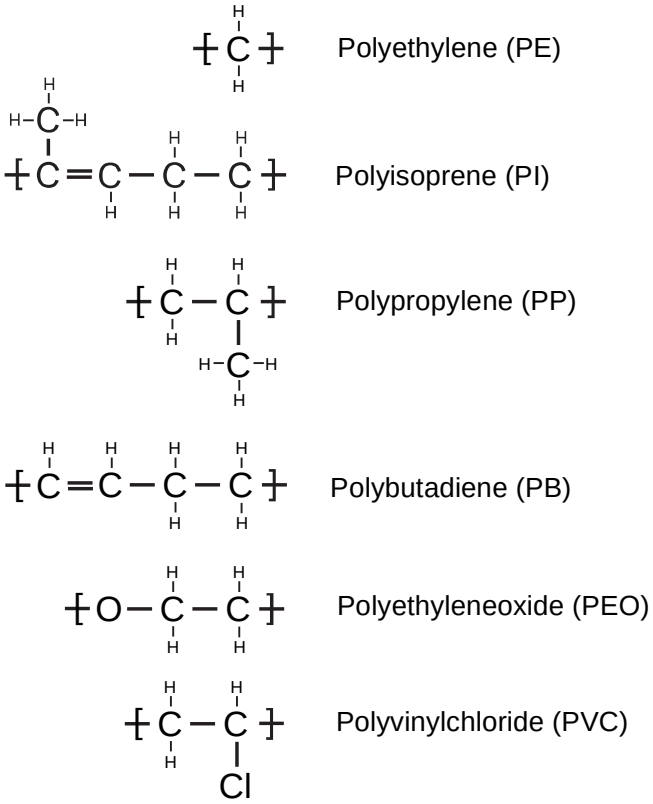

Figure 1.2: Chemical structure of some common monomers used to form polymer molecules.

proximations. In most applications, the theory employs the simple coarse-grained Gaussian model for polymer chains, and treats their interactions by mean-field theory. Section 1.1 begins by justifying the applicability of the Gaussian model, and then Section 1.2 develops the necessary statistical mechanics for a single chain subjected to an external field, $w(\mathbf{r})$. Following that, a number of useful approximations are introduced for handling special cases such as when $w(\mathbf{r})$ is either weak or strong. This provides the necessary background for discussing SCFT.

As with most theories, the framework of SCFT is best described by demonstrating its application on a representative sample of systems. To this end, we focus on the three examples depicted in Fig. 1.3: polymer brushes, homopolymer interfaces, and block copolymer microstructures. Not only do they represent a varied range of applications, but they are also important systems in their own right. A polymeric brush is formed when chains are grafted to a substrate in such high concentration that they create a dense coating with highly extended configurations. Brushes are simple to prepare and provide a convenient way of modifying the properties of a surface, and can, for example, greatly reduce friction, change the wetting behavior, and affect adhesion properties. Polymeric alloys (or blends) provide an economical

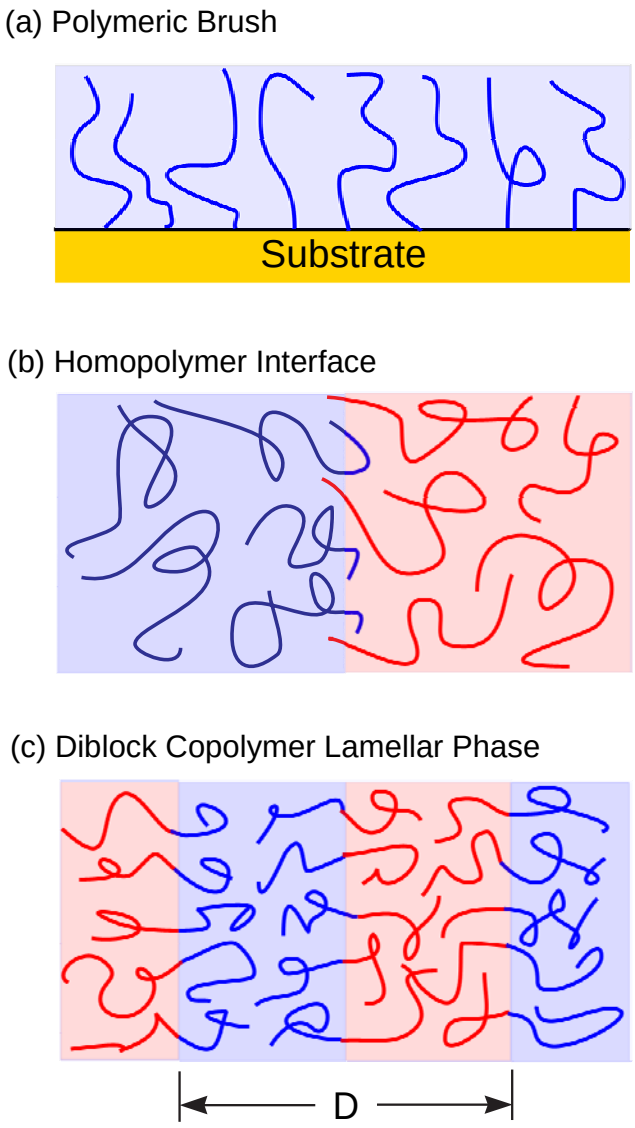

Figure 1.3: (a) Polymeric brush consisting of polymer chains end-grafted to a flat substrate. (b) Polymer interface separating an A-rich phase (blue domain) from a B-rich phase (red domain). (c) Lamellar diblock copolymer microstructure consisting of alternating thin A- and B-rich domains with a repeat period of D.

method of designing new materials with tailored properties. Because large macromolecules possess relatively little translational entropy, the unlike polymers in an alloy tend to segregate while they are being processed in the melt state, leaving the solid material with a domain

structure involving an extensive amount of internal interface. Naturally, the properties of the interface have a pronounced effect on the final material; in particular, a high interfacial tension results in large domains, which is generally undesirable. One way of halting the tendency of domains to coarsen is to chemically bond the unlike polymers together, forming block copolymer molecules. The blocks still segregate into separate domains, but the connectivity of the chain prevents the domains from becoming thicker than the typical size of a single molecule. In fact, the domains tend to form highly-ordered periodic geometrics, of which the lamellar phase of alternating thin layers pictured in Fig. 1.3(c) is the simplest. This ability to self-assemble into ordered nanoscale morphologies of different geometries is a powerful feature that researchers are now beginning to exploit for various high-tech applications.

1.1 Gaussian Chain

To start off, we consider linear homopolymer chains in a homogeneous environment, and disregard, for the moment, all monomer-monomer interactions including the hard-core ones that prevent the chains from overlapping. In the limit of high molecular weights, all such polymers fall into the same universality class of non-avoiding random walks, and as a consequence they exhibit a degree of common behavior. For instance, their typical size scales with their molecular weight to the universal exponent, $\nu = 1/2$. To investigate this common behavior, there is no need to consider realistic polymer chains involving segments such as those denoted in Fig. 1.2. The fact that the behavior is universal means that it is exhibited by all models, including simple artificial ones.

For maximum simplicity, we select the freely-jointed chain, where each monomer has a fixed length, b, and the joint between sequential monomers is completely flexible. Figure 1.4(a) shows a typical configuration of this model, projected onto the two-dimensional page. It was produced by joining together $M = 4000$ vectors, $\mathbf{r}_i$, each generated from the random distribution,

$$p_1(\mathbf{r}_i) = \frac{\delta(r_i - b)}{4\pi b^2} \tag{1.1}$$

where $r_i \equiv |\mathbf{r}_i|$. The factor in the denominator ensures that the distribution is properly normalized such that

$$\int d\mathbf{r}\, p_1(\mathbf{r}) = 4\pi \int_0^\infty dr\, r^2 p_1(\mathbf{r}) = 1 \tag{1.2}$$

The size of the particular configuration displayed in Fig. 1.4(a) can be characterized by the length of its end-to-end vector,

$$\mathbf{R} \equiv \sum_{i=1}^{M} \mathbf{r}_i \tag{1.3}$$

denoted by the arrow at the top of the figure. The length of this vector averaged over all possible configurations, R_0, can then be used as a measure for the typical size of the polymer.

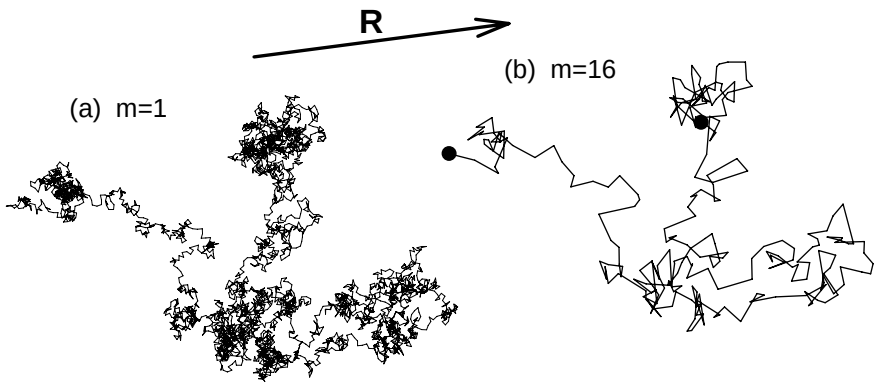

Figure 1.4: (a) Freely-jointed chain with $M = 4000$ fixed-length monomers. (b) Coarse-grained version with $N = 250$ segments, each containing $m = 16$ monomers. The two ends of the polymer are denoted by solid dots and the end-to-end vector, $\mathbf{R}$, is drawn above.

Since the simple average, $\langle|\mathbf{R}|\rangle$, is difficult to evaluate, it is common practice to use the alternative root-mean-square (rms) average,

$$R_0 \equiv \sqrt{\langle \mathbf{R}^2 \rangle} = \sqrt{\left\langle \sum_{i,j} \mathbf{r}_i \cdot \mathbf{r}_j \right\rangle} = bM^{1/2} \tag{1.4}$$

In this case, the formula conveniently simplifies by the fact, $\langle \mathbf{r}_i \cdot \mathbf{r}_j \rangle = 0$ for all $i \neq j$, because the directions of different steps are uncorrelated. The power-law dependence on the degree of polymerization, M, and the exponent, $\nu = 1/2$, are universal properties of non-avoiding random walks, and would have occurred regardless of the actual model and the measure used to characterize the size. The details of the model and the precise definition of size only affect the proportionality constant, which in this case is simply b.

The underlying reason for the universality of non-avoiding random walks emerges when they are examined on a mesoscopic scale, where the chain is viewed in terms of larger repeat units referred to as *coarse-grained* segments. For this, new distribution functions, $p_m(\mathbf{r})$, are defined for the end-to-end vector, $\mathbf{r}$, of segments containing m monomers. These distribution functions can be evaluated by using the recursive relation,

$$p_m(\mathbf{r}) = \int d\mathbf{r}_1 d\mathbf{r}_2 \; p_{m-n}(\mathbf{r}_1) p_n(\mathbf{r}_2) \delta(\mathbf{r}_1 + \mathbf{r}_2 - \mathbf{r}) \tag{1.5}$$

where n is any positive integer less than m. By symmetry, each $p_m(\mathbf{r})$ depends only on the magnitude, r, of its end-to-end vector, $\mathbf{r}$. This fact combined with the constraint, $\mathbf{r}_2 = \mathbf{r} - \mathbf{r}_1$, can be used to reduce the six-dimensional integral in Eq. (1.5) to the two-dimensional one,

$$p_m(\mathbf{r}) = 2\pi \int_0^\infty dr_1 \; r_1^2 p_{m-n}(\mathbf{r}_1) \int_0^\pi d\theta \; \sin(\theta) p_n(\mathbf{r}_2) \tag{1.6}$$

over the length of $\mathbf{r}_1$ and the angle between $\mathbf{r}$ and $\mathbf{r}_1$. In terms of r_1 and θ, the length of $\mathbf{r}_2$ is specified by the cosine law, $r_2^2 = r^2 + r_1^2 - 2rr_1\cos(\theta)$. Using this relation to substitute θ by

r_2, the preceding integral can then be expressed in the slightly more convenient form,

$$p_m(\mathbf{r}) = \frac{2\pi}{r}\int_0^\infty dr_1\; r_1 p_{m-n}(\mathbf{r}_1)\int_{|r-r_1|}^{r+r_1} dr_2\; r_2 p_n(\mathbf{r}_2) \tag{1.7}$$

With the recursion relation in Eq. (1.7), it is now a straightforward exercise to march through calculating $p_m(\mathbf{r})$ for larger and larger segments. Starting with $m = 2$ and $n = 1$, the two-monomer distribution,

$$p_2(\mathbf{r}) = \begin{cases} \frac{1}{8\pi b^2 r}\,, & \text{if } r < 2b \\ 0\,, & \text{if } 2b < r \end{cases} \tag{1.8}$$

is obtained from the single-step distribution in Eq. (1.1). One can easily confirm that this distribution is properly normalized as $p_1(\mathbf{r})$ was in Eq. (1.2). Repeating the process with $m = 4$ and $n = 2$ gives the four-monomer distribution,

$$p_4(\mathbf{r}) = \begin{cases} \frac{8b-3r}{64\pi b^4}\,, & \text{if } r < 2b \\ \frac{(4b-r)^2}{16\pi b^4 r}\,, & \text{if } 2b < r < 4b \\ 0\,, & \text{if } 4b < r \end{cases} \tag{1.9}$$

Although the formulas become increasingly complicated, it is straightforward to continue the iterations numerically.

Figure 1.4(b) displays an equivalent random walk to that in Fig. 1.4(a), but where each segment corresponds to $m = 16$ monomers with a distribution given by $p_{16}(\mathbf{r})$. The act of combining m monomers into larger units, or segments, makes the chain appear smoother and buries microscopic degrees of freedom into the probability distribution, $p_m(\mathbf{r})$. This procedure, where the number of units is reduced from M down to $N \equiv M/m$, is referred to as coarse graining. It does away with M and b, and replaces them by N and a statistical segment length,

$$a \equiv R_0 N^{-1/2} = b m^{1/2} \tag{1.10}$$

defined such that $R_0 = aN^{1/2}$.

When the probability distributions, $p_m(\mathbf{r})$, are scaled with respect to the statistical segment length, a, they approach the asymptotic limit,

$$p_m(\mathbf{r}) \to \left(\frac{3}{2\pi a^2}\right)^{3/2} \exp\left(-\frac{3r^2}{2a^2}\right) \tag{1.11}$$

as $m \to \infty$. Figure 1.5 demonstrates this by comparing distributions of finite m (solid curves) against the asymptotic limit (dashed curve). This convergence to a simple Gaussian distribution is well known in statistics and goes by the name of the *central limit* theorem. The Gaussian (or normal) distribution applies to the average of any large random sample, in this case the displacement vectors of m monomers. Even if the lengths of the individual monomers were not fixed, but varied according to some arbitrary distribution, the coarse-grained segments would still develop Gaussian distributions, albeit with a different expression for a. This universality occurs because the Gaussian distribution represents a fixed point of the recursion

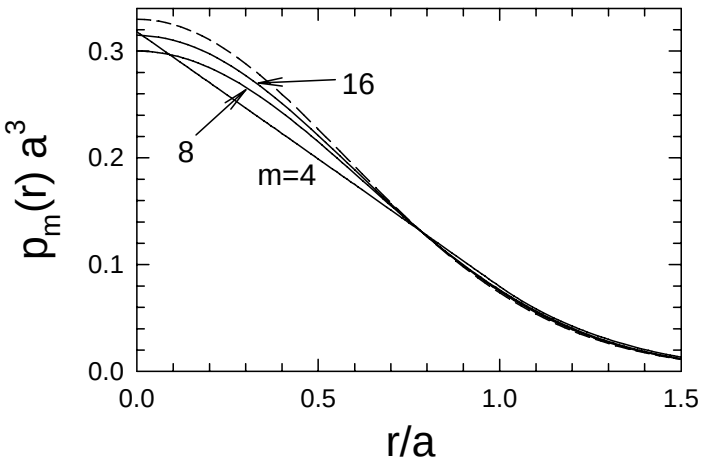

Figure 1.5: Probability distribution, $p_m(\mathbf{r})$, for a coarse-grained segment with m monomers. The dashed curve denotes the asymptotic limit in Eq. (1.11) for $m \to \infty$.

relation in Eq. (1.5); in other words, if $p_{m-n}(\mathbf{r}_1)$ and $p_n(\mathbf{r}_2)$ are both Gaussians, then so is $p_m(\mathbf{r})$.

This universality actually extends beyond freely-jointed chains to a more general class that can be referred to as Markov chains. An equilibrium configuration of a Markov chain can still be generated by starting at one end and attaching monomers one-by-one according to a given probability distribution. However, in this case, the displacement of the i'th monomer, $\mathbf{r}_i$, can have a distribution, $p_1(\mathbf{r}_i; \mathbf{r}_{i-1})$, that depends on the $\mathbf{r}_{i-1}$ of the preceding monomer. In fact, this can be generalized such that the probability of $\mathbf{r}_i$ depends on $\mathbf{r}_{i-1}$, $\mathbf{r}_{i-2}$,..., $\mathbf{r}_{i-I}$ so long as I remains finite. If this is the case, then sufficiently large coarse-grained segments will still develop a Gaussian distribution with an average chain size obeying $R_0 = aN^{1/2}$.

While the universality class of random walks applies to an impressive range of models, it does not include those with self-avoiding interactions. In that case, the position and orientation of a particular monomer is dependent upon all others in the chain. Nevertheless, such polymer configurations can still be generated with random walks, but those configurations containing overlaps must now be disregarded. The smaller compact configurations are more likely to contain overlapping monomers, and therefore self-avoidance favors larger and more open configurations. Consequently, the size of an isolated polymer in solution scales as $R_0 \propto N^\nu$ with a larger exponent of $\nu \approx 0.6$ (de Gennes 1979). However, when the polymer is in a melt with other polymers, it has to avoid them as well as itself. In this case, the advantage of the more open configurations is lost, and the polymer reverts back to random-walk statistics with the Gaussian probability in Eq. (1.11), although with a modified statistical segment length (Wang 1995).

Fetters et al. (1994) provide a library of experimental results for R_0 as a function of

molecular weight and bulk mass densities for various common polymer types, such as those depicted in Fig. 1.2. Given the chemical composition and thus the molecular weight of a monomer, it is then possible to calculate the statistical segment length, a, and the bulk segment density, ρ_0. However, the values obtained depend on the definition of the segment (i.e., the value selected for m). Of course, none of the physical quantities can be affected by such a choice, and indeed this is always the case. If, for example, the number of monomers in each segment is doubled, then N decreases by a factor of 2 and a increases by $\sqrt{2}$, such that the quantity, $R_0 = aN^{1/2}$, remains unchanged.

The freedom to redefine segments is linked to the scaling behavior and thus the universality of polymeric systems. However, it can be confusing because the size of N no longer has any absolute meaning, or in other words, it is impossible to judge whether a polymer is long or short based solely on its value of N. Fortunately, there is a special invariant definition,

$$\mathcal{N} \equiv \left(\frac{R_0^3}{N/\rho_0} \right)^2 = a^6 \rho_0^2 N \tag{1.12}$$

with a real physical significance that provides a true measure of the polymeric nature of the molecule. It is based on the ratio of the typical volume spanned by a polymer, R_0^3, to its physical volume, N/ρ_0. Thus, small values of $\mathcal{N}$ correspond to compact molecules and large values imply open configurations with many intermolecular contacts. Be aware that some authors assume, without mentioning, that $N = \mathcal{N}$ by innocuously setting the segment volume to $\rho_0^{-1} = a^3$.

1.2 Gaussian Chain in an External Field

The preceding section examined polymers in an ideal homogeneous environment, where no forces were exerted on the chains. In the more interesting situations depicted in Fig. 1.3, the polymers do experience interactions that vary with respect to position, $\mathbf{r}$. Their net effect can generally be represented by a static field, $w(\mathbf{r})$, determined self-consistently from the overall segment distribution in the system. However, we ignore for now the source of the field and start by developing the statistical mechanics for a single polymer acted upon by an arbitrary external field. Although fields are generally real quantities, the derivations that follow hold even when $w(\mathbf{r})$ is complex; this fact will be needed in the derivation of self-consistent field theory (SCFT).

We assume that the field varies slowly enough that the chain can be divided into N appropriately sized coarse-grained segments of volume, ρ_0^{-1}, each small enough such that their local environment is more or less homogeneous, but also large enough so that they obey Gaussian statistics with a statistical segment length, a. The coarse-grained trajectory of the polymer (e.g., the path in Fig. 1.4(b)) is then specified by a function, $\mathbf{r}_\alpha(s)$, where the parameter, $0 \le s \le 1$, runs along the backbone of the polymer such that equal intervals of s have the same molecular weight. (The subscript α will be used to label different molecules when we eventually treat complete systems.) Having specified the trajectory, a dimensionless segment concentration can be defined as

$$\hat{\phi}_\alpha(\mathbf{r}) = \frac{N}{\rho_0} \int_0^1 ds\, \delta(\mathbf{r} - \mathbf{r}_\alpha(s)) \tag{1.13}$$

The energy of a polymer configuration, $\mathbf{r}_\alpha(s)$, turns out to be a local property, meaning that any given interval of the chain, $s_1 \le s \le s_2$, can be assigned a definite quantity of energy, $E[\mathbf{r}_\alpha, s_1, s_2]$, independent of the rest of the chain. This will become a crucial property in the derivation that follows. The formula for the energy,

$$\frac{E[\mathbf{r}_\alpha; s_1, s_2]}{k_B T} = \int_{s_1}^{s_2} ds \left(\frac{3}{2a^2 N} |\mathbf{r}'_\alpha(s)|^2 + w(\mathbf{r}_\alpha(s)) \right) \tag{1.14}$$

involves one term that accounts for the Gaussian probability from Eq. (1.11) and another term for the energy of the field. Note that square brackets are used for $E[\mathbf{r}_\alpha; s_1, s_2]$ to denote that it is a functional (i.e., a function of a function).

The two primary quantities of the polymer that need to be calculated are the ensemble-averaged concentration, $\phi_\alpha(\mathbf{r}) \equiv \left\langle \hat{\phi}_\alpha(\mathbf{r}) \right\rangle$, and the configurational entropy, S. In order to evaluate these, some partition functions are required. To begin, consider the first sN segments ($0 \le s \le 1$) of the chain constraining the two ends at $\mathbf{r}_\alpha(0) = \mathbf{r}_0$ and $\mathbf{r}_\alpha(s) = \mathbf{r}$. The energy of this fragment is $E[\mathbf{r}_\alpha; 0, s]$ and thus its partition function is

$$q(\mathbf{r}, \mathbf{r}_0, s) \propto \int \mathcal{D}\mathbf{r}_\alpha \exp\left(-\frac{E[\mathbf{r}_\alpha; 0, s]}{k_B T} \right) \delta(\mathbf{r}_\alpha(0) - \mathbf{r}_0) \delta(\mathbf{r}_\alpha(s) - \mathbf{r}) \tag{1.15}$$

This is a functional integral over all configurations, $\mathbf{r}_\alpha(t)$, for $0 < t < s$, weighted by the appropriate Boltzmann factor; the delta functions simply exclude those configurations where the two ends are not at $\mathbf{r}_0$ and $\mathbf{r}$. (Those unfamiliar with functional integrals should refer to the Appendix.) In principle, the Boltzmann factor in the partition function should also contain the kinetic energy, and the functional integration should also extend over the momenta of all the monomers. However, the form of the kinetic energy allows the momentum coordinates to be integrated out and included in the proportionality factor (Hong and Noolandi 1981), which in any case has been omitted from Eq. (1.15). A proper evaluation of the proportionality constant would require a detailed account of the exact degrees of freedom available to all the atoms in the polymer molecule, but such information is lost in the coarse-graining procedure. Fortunately, the proportionality constant has no effect on the evaluation of $\phi_\alpha(\mathbf{r})$. Although it does affect S, it does so simply by an additive constant, which is immaterial since we will only be concerned with changes in entropy. Thus, the proportionality relationship in Eq. (1.15) is sufficient for our purposes.

The local property of the polymer energy is manifest mathematically by the equality, $E[\mathbf{r}_\alpha; 0, s] = E[\mathbf{r}_\alpha; 0, t] + E[\mathbf{r}_\alpha; t, s]$ for any $t \in [0, s]$. This implies the recursive relation,

$$q(\mathbf{r}, \mathbf{r}_0, s) = \frac{1}{(a^2 N)^{3/2}} \int d\mathbf{r}_1 \; q(\mathbf{r}, \mathbf{r}_1, t) q(\mathbf{r}_1, \mathbf{r}_0, s - t) \tag{1.16}$$

which gives the partition function for a fragment of sN segments in terms of the partition functions of two shorter fragments. By including an equality sign in Eq. (1.16), we have effectively chosen a value for the missing proportionality factor in Eq. (1.15); not one that has any actual meaning, but merely the simplest one that renders $q(\mathbf{r}, \mathbf{r}_0, s)$ dimensionless. This recursion relation also implies

$$q(\mathbf{r}, \mathbf{r}_0, 0) = (a^2 N)^{3/2} \delta(\mathbf{r} - \mathbf{r}_0) \tag{1.17}$$

because Eq. (1.16) must hold for $t \to 0$. Naturally $q(\mathbf{r}, \mathbf{r}_0, 0) = 0$ when $\mathbf{r} \neq \mathbf{r}_0$, since $s = 0$ implies that $\mathbf{r}$ and $\mathbf{r}_0$ both correspond to the same point on the chain.

The recursion relation, Eq. (1.16), provides a means of building up the partition function for a long chain fragment from those of very short fragments. This reduces the problem to the easier one of finding $q(\mathbf{r}, \mathbf{r}_0, \epsilon)$, where ϵ is small enough that the field can be treated as a constant for typical chain extensions of $|\mathbf{r} - \mathbf{r}_0| \lesssim a(\epsilon N)^{1/2}$. In this case, the field simply adds a constant energy of $\epsilon w(\mathbf{r}) k_B T$ to each configuration, and thus does not affect the relative probability of its configurations. Therefore, the partition function can be expressed as

$$q(\mathbf{r}, \mathbf{r}_0, \epsilon) \approx \left(\frac{3}{2\pi\epsilon}\right)^{3/2} \exp\left(-\frac{3|\mathbf{r} - \mathbf{r}_0|^2}{2a^2 N\epsilon} - \epsilon w(\mathbf{r})\right) \tag{1.18}$$

which assumes the Gaussian distribution in Eq. (1.11) for a chain of ϵN segments in a homogeneous environment, adjusted for the constant energy of the field and normalized so that it reduces to Eq. (1.17) in the limit $\epsilon \to 0$. For extensions, $|\mathbf{r} - \mathbf{r}_0|$, significantly beyond $a(\epsilon N)^{1/2}$, the partition function approaches zero regardless of whether or not the field energy is well-approximated by $\epsilon w(\mathbf{r}) k_B T$. Hence, Eq. (1.18) remains accurate over all extensions, provided that $a(\epsilon N)^{1/2}$ is sufficiently small relative to the spatial variations in $w(\mathbf{r})$.

Now the partition function for large fragments can be calculated iteratively using

$$q(\mathbf{r}, \mathbf{r}_0, s + \epsilon) = \frac{1}{(a^2 N)^{3/2}} \int d\mathbf{r}_\epsilon \, q(\mathbf{r}, \mathbf{r} + \mathbf{r}_\epsilon, \epsilon) q(\mathbf{r} + \mathbf{r}_\epsilon, \mathbf{r}_0, s) \tag{1.19}$$

The first partition function, $q(\mathbf{r}, \mathbf{r} + \mathbf{r}_\epsilon, \epsilon)$, under the integral implies that we only need to know the second one, $q(\mathbf{r} + \mathbf{r}_\epsilon, \mathbf{r}_0, \epsilon)$, accurately for $|\mathbf{r}_\epsilon| \lesssim a(\epsilon N)^{1/2}$. We therefore expand it in the Taylor series,

$$\begin{aligned} q(\mathbf{r}, \mathbf{r}_0, s + \epsilon) &= \frac{1}{(a^2 N)^{3/2}} \int d\mathbf{r}_\epsilon \, q(\mathbf{r}, \mathbf{r} + \mathbf{r}_\epsilon, \epsilon) \times \\ &\qquad \left[1 + \mathbf{r}_\epsilon \cdot \nabla + \frac{1}{2}\mathbf{r}_\epsilon \mathbf{r}_\epsilon : \nabla\nabla\right] q(\mathbf{r}, \mathbf{r}_0, s) \end{aligned} \tag{1.20}$$

to second order in $\mathbf{r}_\epsilon$. Here, we have used the dyadic notation (Goldstein 1980) for the second-order term. The expansion now makes it possible to explicitly integrate over $\mathbf{r}_\epsilon$, giving

$$q(\mathbf{r}, \mathbf{r}_0, s + \epsilon) \approx \exp\left(-\epsilon w(\mathbf{r})\right) \left[1 + \frac{a^2 N}{6}\epsilon\nabla^2\right] q(\mathbf{r}, \mathbf{r}_0, s) \tag{1.21}$$

$$\approx \left[1 + \frac{a^2 N}{6}\epsilon\nabla^2 - \epsilon w(\mathbf{r})\right] q(\mathbf{r}, \mathbf{r}_0, s) \tag{1.22}$$

to first order in ϵ. Alternatively, a Taylor-series expansion in s gives

$$q(\mathbf{r}, \mathbf{r}_0, s + \epsilon) \approx \left[1 + \epsilon\frac{\partial}{\partial s}\right] q(\mathbf{r}, \mathbf{r}_0, s) \tag{1.23}$$

By direct comparison, it immediately follows that

$$\frac{\partial}{\partial s} q(\mathbf{r}, \mathbf{r}_0, s) = \left[\frac{a^2 N}{6}\nabla^2 - w(\mathbf{r})\right] q(\mathbf{r}, \mathbf{r}_0, s) \tag{1.24}$$

which is the modified diffusion equation normally used to evaluate $q(\mathbf{r}, \mathbf{r}_0, s)$. Likewise, a partial partition function,

$$q(\mathbf{r}, s) \propto \int \mathcal{D}\mathbf{r}_\alpha \exp\left(-\frac{E[\mathbf{r}_\alpha; 0, s]}{k_B T}\right) \delta(\mathbf{r}_\alpha(s) - \mathbf{r}) \tag{1.25}$$

can be defined for a chain fragment with a free $s = 0$ end. The fact that

$$q(\mathbf{r}, s) = \frac{1}{(a^2 N)^{3/2}} \int d\mathbf{r}_0 \, q(\mathbf{r}, \mathbf{r}_0, s) \tag{1.26}$$

implies that it also satisfies Eq. (1.24), given that the diffusion equation is linear. Furthermore, Eq. (1.17) implies the initial condition, $q(\mathbf{r}, 0) = 1$.

In a completely analogous way, complementary partition functions are defined for the last $(1 - s)N$ segments of the chain. The one for a fixed $s = 1$ end is defined as

$$q^\dagger(\mathbf{r}, \mathbf{r}_0, s) \propto \int \mathcal{D}\mathbf{r}_\alpha \exp\left(-\frac{E[\mathbf{r}_\alpha; s, 1]}{k_B T}\right) \delta(\mathbf{r}_\alpha(s) - \mathbf{r}) \delta(\mathbf{r}_\alpha(1) - \mathbf{r}_0) \tag{1.27}$$

and satisfies the diffusion equation,

$$\frac{\partial}{\partial s} q^\dagger(\mathbf{r}, \mathbf{r}_0, s) = -\left[\frac{a^2 N}{6} \nabla^2 - w(\mathbf{r})\right] q^\dagger(\mathbf{r}, \mathbf{r}_0, s) \tag{1.28}$$

subject to the condition, $q^\dagger(\mathbf{r}, \mathbf{r}_0, 1) = (a^2 N)^{3/2} \delta(\mathbf{r} - \mathbf{r}_0)$. For an unconstrained end, the complementary partition function becomes

$$q^\dagger(\mathbf{r}, s) = \frac{1}{(a^2 N)^{3/2}} \int d\mathbf{r}_0 \, q^\dagger(\mathbf{r}, \mathbf{r}_0, s) \tag{1.29}$$

satisfying Eq. (1.28) with $q^\dagger(\mathbf{r}, 1) = 1$. The full partition function, $\mathcal{Q}[w]$, for a polymer in the field, $w(\mathbf{r})$, is then related to the integral of the two partial partition functions. In the case where both ends of the polymer are free,

$$\mathcal{Q}[w] = \int d\mathbf{r} \, q(\mathbf{r}, s) q^\dagger(\mathbf{r}, s) \propto \int \mathcal{D}\mathbf{r}_\alpha \exp\left(-\frac{E[\mathbf{r}_\alpha; 0, 1]}{k_B T}\right) \tag{1.30}$$

Again, the square brackets on $\mathcal{Q}[w]$ denote that it is a functional that depends on the function, $w(\mathbf{r})$.

With the partition functions in hand, the average segment distribution, $\phi_\alpha(\mathbf{r})$, can now be evaluated. Here the calculation is shown for an unconstrained polymer, but the procedure is essentially the same if one or both ends are constrained. Following standard statistical mechanics, the average is computed by weighting each configuration by the appropriate Boltzmann factor;

$$\begin{aligned}
\phi_\alpha(\mathbf{r}) &= \frac{1}{\mathcal{Q}[w]} \int \mathcal{D}\mathbf{r}_\alpha \hat{\phi}_\alpha(\mathbf{r}) \exp\left(-\frac{E[\mathbf{r}_\alpha; 0, 1]}{k_B T}\right) \\
&= \frac{N}{\rho_0 \mathcal{Q}[w]} \int_0^1 ds \int \mathcal{D}\mathbf{r}_\alpha \delta(\mathbf{r} - \mathbf{r}_\alpha(s)) \exp\left(-\frac{E[\mathbf{r}_\alpha; 0, 1]}{k_B T}\right) \\
&= \frac{N}{\rho_0 \mathcal{Q}[w]} \int_0^1 ds \, q(\mathbf{r}, s) q^\dagger(\mathbf{r}, s)
\end{aligned} \tag{1.31}$$

This equation provides the practical means of calculating the average segment concentration, but there will also be instances where we need to identify it by the functional derivative,

$$\phi_\alpha(\mathbf{r}) = -\frac{N}{\rho_0}\,\frac{\mathcal{D}\ln(\mathcal{Q}[w])}{\mathcal{D}w(\mathbf{r})} \equiv -\frac{N}{\rho_0}\lim_{\epsilon\to 0}\frac{\ln(\mathcal{Q}[w+\epsilon\delta]) - \ln(\mathcal{Q}[w])}{\epsilon} \tag{1.32}$$

The equivalence of this functional derivative to Eq. (1.31) follows almost immediately from the alternative expression,

$$\mathcal{Q}[w] \propto \int \mathcal{D}\mathbf{r}_\alpha \exp\left(-\frac{3}{2a^2N}\int_0^1 ds|\mathbf{r}'_\alpha(s)|^2 - \frac{\rho_0}{N}\int d\mathbf{r}_1\; w(\mathbf{r}_1)\hat{\phi}_\alpha(\mathbf{r}_1)\right) \tag{1.33}$$

for the partition function. Note that $\mathcal{Q}[w+\epsilon\delta]$ simply refers to the partition function evaluated with $w(\mathbf{r}_1)$ replaced by $w(\mathbf{r}_1) + \epsilon\delta(\mathbf{r}_1 - \mathbf{r})$. (See the Appendix for further information on functional differentiation.)

Lastly, we calculate the entropy, S, or equivalently the entropic free energy, $f_e \equiv -TS$, which, for reasons that will become apparent, is also called the elastic free energy of the polymer. In accord with standard statistical mechanics, the entropic energy is

$$\frac{f_e}{k_BT} = -\ln\left(\frac{\mathcal{Q}[w]}{\mathcal{V}}\right) - \frac{\rho_0}{N}\int d\mathbf{r}\; w(\mathbf{r})\phi_\alpha(\mathbf{r}) \tag{1.34}$$

The logarithm of $\mathcal{Q}[w]$ gives the total free energy of the polymer in the field, while the integral removes the average internal energy acquired from the field, leaving behind the entropic energy. The extra factor of $\mathcal{V}$ in the logarithm simply adds a constant to f_e such that the entropic energy is measured relative to the homogeneous state; it is easily confirmed that Eq. (1.34) gives $f_e = 0$ for the case of a uniform field.

Since the force exerted on the segments is given by the gradient of the field, an additive constant to the field should have no effect on any physical quantities. Indeed, this is the case. If a constant, w_0, is added to the field such that $w(\mathbf{r}) \Rightarrow w(\mathbf{r}) + w_0$, the partition functions transform as

$$q(\mathbf{r},s) \;\Rightarrow\; q(\mathbf{r},s)\exp(-sw_0) \tag{1.35}$$

$$q^\dagger(\mathbf{r},s) \;\Rightarrow\; q^\dagger(\mathbf{r},s)\exp(-(1-s)w_0) \tag{1.36}$$

$$\mathcal{Q}[w] \;\Rightarrow\; \mathcal{Q}[w]\exp(-w_0) \tag{1.37}$$

When these substitutions are entered into Eq. (1.31), all the exponential factors cancel, leaving $\phi_\alpha(\mathbf{r})$ unaffected. Likewise, w_0 cancels out of Eq. (1.34) for f_e, using the fact that the average segment concentration is $\bar{\phi}_\alpha = N/\rho_0\mathcal{V}$. This invariance will generally be used to set the spatial average of the field, $\bar{w}$, to zero.

1.3 Strong-Stretching Theory (SST): The Classical Path

In circumstances where the field energy becomes large relative to the thermal energy, k_BT, the polymer is effectively restricted to those configurations close to the ground state, referred to as the *classical path* for reasons that will become apparent in the following section. This

opens up the possibility of low-temperature series approximations, but one first needs to locate the ground-state trajectory by minimizing

$$E[\mathbf{r}_\alpha; 0, 1] = \int_0^1 ds \mathcal{L}(\mathbf{r}_\alpha(s), \mathbf{r}'_\alpha(s)) \tag{1.38}$$

where

$$\mathcal{L}(\mathbf{r}_\alpha(s), \mathbf{r}'_\alpha(s)) \equiv \frac{3}{2a^2N}|\mathbf{r}'_\alpha(s)|^2 + w(\mathbf{r}_\alpha(s)) \tag{1.39}$$

This is a standard *calculus of variations* problem, which, as demonstrated in the Appendix, is equivalent to solving the Euler-Lagrange equation,

$$\frac{d}{ds}\left(\frac{\partial \mathcal{L}}{\partial \mathbf{r}'_\alpha}\right) - \frac{\partial \mathcal{L}}{\partial \mathbf{r}_\alpha} = 0 \tag{1.40}$$

This is a slight generalization of Eq. (1.331), due to the fact that $\mathbf{r}_\alpha(s)$ is a vector rather than a scalar function. Nevertheless, the differentiation of $\mathcal{L}$ in Eq. (1.40) is easily performed and leads to the differential equation,

$$\frac{3}{a^2N}\mathbf{r}''_\alpha(s) - \nabla w(\mathbf{r}_\alpha(s)) = 0 \tag{1.41}$$

Solving this vector equation subject to possible boundary conditions for $\mathbf{r}_\alpha(0)$ and $\mathbf{r}_\alpha(1)$ provides the classical path.

Although Eq. (1.41) is sufficient, we can derive an alternative equation that provides a useful relation between the local chain extension, $|\mathbf{r}'_\alpha(s)|$, and the field energy, $w(\mathbf{r}_\alpha(s))$. This is done by dotting Eq. (1.41) with $\mathbf{r}'_\alpha(s)$ to give

$$\frac{3}{a^2N}\mathbf{r}'_\alpha(s) \cdot \mathbf{r}''_\alpha(s) - \mathbf{r}'_\alpha(s) \cdot \nabla w(\mathbf{r}_\alpha(s)) = 0 \tag{1.42}$$

which, in turn, can be rewritten as

$$\frac{d}{ds}\left(\frac{3|\mathbf{r}'_\alpha(s)|^2}{2a^2N}\right) - \frac{d}{ds}w(\mathbf{r}_\alpha(s)) = 0 \tag{1.43}$$

Performing an integration reduces this to the first-order differential equation,

$$\frac{3|\mathbf{r}'_\alpha(s)|^2}{2a^2N} - w(\mathbf{r}_\alpha(s)) = \text{constant} \tag{1.44}$$

In cases of appropriate symmetry, the classical trajectory can be derived from this scalar equation alone.

Once the classical path is known, the average segment concentration is given by

$$\phi_\alpha(\mathbf{r}) = \frac{N}{\rho_0}\int_0^1 ds\, \delta(\mathbf{r} - \mathbf{r}_\alpha(s)) \tag{1.45}$$

and the entropic free energy is

$$\frac{f_e}{k_BT} = \frac{3}{2a^2N}\int_0^1 ds\, |\mathbf{r}'_\alpha(s)|^2 \tag{1.46}$$

This entropic energy is often referred to as the elastic or stretching energy, because it has the equivalent form to the stretching energy of a thin, elastic thread.

1.4 Analogy with Quantum/Classical Mechanics

Every so often, mathematics and physics are bestowed with a powerful mapping that equates two diverse topics. In one giant leap, years of accumulated knowledge on one topic can be instantly transferred to another. Here, we encounter such an example by the fact that a Gaussian chain in an external field maps onto the quantum mechanics of a single particle in a potential. For those without a background in quantum mechanics, the section can be skimmed over without seriously compromising one's understanding of the remaining sections.

The mapping becomes apparent when examining the path-integral formalism of quantum mechanics introduced by Feynman and Hibbs (1965). With incredible insight, they demonstrate that the quantum mechanical wavefunction, $\Psi(\mathbf{r},t)$, for a particle of mass, m, in a potential, $U(\mathbf{r})$, is given by the path integral,

$$\Psi(\mathbf{r},t) = \int \mathcal{D}\mathbf{r}_p \exp(iS/\hbar)\delta(\mathbf{r}_p(t)-\mathbf{r}) \tag{1.47}$$

over all possible trajectories, $\mathbf{r}_p(t)$, where the particle terminates at position, $\mathbf{r}$, at time, t. (Note that $i \equiv \sqrt{-1}$.) In this definition, each trajectory contributes a phase factor given by the classical action,

$$S \equiv \int dt \ \left[\frac{m}{2}|\mathbf{r}_p'(t)|^2 - U(\mathbf{r}_p(t))\right] \tag{1.48}$$

which, in this case, is kinetic energy minus potential energy integrated along the particle trajectory. Naturally, Feynman justified this by showing that Eq. (1.47) is equivalent to the usual time-dependent Schrödinger equation,

$$i\hbar\frac{\partial}{\partial t}\Psi(\mathbf{r},t) = \left[-\frac{\hbar^2}{2m}\nabla^2 + U(\mathbf{r})\right]\Psi(\mathbf{r},t) \tag{1.49}$$

in much the same way Section 1.2 derived the diffusion equation for $q(\mathbf{r},s)$.

Taking a closer look, the mathematics of this quantum mechanical problem is exactly that of our polymer in an external field. A precise mapping merely requires the associations,

$$t \quad \Leftrightarrow \quad s \tag{1.50}$$

$$m \quad \Leftrightarrow \quad \frac{3}{a^2 N} \tag{1.51}$$

$$U(\mathbf{r}) \quad \Leftrightarrow \quad -w(\mathbf{r}) \tag{1.52}$$

$$S \quad \Leftrightarrow \quad \frac{E[\mathbf{r}_\alpha;0,s]}{k_B T} \tag{1.53}$$

$$\mathbf{r}_p(t) \quad \Leftrightarrow \quad \mathbf{r}_\alpha(s) \tag{1.54}$$

$$\hbar \quad \Leftrightarrow \quad -i \tag{1.55}$$

$$\Psi(\mathbf{r},t) \quad \Leftrightarrow \quad q(\mathbf{r},s) \tag{1.56}$$

Indeed, these substitutions transform Eq. (1.47) for the wavefunction into Eq. (1.25) for the partition function of sN polymer segments, and likewise the Schrödinger Eq. (1.49) transforms into the diffusion Eq. (1.24).

Extending this analogy further, the strong-stretching theory (SST) developed in Section 1.3 is found to be equivalent to classical mechanics. In Feynman's formulation, the connection between quantum mechanics and classical mechanics becomes exceptionally transparent. When the action, S, of a particle is large relative to $\hbar$, the path integral becomes dominated by the extremum of S, because all paths close to the extremum contribute the same phase factor, and thus add constructively. (This is the basis of Fermat's principle in optics by which the full wave treatment of light can be reduced to classical ray optics (Hecht and Zajac 1974).) However, the procedure of finding the extremum of S is precisely the Lagrangian formalism of classical mechanics (Goldstein 1980). Thus, in the limit of large S, the particle follows the classical mechanical trajectory determined by Newton's equation of motion (i.e, $m\mathbf{a} = \mathbf{F}$),

$$m\mathbf{r}_p''(t) = -\nabla U(\mathbf{r}_p(t)) \tag{1.57}$$

Equally familiar in classical mechanics is the equation for the conservation of energy,

$$\frac{m}{2}|\mathbf{r}_p'(t)|^2 + U(\mathbf{r}_p(t)) = \text{constant} \tag{1.58}$$

In terms of the analogy, classical mechanics corresponds to the case where $E[\mathbf{r}_\alpha; s_1, s_2]/k_BT$ is large relative to one, which is the condition for the strong-stretching theory (SST) discussed in the preceding section. Indeed, Eq. (1.57) matches precisely with Eq. (1.41) for the ground-state polymer trajectory, as does Eq. (1.58) with Eq. (1.44). It is this analogy from which the ground-state trajectory acquires its name, the *classical* path.

1.5 Mathematical Techniques and Approximations

Quantum mechanics has experienced a massive activity of research since its introduction midway through the last century. The accumulated knowledge is staggering, and the fact that our problem maps onto it means that we can make significant progress without having to reinvent the wheel. This section demonstrates several useful calculations that draw upon what are now standard techniques in quantum mechanics.

1.5.1 Spectral Method

One of the most widely used and fruitful techniques in quantum mechanics is the spectral method for solving the time-dependent wavefunction, $\Psi(\mathbf{r}, t)$. Here, the method is adapted to the evaluation of the partial partition functions, $q(\mathbf{r}, s)$ and $q^\dagger(\mathbf{r}, s)$, for a homopolymer in an external field, $w(\mathbf{r})$. The first step is to solve the analog of the time-independent Schrödinger equation,

$$\left[\frac{a^2N}{6}\nabla^2 - w(\mathbf{r})\right] f_i(\mathbf{r}) = -\lambda_i f_i(\mathbf{r}) \tag{1.59}$$

for all the eigenvalues, λ_i, and eigenfunctions, $f_i(\mathbf{r})$, where $i = 0$,1,2,... For reasons that will be discussed at the end of this section, the eigenvalues are ordered from smallest to largest. As

in quantum mechanics, the eigenfunctions are orthogonal and can be normalized to satisfy,

$$\frac{1}{\mathcal{V}}\int d\mathbf{r}\; f_i(\mathbf{r})f_j(\mathbf{r}) = \delta_{ij} \tag{1.60}$$

where $\mathcal{V}$ is the total volume of the system. Furthermore, the eigenfunctions form a complete basis, which implies that any function of position, $g(\mathbf{r})$, can be expanded as

$$g(\mathbf{r}) = \sum_{i=0}^{\infty} g_i f_i(\mathbf{r}) \tag{1.61}$$

The coefficients, g_i, of the expansion are determined by multiplying Eq. (1.61) by $f_j(\mathbf{r})$, integrating over $\mathbf{r}$, and using the orthonormal condition from Eq. (1.60). This gives the formula,

$$g_i = \frac{1}{\mathcal{V}}\int d\mathbf{r} f_i(\mathbf{r})g(\mathbf{r}) \tag{1.62}$$

Once the orthonormal basis functions have been obtained, it is a trivial matter to evaluate $q(\mathbf{r}, s)$. One starts by expanding it as

$$q(\mathbf{r}, s) = \sum_{i=0}^{\infty} q_i(s) f_i(\mathbf{r}) \tag{1.63}$$

and substituting the expansion into Eq. (1.24). Given the inherent property of the eigenfunctions, Eq. (1.59), the diffusion equation reduces to

$$\sum_{i=0}^{\infty} q_i'(s) f_i(\mathbf{r}) = -\sum_{i=0}^{\infty} \lambda_i q_i(s) f_i(\mathbf{r}) \tag{1.64}$$

With the same steps used to derive Eq. (1.62), it follows that

$$q_i'(s) = -\lambda_i q_i(s) \tag{1.65}$$

for all $i = 0$,1,2,.... Differential equations do not come any simpler. Inserting the solution into Eq. (1.63) gives the final result,

$$q(\mathbf{r}, s) = \sum_{i=0}^{\infty} c_i \exp(-\lambda_i s) f_i(\mathbf{r}) \tag{1.66}$$

where the constant,

$$c_i \equiv q_i(0) = \frac{1}{\mathcal{V}}\int d\mathbf{r}\; f_i(\mathbf{r})q(\mathbf{r}, 0) \tag{1.67}$$

is determined by the initial condition. Similarly, the expression for the complementary partition function is

$$q^\dagger(\mathbf{r}, s) = \sum_{i=0}^{\infty} c_i^\dagger \exp(-\lambda_i(1-s)) f_i(\mathbf{r}) \tag{1.68}$$

where

$$c_i^\dagger = \frac{1}{\mathcal{V}} \int d\mathbf{r}\ f_i(\mathbf{r}) q^\dagger(\mathbf{r}, 1) \tag{1.69}$$

In practice, it is impossible to complete the infinite sums in Eqs. (1.66) and (1.68), but the eigenvalues are appropriately ordered such that the terms become less and less important. Therefore, the sums can be truncated at some point, $i = M$, where the number of terms retained, $M + 1$, is guided by the desired level of accuracy.

1.5.2 Ground-State Dominance

The previous expansion for $q(\mathbf{r}, s)$ in Eq. (1.66) becomes increasingly dominated by the first term involving the *ground-state* eigenvalue, λ_0, the further s is from the end of the chain. For a high-molecular-weight polymer, the approximations,

$$q(\mathbf{r}, s) \approx c_0 \exp(-\lambda_0 s) f_0(\mathbf{r}) \tag{1.70}$$

and

$$q^\dagger(\mathbf{r}, s) \approx c_0^\dagger \exp(-\lambda_0 (1 - s)) f_0(\mathbf{r}) \tag{1.71}$$

become accurate over the vast majority of the chain. In this case, it follows that the partition function of the entire chain is

$$\mathcal{Q}[w] \approx \mathcal{V} c_0 c_0^\dagger \exp(-\lambda_0) \tag{1.72}$$

and that the segment concentration is

$$\phi_\alpha(\mathbf{r}) \approx \frac{N}{\rho_0 \mathcal{V}} f_0^2(\mathbf{r}) \tag{1.73}$$

These simplifications permit us to derive an analytical Landau-Ginzburg free energy expression for the entropic energy, f_e, of the polymer as a function of its concentration profile, $\phi_\alpha(\mathbf{r})$. Our derivation will assume that concentration gradient,

$$\nabla \phi_\alpha(\mathbf{r}) = \frac{2N}{\rho_0 \mathcal{V}} f_0(\mathbf{r}) \nabla f_0(\mathbf{r}) \tag{1.74}$$

is zero at the extremities (i.e., boundaries) of our system, $\mathcal{V}$.

The first step of the derivation is to multiply Eq. (1.59) for $i = 0$ by $f_0(\mathbf{r})$ and integrate over $\mathcal{V}$, producing the result,

$$\frac{\rho_0}{N} \int d\mathbf{r}\ w(\mathbf{r}) \phi_\alpha(\mathbf{r}) = \frac{a^2 N}{6\mathcal{V}} \int d\mathbf{r}\ f_0(\mathbf{r}) \nabla^2 f_0(\mathbf{r}) + \lambda_0 \tag{1.75}$$

Next, this expression for the field energy along with Eq. (1.72) for $\mathcal{Q}[w]$ are inserted into Eq. (1.34) giving the expression,

$$\frac{f_e}{k_B T} = -\frac{a^2 N}{6\mathcal{V}} \int d\mathbf{r}\ f_0(\mathbf{r}) \nabla^2 f_0(\mathbf{r}) - \ln(c_0 c_0^\dagger) \tag{1.76}$$

for the entropic free energy. The logarithmic term can be dropped in the large-N limit. An integration by parts is then performed to reexpress the equation as

$$\frac{f_e}{k_BT} = \frac{a^2N}{6\mathcal{V}} \int d\mathbf{r}\, |\nabla f_0(\mathbf{r})|^2 \tag{1.77}$$

where the boundary term vanishes as a result of the assumption, $\nabla\phi_\alpha(\mathbf{r}) = 0$, along the edge of $\mathcal{V}$. For the final step of the derivation, the eigenfunction, $f_0(\mathbf{r})$, is replaced by the segment concentration, $\phi_\alpha(\mathbf{r})$, using Eqs. (1.73) and (1.74). This produces the Landau-Ginzburg free energy expression,

$$\frac{f_e}{k_BT} = \frac{a^2\rho_0}{24} \int d\mathbf{r}\, \frac{|\nabla\phi_\alpha(\mathbf{r})|^2}{\phi_\alpha(\mathbf{r})} \tag{1.78}$$

which gives the entropic energy without the need to evaluate the underlying field, $w(\mathbf{r})$. The derivation assumes only that the molecular weight (i.e., N) of the polymer is large.

1.5.3 Fourier Representation

Quantum mechanical problems are often made more tractable by reexpressing them in so-called momentum space. The principle is very similar to that of the spectral method, where quantities are expanded in terms of energy eigenstates. The main difference is that the expansions are now in terms of eigenfunctions, $\exp(i\mathbf{k}\cdot\mathbf{r})$, of the momentum operator, $\hat{p} \equiv -i\hbar\nabla$. (Here, $i \equiv \sqrt{-1}$.) The other difference is that the momentum eigenvalue, $\mathbf{k}$, is continuous, which implies that sums are now replaced by integrals and Kronecker delta functions are substituted by Dirac delta functions. For example, the orthogonality condition in Eq. (1.60) becomes

$$\frac{1}{(2\pi)^3} \int d\mathbf{r} \exp(i(\mathbf{k}_1 - \mathbf{k}_2)\cdot\mathbf{r}) = \delta(\mathbf{k}_1 - \mathbf{k}_2) \tag{1.79}$$

Furthermore, the expansion of an arbitrary function, $g(\mathbf{r})$, becomes the integral,

$$g(\mathbf{r}) = \frac{1}{(2\pi)^3} \int d\mathbf{k}\, g(\mathbf{k}) \exp(i\mathbf{k}\cdot\mathbf{r}) \tag{1.80}$$

and the coefficient of the expansion,

$$g(\mathbf{k}) \equiv \int d\mathbf{r}\, g(\mathbf{r}) \exp(-i\mathbf{k}\cdot\mathbf{r}) \tag{1.81}$$

is now a continuous function, referred to as the Fourier transform of $g(\mathbf{r})$. Although $g(\mathbf{k})$ is complex, its complex conjugate satisfies $g^*(\mathbf{k}) = g(-\mathbf{k})$, which implies that $|g(\mathbf{k})|^2 = g(-\mathbf{k})g(\mathbf{k})$. Before moving on, we quote a useful identity,

$$\int d\mathbf{r}\, g_1(\mathbf{r})g_2(\mathbf{r}) = \frac{1}{(2\pi)^3} \int d\mathbf{k}\, g_1(-\mathbf{k})g_2(\mathbf{k}) \tag{1.82}$$

for the integral of two functions. It can be proved by substituting the expansions for $g_1(\mathbf{r})$ and $g_2(\mathbf{r})$ into the left-hand side, identifying the integral over $\mathbf{r}$ as the Dirac delta function in Eq. (1.79), and using the sifting property of the delta function from Eq. (1.329).

Now we are ready to Fourier transform the diffusion equation for $q(\mathbf{r}, s)$. The first step is to insert the Fourier representations, Eq. (1.80), of $q(\mathbf{r}, s)$ and $w(\mathbf{r})$ into the diffusion Eq. (1.24), giving

$$\frac{\partial}{\partial s}\int d\mathbf{k}_2 q(\mathbf{k}_2, s)\exp(i\mathbf{k}_2\cdot\mathbf{r}) = -\frac{a^2N}{6}\int d\mathbf{k}_2 k_2^2 q(\mathbf{k}_2, s)\exp(i\mathbf{k}_2\cdot\mathbf{r}) - \frac{1}{(2\pi)^3}\int d\mathbf{k}_1 d\mathbf{k}_2 w(\mathbf{k}_1)q(\mathbf{k}_2, s)\exp(i(\mathbf{k}_1+\mathbf{k}_2)\cdot\mathbf{r}) \tag{1.83}$$

Next the equation is multiplied through by $\exp(-i\mathbf{k}\cdot\mathbf{r})$ and integrated over $\mathbf{r}$. Using the orthogonality relation in Eq. (1.79), the expression simplifies to

$$\frac{\partial}{\partial s}\int d\mathbf{k}_2 q(\mathbf{k}_2, s)\delta(\mathbf{k}_2-\mathbf{k}) = -\frac{a^2N}{6}\int d\mathbf{k}_2 k_2^2 q(\mathbf{k}_2, s)\delta(\mathbf{k}_2-\mathbf{k}) - \frac{1}{(2\pi)^3}\int d\mathbf{k}_1 d\mathbf{k}_2 w(\mathbf{k}_1)q(\mathbf{k}_2, s)\delta(\mathbf{k}_1+\mathbf{k}_2-\mathbf{k}) \tag{1.84}$$

Now we apply the sifting property of the delta function to arrive at the final expression,

$$\frac{\partial}{\partial s}q(\mathbf{k}, s) = -\frac{k^2a^2N}{6}q(\mathbf{k}, s) - \frac{1}{(2\pi)^3}\int d\mathbf{k}_1 w(\mathbf{k}_1)q(\mathbf{k}-\mathbf{k}_1, s) \tag{1.85}$$

This equation is then solved for $q(\mathbf{k}, s)$ subject to the initial condition

$$q(\mathbf{k}, 0) = \int d\mathbf{r}\; q(\mathbf{r}, 0)\exp(-i\mathbf{k}\cdot\mathbf{r}) \tag{1.86}$$

For a polymer with a free end,

$$q(\mathbf{k}, 0) = (2\pi)^3\delta(\mathbf{k}) \tag{1.87}$$

whereas when the $s = 0$ end is fixed at $\mathbf{r}_0$,

$$q(\mathbf{k}, 0) = (aN^{1/2})^3\exp(i\mathbf{k}\cdot\mathbf{r}_0) \tag{1.88}$$

In either case, the solution to Eq. (1.85) for a homogeneous environment (i.e., $w(\mathbf{r}) = 0$) is readily expressed as

$$q(\mathbf{k}, s) = q(\mathbf{k}, 0)\exp(-k^2a^2Ns/6) \tag{1.89}$$

from which $q(\mathbf{r}, s)$ immediately follows. The aim of the next section will be to extend this result to polymers in a weak field.

1.5.4 Random-Phase Approximation

Here, a Landau-Ginzburg free energy expression is derived for the entropic free energy, f_e, of a polymer molecule in a weakly-varying field, $w(\mathbf{r})$. As before in Section 1.5.2, this calculation will assume that the two ends of the chain are free, by imposing the initial condition in Eq. (1.87). We will also use the invariance discussed at the end of Section 1.2 to fix the spatial average of the field to $\bar{w} = 0$. Given that $w(\mathbf{r})$ only deviates slightly from zero, it is safe to assume that the ensemble-averaged segment concentration, $\phi_\alpha(\mathbf{r})$, never strays far from its spatial average,

$$\bar{\phi}_\alpha \equiv \frac{1}{\mathcal{V}} \int d\mathbf{r}\, \phi_\alpha(\mathbf{r}) = \frac{N}{\rho_0 \mathcal{V}} \tag{1.90}$$

The first step is to find an approximate solution for $q(\mathbf{k} \neq 0, s)$. Since the integral in Eq. (1.85) involves $w(\mathbf{k}_1)$, which is small, the multiplicative factor of $q(\mathbf{k} - \mathbf{k}_1, s)$ need not be particularly accurate. Approximating it by $q(\mathbf{k} - \mathbf{k}_1, 0)$ from Eq. (1.87) gives

$$\frac{\partial}{\partial s} q(\mathbf{k}, s) \approx -xq(\mathbf{k}, s) - \frac{1}{(2\pi)^3} \int d\mathbf{k}_1 w(\mathbf{k}_1) q(\mathbf{k} - \mathbf{k}_1, 0) \tag{1.91}$$

$$= -xq(\mathbf{k}, s) - w(\mathbf{k}) \tag{1.92}$$

where $x \equiv k^2 a^2 N/6$. Given that $q(\mathbf{k}, 0) = 0$ for $\mathbf{k} \neq 0$, the solution becomes

$$q(\mathbf{k}, s) \approx -w(\mathbf{k}) h(x, s) \tag{1.93}$$

where

$$h(x, s) \equiv \frac{1 - \exp(-sx)}{x} \tag{1.94}$$

The second step is to solve for $q(\mathbf{k} = 0, s)$, in which case Eq. (1.85) reduces to

$$\frac{\partial}{\partial s} q(\mathbf{k}, s) = -\frac{1}{(2\pi)^3} \int d\mathbf{k}_1 w(\mathbf{k}_1) q(-\mathbf{k}_1, s) \tag{1.95}$$

Since we have set $\bar{w} = 0$, it follows that $w(\mathbf{k}_1) = 0$ for $\mathbf{k}_1 = 0$, which in turn implies that the approximation from Eq. (1.93) can be inserted inside the integral to give

$$\frac{\partial}{\partial s} q(\mathbf{k}, s) \approx \frac{1}{(2\pi)^3} \int d\mathbf{k}_1 w(\mathbf{k}_1) w(-\mathbf{k}_1) h(x_1, s) \tag{1.96}$$

The solution of this is

$$q(\mathbf{k}, s) \approx q(\mathbf{k}, 0) \left[1 + \frac{1}{2(2\pi)^3 \mathcal{V}} \int d\mathbf{k}_1 w(-\mathbf{k}_1) w(\mathbf{k}_1) g(x_1, s) \right] \tag{1.97}$$

where

$$g(x, s) \equiv \frac{2[\exp(-sx) + sx - 1]}{x^2} \tag{1.98}$$

Note that we have used the fact that $q(\mathbf{k}=0,0)=\mathcal{V}$, which follows from Eq. (1.81) and the initial condition, $q(\mathbf{r},0)=1$. Now that the Fourier transform, $q(\mathbf{k},s)$, is known for all $\mathbf{k}$, it can be converted back to

$$q(\mathbf{r},s) \approx 1 + \frac{1}{2(2\pi)^3\mathcal{V}} \int d\mathbf{k}\; w(-\mathbf{k})w(\mathbf{k})g(x,s) - \frac{1}{(2\pi)^3} \int d\mathbf{k}\; w(\mathbf{k})h(x,s)\exp(i\mathbf{k}\cdot\mathbf{r}) \tag{1.99}$$

using the inverse Fourier transform, Eq. (1.80). In principle, the second integral in Eq. (1.99) should exclude $\mathbf{k}=0$, but it can be extended to all $\mathbf{k}$, since $w(\mathbf{k}=0)=0$. The analogous calculation for the complementary partition function gives

$$q^\dagger(\mathbf{r},s) \approx 1 + \frac{1}{2(2\pi)^3\mathcal{V}} \int d\mathbf{k}\; w(-\mathbf{k})w(\mathbf{k})g(x,1-s) - \frac{1}{(2\pi)^3} \int d\mathbf{k}\; w(\mathbf{k})h(x,1-s)\exp(i\mathbf{k}\cdot\mathbf{r}) \tag{1.100}$$

From the partial partition functions, it follows that the partition for the entire chain is

$$\frac{\mathcal{Q}[w]}{\mathcal{V}} \approx 1 + \frac{1}{2(2\pi)^3\mathcal{V}} \int d\mathbf{k}\; w(-\mathbf{k})w(\mathbf{k})g(x,1) \tag{1.101}$$

The Fourier amplitudes of the segment concentration are most easily evaluated using the functional derivative,

$$\phi_\alpha(\mathbf{k}) = -\frac{N(2\pi)^3}{\rho_0}\frac{\mathcal{D}\ln(\mathcal{Q}[w])}{\mathcal{D}w(-\mathbf{k})} \tag{1.102}$$

which is derived similarly to Eq. (1.32) by making the substitution

$$\frac{\rho_0}{N}\int d\mathbf{r}\; w(\mathbf{r})\hat{\phi}_\alpha(\mathbf{r}) = \frac{\rho_0}{N(2\pi)^3}\int d\mathbf{k}\; w(-\mathbf{k})\hat{\phi}_\alpha(\mathbf{k}) \tag{1.103}$$

in Eq. (1.33). Note that the differentiation cannot be used for $\mathbf{k}=0$, because $\mathcal{Q}[w]$ has been calculated under the assumption $w(\mathbf{k}=0)=0$. Nevertheless, we already know that $\phi_\alpha(\mathbf{k}=0)=\bar{\phi}_\alpha\mathcal{V}=N/\rho_0$. For $\mathbf{k}\neq 0$, we have

$$\phi_\alpha(\mathbf{k}) = -\bar{\phi}_\alpha w(\mathbf{k})g(x,1) \tag{1.104}$$

It is now just a simple matter of substituting our results into Eq. (1.34) to obtain an expression for the entropic free energy. First, the logarithm of $\mathcal{Q}[w]$ is evaluated with the Taylor-series approximation, $\ln(1+x)\approx x$, applied to Eq. (1.101). Then the field energy is rewritten in terms of Fourier coefficients as in Eq. (1.103), and lastly all occurrences of $w(\mathbf{k})$ are eliminated in favor of $\phi(\mathbf{k})$ using Eq. (1.104). The final result is

$$\frac{f_e}{k_BT} = \frac{\rho_0}{2N\bar{\phi}_\alpha(2\pi)^3}\int_{\mathbf{k}\neq 0} d\mathbf{k}\frac{\phi_\alpha(-\mathbf{k})\phi_\alpha(\mathbf{k})}{g(x,1)} \tag{1.105}$$

to second order in $|\phi_\alpha(\mathbf{k})|$. As in Section 1.5.2, this is a Landau-Ginzburg free energy expression that provides the entropic free energy, f_e, for a specified segment profile, $\phi_\alpha(\mathbf{r})$, without the need to solve for the underlying field, $w(\mathbf{r})$.

This time, the derivation assumes small variations in $\phi_\alpha(\mathbf{r})$, whereas the previous expression in Eq. (1.78) instead assumed that N is large. If we now make this additional assumption that the molecules are large relative to the wavelengths of all the concentration fluctuations (i.e., $x \gg 1$), then $g(x,1) \approx 2/x$ and Eq. (1.105) reduces to

$$\frac{f_e}{k_B T} \approx \frac{a^2 \rho_0}{24 \bar{\phi}_\alpha} \int d\mathbf{r} |\nabla \phi_\alpha(\mathbf{r})|^2 \tag{1.106}$$

where we have made use of the identity,

$$\frac{1}{(2\pi)^3} \int d\mathbf{k} k^2 \phi_\alpha(-\mathbf{k}) \phi_\alpha(\mathbf{k}) = \int d\mathbf{r} |\nabla \phi_\alpha(\mathbf{r})|^2 \tag{1.107}$$

Hence, Eq. (1.105) becomes equivalent to Eq. (1.78), provided that $\phi_\alpha(\mathbf{r}) \approx \bar{\phi}_\alpha$, which indeed was the assumption used to arrive at Eq. (1.105).

1.6 Polymer Brushes

To proceed further with the theory, it is useful to discuss a specific example, and for that we now examine the polymer brush depicted in Fig. 1.3(a), where n polymers are grafted to a planar substrate of area $\mathcal{A}$. (Brushes are often examined in solvent environments, but for simplicity we will treat only the dry-brush case.) The grafting is enforced by requiring the z component of the trajectories to satisfy, $z_\alpha(1) = 0$, for $\alpha = 1$, 2,..., n. Pinning the $s = 1$ end of each molecule to $z = 0$ tends to cause the total segment concentration,

$$\hat{\phi}(\mathbf{r}) \equiv \sum_{\alpha=1}^{n} \hat{\phi}_\alpha(\mathbf{r}) \tag{1.108}$$

to accumulate near the substrate, exceeding the bulk segment density, ρ_0, permitted by the hard-core repulsive interactions. To correct for this, a static field, $w(\mathbf{r})$, is introduced to mimic the hard-core interactions and force the chains to extend outwards from the substrate in order to avoid overcrowding. More specifically, the field is selected such that it produces a uniform bulk segment concentration, $\hat{\phi}(\mathbf{r}) = 1$, up to the brush edge at $z = L$, determined by the total quantity of polymer, $\mathcal{A}L = \mathcal{V} \equiv nN/\rho_0$.

We assume the grafting is uniform and sufficiently thick that the brush exhibits translational symmetry, from which it follows that the field, $w(z)$, varies only in the z direction. This, in turn, allows us to separate the energy of a polymer fragment as

$$E[\mathbf{r}_\alpha; s_1, s_2] = E_\parallel[x_\alpha; s_1, s_2] + E_\parallel[y_\alpha; s_1, s_2] + E_\perp[z_\alpha; s_1, s_2] \tag{1.109}$$

where

$$E_\parallel[x_\alpha; s_1, s_2] = \frac{3}{2a^2 N} \int_{s_1}^{s_2} ds [x'_\alpha(s)]^2 \tag{1.110}$$

$$E_\perp[z_\alpha; s_1, s_2] = \int_{s_1}^{s_2} ds \left(\frac{3}{2a^2 N} [z'_\alpha(s)]^2 + w(z_\alpha(s)) \right) \tag{1.111}$$

This separation implies that the $x_\alpha(s)$ and $y_\alpha(s)$ components of the trajectory are unaffected by the field and continue to perform simple, unperturbed random walks. Consequently, we need only to consider the one-dimensional problem involving the z component of the trajectory, $z_\alpha(s)$.

Rather than starting with the full self-consistent field theory (SCFT), we first present the analytical strong-stretching theory (SST) (Semenov 1985) for thick brushes in which the chains are, effectively, restricted to their classical trajectories. In this limit, a powerful analogy with classical mechanics (Milner et al. 1988) allows us to deduce that $w(z)$ is parabolic, without having to invoke the incompressibility condition, $\hat{\phi}(\mathbf{r}) = 1$. Following that, the effect of fluctuations about the classical path are examined using both the path-integral formulation and the diffusion equation, but still assuming the parabolic potential. We then conclude by describing the SCFT for determining the proper $w(z)$ in the presence of chain fluctuations, and presenting direct comparisons with the preceding SST predictions.

1.6.1 SST for a Brush: The Parabolic Potential

For very thick brushes (i.e., $L/aN^{1/2} \gg 1$), the polymer chains are generally so extended that fluctuations about the classical paths of lowest energy can be ignored to a first approximation. We therefore start by identifying the classical trajectory of a chain with its $s = 0$ end extended to $z = z_0$. The one-dimensional version of Eq. (1.44) implies that the classical path must satisfy

$$\frac{3[z'_\alpha(s)]^2}{2a^2N} - w(z_\alpha(s)) = \text{constant} \tag{1.112}$$

Normally, the unknown field, $w(z)$, would be determined using the incompressibility condition, but in this particular situation it can be deduced by exploiting an analogy with classical mechanics (Milner et al. 1988). On physical grounds, the tension of the chain should vanish at the free end (i.e., $z'_\alpha(0) = 0$), just as it would for a heavy length of rope hanging in a gravitational potential. Add to this the fact that the trajectory must finish at the substrate (i.e., $z_\alpha(1) = 0$) regardless of the starting point (i.e., $z_\alpha(0) = z_0$), and we are ready to exploit the analogy with classical mechanics developed in Section 1.4. The analogy maps this polymer problem onto that of a particle that starts from rest and reaches $z = 0$ in exactly one unit of time, regardless of the starting point. As any undergraduate student will know, this is the property of a pendulum (or simple harmonic oscillator) with a period of 4, for which they would have no trouble working out the potential, $U(z)$. Then, from the correspondence in Eq. (1.52), it immediately follows that

$$w(z) = -\frac{3\pi^2 z^2}{8a^2N} \tag{1.113}$$

for which the corresponding trajectory is

$$z_\alpha(s) = z_0 \cos(\pi s/2) \tag{1.114}$$

Inserting the trajectory into Eq. (1.111), the total energy, $E_\perp[z_\alpha; 0, 1]$, of the chain is found to be precisely zero. In reality, there should be a small dependence on z_0 related to

the distribution, $g(z_0)$, of the free end, but that is lost in this simple treatment. In the more complete theory (Matsen 2002b) where $g(z_0) \propto \exp(-E_\perp[z_\alpha;0,1]/k_BT)$, there is a small entopic tension at the free end of the chain produced by the tendency for a broad $g(z_0)$ distribution, which incidentally negates the argument for the parabolic potential. However, let us stick with the simpler theory for now.

In the simpler version of the theory, $g(z_0)$ has to be determined by requiring the overall segment concentration to be uniform. When a chain with a given end-point z_0 is unable to fluctuate about its classical path, the sN'th segment has the delta (i.e., infinitely narrow) distribution,

$$\rho(z;z_0,s) = aN^{1/2}\delta(z - z_\alpha(s)) \tag{1.115}$$

Summing this distribution over all the segments gives the concentration,

$$\phi(z;z_0) \equiv \int_0^1 ds\ \rho(z;z_0,s) \tag{1.116}$$

$$= \begin{cases} \frac{2aN^{1/2}}{\pi\sqrt{z_0^2-z^2}}\,, & \text{if } z < z_0 \\ 0\,, & \text{if } z > z_0 \end{cases} \tag{1.117}$$

of an entire chain with its free end at $z = z_0$. From this, the average concentration over all the chains becomes

$$\phi(z) = \frac{L}{a^2N}\int_0^1 dz_0\ g(z_0)\phi(z;z_0) \tag{1.118}$$

By requiring $\phi(z) = 1$ over the thickness of the brush, this integral equation can be inverted giving the end-segment distribution,

$$g(z_0) = \frac{z_0 aN^{1/2}}{L\sqrt{L^2 - z_0^2}} \tag{1.119}$$

Although the inversion (Netz and Schick 1998) is complicated, the above solution is easily confirmed.

Now that $g(z_0)$ is known, the calculation of the average stretching energy, f_e, of the brush is straightforward. First, the stretching energy of an individual chain is

$$\frac{f_e(z_0)}{k_BT} = \frac{3}{2a^2N}\int_0^1 ds[z'_\alpha(s)]^2 = \frac{3\pi^2 z_0^2}{16a^2N} \tag{1.120}$$

Weighting this with respect to $g(z_0)$ gives an average stretching energy per chain of

$$\frac{f_e}{k_BT} = \frac{1}{aN^{1/2}}\int_0^L dz_0 g(z_0)\frac{f_e(z_0)}{k_BT} = \frac{\pi^2L^2}{8a^2N} \tag{1.121}$$

Although the predictions of SST are not particularly accurate under realistic experimental conditions, the value of simple analytical expressions cannot be overstated. Comparisons with SCFT in Section 1.6.6 will show that SST does properly capture the general qualitative trends.

Before moving on, we present a useful trick for evaluating f_e that avoids the difficult step of calculating $g(z_0)$. It derives from the fact that $E_\perp[z_\alpha; 0, 1] = 0$, which implies that for each and every individual chain, the stretching energy equals minus the field energy. Thus,

$$\frac{f_e(z_0)}{k_BT} = -\frac{1}{aN^{1/2}} \int_0^L dz\; w(z)\phi(z; z_0) \tag{1.122}$$

Substituting this into the integral of Eq. (1.121) gives

$$\frac{f_e}{k_BT} = -\frac{1}{L} \int_0^L dz\; w(z)\phi(z) = \frac{3\pi^2}{8a^2NL} \int_0^L dz\; z^2 \tag{1.123}$$

where we have made use of Eq. (1.118). The trivial integral of z^2 gives the previous result in Eq. (1.121). An important advantage of this formula is that it easily extends to brushes grafted to curved substrates, a fact that we will use in Section 1.8.4 for block copolymer morphologies.

1.6.2 Path-Integral Formalism for a Parabolic Potential

While the classical trajectory is the most probable, there are, nevertheless, nearby trajectories that make a significant contribution to the partition function. To calculate their effect, we expand about the lowest energy path in a Fourier sine series,

$$z_\alpha(s) = z_0 \cos(\pi s/2) + \sum_{n=1}^{\infty} z_n \sin(n\pi s) \tag{1.124}$$

that constrains the two ends of the chain to $z = 0$ and $z = z_0$. This allows the integrals to be performed analytically, giving

$$\frac{E_\perp[z_\alpha; 0, 1]}{k_BT} = \sum_{n=1}^{\infty} k_n z_n^2 \tag{1.125}$$

where

$$k_n = \frac{3\pi^2(4n^2 - 1)}{16a^2N} \tag{1.126}$$

As required, $k_n > 0$ for all n, implying that fluctuations about the classical path (i.e., $z_n \neq 0$) increase the energy of the chain, more so for the higher harmonics.

Now we can evaluate the partition function, integrating over all possible paths, or equivalently all possible amplitudes, z_n, of each harmonic, n. The result is

$$q(0, z_0, 1) \propto \prod_{n=1}^{\infty} \int_{-\infty}^{\infty} dz_n\; \exp(-k_n z_n^2) = \prod_{n=1}^{\infty} \sqrt{\frac{\pi}{k_n}} = \text{constant} \tag{1.127}$$

It might be disturbing that the product tends to zero as more factors are included, but there is in reality a cutoff at $n \approx M$, since sinusoidal fluctuations in the chain trajectory cease to make any sense when the wavelength becomes smaller than the actual monomer size. What

is important is that $q(0, z_0, 1)$ does not actually depend on z_0. So, just as in the classical treatment, the free energy of a chain in the parabolic potential is independent of its extension.

The main effect of the fluctuations is to broaden the single-segment distribution, $\rho(z; z_0, s)$, from the delta function predicted by SST in Eq. (1.115). With fluctuations, the distribution is defined as

$$\rho(z; z_0, s) = aN^{1/2} \int \left(\prod_{n=1}^{\infty} dz_n \; P_n(z_n) \right) \delta(z - z_\alpha(s)) \tag{1.128}$$

where

$$P_n(z_n) = \sqrt{\frac{k_n}{\pi}} \exp(-k_n z_n^2) \tag{1.129}$$

is the Boltzmann distribution for a n'th harmonic fluctuation of amplitude, z_n. Using the integral representation,

$$\delta(x) = \frac{1}{2\pi} \int_{-\infty}^{\infty} dk \; \exp(ikx) \tag{1.130}$$

of the Dirac delta function, the single-segment distribution can be rewritten as

$$\rho(z; z_0, s) = \frac{aN^{1/2}}{2\pi} \int dk \exp(ik(z - z_0 \cos(\pi s/2))) \times \left(\prod_{n=1}^{\infty} \sqrt{\frac{k_n}{\pi}} \int_{-\infty}^{\infty} dz_n \exp(-k_n z_n^2 - ikz_n \sin(n\pi s)) \right) \tag{1.131}$$

This allows us to integrate over z_n, which leads to the expression,

$$\rho(z; z_0, s) = \frac{aN^{1/2}}{2\pi} \int dk \exp \left[ik(z - z_0 \cos(\pi s/2)) - \frac{k^2}{4} \sum_{n=1}^{\infty} \frac{\sin^2(n\pi s)}{k_n} \right] \tag{1.132}$$

The summation can then be eliminated using the Fourier series expansion,

$$|\sin(\pi s)| = \frac{2}{\pi} - \frac{4}{\pi} \sum_{n=1}^{\infty} \frac{\cos(n2\pi s)}{4n^2 - 1} = \frac{8}{\pi} \sum_{n=1}^{\infty} \frac{\sin^2(n\pi s)}{4n^2 - 1} \tag{1.133}$$

With that gone, the final integration over k gives the relatively simple result,

$$\rho(z; z_0, s) = \left(\frac{3}{2\sin(\pi s)} \right)^{1/2} \exp \left(-\frac{3\pi [z - z_0 \cos(\pi s/2)]^2}{2a^2 N \sin(\pi s)} \right) \tag{1.134}$$

Hence, the chain fluctuations transform the delta function distributions, Eq. (1.115), predicted by SST into Gaussian distributions centered about the classical trajectory with a standard deviation (i.e., width) of $\sqrt{a^2 N \sin(\pi s)/3\pi}$. The total concentration of the chain, $\phi(z; z_0)$, has to be performed numerically, but that is a relatively trivial calculation. Figure 1.6 shows the result for several different extensions compared with the SST prediction from Eq. (1.117).

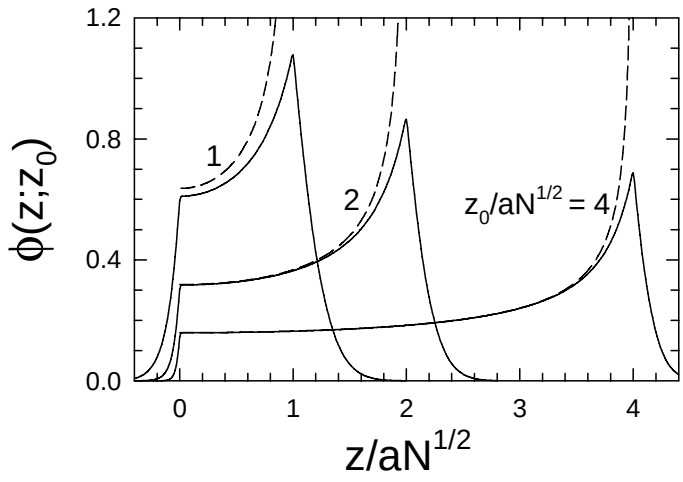

Figure 1.6: Segment distributions, $\phi(z; z_0)$, of polymers extended to various $z = z_0$ in the parabolic potential, Eq. (1.113). The dashed curves denote the distributions, Eq. (1.117), of the classical paths.

The strong-stretching approximation is inaccurate until $z_0/aN^{1/2} \gtrsim 1$, and even then it is rather poor for $z \approx z_0$. Of course this should not be surprising, as there is relatively little tension at the free end of the chain.

Now we evaluate the average elastic energy, $f_e(z_0)$, of a fluctuating chain extended to $z = z_0$. This is obtained by taking the free energy of a chain in the parabolic potential and subtracting off the average field energy. In mathematical terms,

$$\frac{f_e(z_0)}{k_BT} = -\ln q(0, z_0, 1) - \int dz\, w(z)\phi(z; z_0) \tag{1.135}$$

Although there is no analytical formula for $\phi(z; z_0)$, Eq. (1.116) allows the field energy to be expressed as

$$\int_0^1 ds \int_0^L dz\, w(z)\rho(z; z_0, s) = -\frac{3\pi^2 z_0^2}{16a^2N} - \frac{1}{4} \tag{1.136}$$

which can be evaluated by integrating first over z and then s. Therefore, the entropic free energy of the chain is

$$\frac{f_e(z_0)}{k_BT} = \frac{3\pi^2 z_0^2}{16a^2N} + \text{constant} \tag{1.137}$$

which is precisely the same as predicted by SST, Eq. (1.120), apart from the additive constant. The unknown constant appears because we are unable to specify the proportionality constant in Eq. (1.127), which in turn is because the coarse-graining procedure prevents us from knowing the absolute entropy of the chain; the best we can do is calculate relative changes in entropy.

1.6.3 Diffusion Equation for a Parabolic Potential

In Section 1.2, we established that the path-integral definition of the partition function is equivalent to the one based on the diffusion equation, just as Feynman's path-integral formalism of quantum mechanics coincides with Schrödinger's differential equation. As in quantum mechanics, the differential equation approach is generally the more practical method of calculating $q(z, z_0, s)$. Here, we demonstrate that it indeed gives identical results to those obtained in the previous section, where the path-integral approach was used.

Normally the diffusion Eq. (1.24) has to be solved numerically, but there already exists a known analytical solution for parabolic potentials (Merzbacher 1970). In fact, it was originally derived for the wavefunction of a simple harmonic oscillator; once again, we benefit from the analogy with quantum mechanics. Transforming the quantum mechanical wavefunction in Merzbacher (1970), according to Eqs. (1.50)-(1.56) for the parabolic potential in Eq. (1.113), gives

$$q(z, z_0, s) = \left(\frac{3}{4\sin(\pi s/2)}\right)^{1/2} \exp\left(-\frac{3\pi[(z^2+z_0^2)\cos(\pi s/2) - 2zz_0]}{4a^2N\sin(\pi s/2)}\right) \quad (1.138)$$

Although the derivation of this expression is complicated, it is relatively trivial to confirm that it is in fact the proper solution to Eq. (1.24) for the initial condition, $q(z, z_0, 0) = aN^{1/2}\delta(z - z_0)$.

Substituting $z = 0$ and $s = 1$ into Eq. (1.138), we find that $q(0, z_0, 1) = \sqrt{3/4}$, consistent with the path-integral calculation in Eq. (1.127). In terms of the partition function, the distribution of the sN'th segment is given by

$$\rho(z; z_0; s) = \frac{q(0, z, 1-s)q(z, z_0, s)}{q(0, z, 1)} \quad (1.139)$$

The derivation is essentially the same as that for Eq. (1.31). Inserting Eq. (1.138) and simplifying with some basic trigonometric identities gives the identical expression to that in Eq. (1.134), as required by the equivalence of the two approaches. Given this, the remaining results of the preceding section follow. One slight difference is that we now obtain a specific value for the unknown constant in Eq. (1.137), because the initial condition for $q(z, z_0, s)$, in effect, selects a proportionality constant for Eq. (1.127), but not one with any physical significance. Nevertheless, this provides us with a standard reference by which to compare calculations.

1.6.4 Self-Consistent Field Theory (SCFT) for a Brush

The parabolic potential used up to now is only approximate. The argument for it assumes that the tension at the free chain-end is zero, but there is in fact a small entropic force that acts to broaden the end-segment distribution, $g(z_0)$ (Matsen 2002b). Here, the self-consistent field theory (SCFT) is described for determining the field in a more rigorous manner. The theory starts with the partition function for the entire system, which is written as

$$Z \propto \int \left(\prod_{\alpha=1}^{n} \tilde{\mathcal{D}}\mathbf{r}_\alpha \delta(z_\alpha(1) - \epsilon)\right) \delta[1 - \hat{\phi}] \quad (1.140)$$

where the tildes, $\tilde{\mathcal{D}}\mathbf{r}_\alpha \equiv \mathcal{D}\mathbf{r}_\alpha P[\mathbf{r}_\alpha]$, denote that the functional integrals are weighted by

$$P[\mathbf{r}_\alpha] = \exp\left(-\frac{3}{2a^2N}\int_0^1 ds|\mathbf{r}'_\alpha(s)|^2\right) \tag{1.141}$$

so as to account for the internal entropy of each coarse-grained segment. The functional integrals over each $\mathbf{r}_\alpha(s)$ are, in principle, restricted to the volume of the system, $\mathcal{V} = \mathcal{A}L$. To ensure that the chains are properly grafted to the substrate, there are Dirac delta functions constraining the $s = 1$ end of each chain to $z = \epsilon$; we will eventually take the limit $\epsilon \to 0$. Furthermore, there is a Dirac delta functional that constrains the overall concentration, $\hat{\phi}(\mathbf{r})$, to be uniform over all $\mathbf{r} \in \mathcal{V}$.

Although the expression for Z is inherently simple, its evaluation is far from trivial. Progress is made by first replacing the delta functional by the integral representation,

$$\delta[1-\hat{\phi}] \propto \int \mathcal{D}W \exp\left(\frac{\rho_0}{N}\int d\mathbf{r}\, W(\mathbf{r})[1-\hat{\phi}(\mathbf{r})]\right) \tag{1.142}$$

This expression is equivalent to Eq. (1.335) derived in the Appendix, but with $k(x)$ substituted by $-i\rho_0 W(\mathbf{r})/N$. The constants, ρ_0 and N, have no effect on the limits of integration, but the i implies that $W(\mathbf{r})$ must be integrated in the complex plane along the imaginary axis. Inserting Eq. (1.142) into Eq. (1.140) and substituting $\hat{\phi}(\mathbf{r})$ by Eqs. (1.13) and (1.108) allows the integration over the chain trajectories to be performed. This results in the revised expression,

$$Z \propto \int \mathcal{D}W\, (\mathcal{Q}[W])^n \exp\left(\frac{\rho_0}{N}\int d\mathbf{r}\, W(\mathbf{r})\right) \tag{1.143}$$

where

$$\mathcal{Q}[W] \propto \int \tilde{\mathcal{D}}\mathbf{r}_\alpha \exp\left(-\int_0^1 ds\, W(\mathbf{r}_\alpha(s))\right)\delta(z_\alpha(1)-\epsilon) \tag{1.144}$$

is the partition function of a single polymer in the external field, $W(\mathbf{r})$. For convenience, the partition function of the system is reexpressed as

$$Z \propto \int \mathcal{D}W \exp\left(-\frac{F[W]}{k_BT}\right) \tag{1.145}$$

where

$$\frac{F[W]}{nk_BT} \equiv -\ln\left(\frac{\mathcal{Q}[W]}{\mathcal{A}aN^{1/2}}\right) - \frac{1}{\mathcal{V}}\int d\mathbf{r}\, W(\mathbf{r}) \tag{1.146}$$

There are a couple of subtle points that need to be mentioned. Firstly, the present calculation of Z allows the grafted ends to move freely in the $z = \epsilon$ plane, when actually they are grafted to particular spots on the substrate. As long as the chains are densely grafted, the only real consequence of treating the ends as a two-dimensional gas is that $\mathcal{Q}[W]$ becomes proportional to $\mathcal{A}$, the area available to each chain end. To correct for this, the $\mathcal{Q}[W]$ in Eq.

(1.146) is divided by $\mathcal{A}$, which is necessary for $F[W]$ to be a proper extensive quantity that scales with the size of the system. Alternatively, we could imagine that the chain ends are free to move, but then the molecules would become indistinguishable and Z would have to be divided by a factor of $n!$ to avoid the Gibbs paradox (Reif 1965). Either way, we arrive at the same expression for $F[W]$ apart from additive constants. That bring us to the second point that additive constants to $F[W]$ are of no consequence, since they can be absorbed into the proportionality constant omitted in Eq. (1.145). This fact has been used to insert an extra factor of $aN^{1/2}$ into Eq. (1.146) to make the argument of the logarithm dimensionless.

Even though $W(\mathbf{r})$ takes on imaginary values, $\mathcal{Q}[W]$ is solved by the exact same methods derived in Section 1.2, and thus $F[W]$ is readily computed. However, the functional integral in Eq. (1.145) cannot be performed exactly. To proceed further, we use the fact that $F[W]$ is an analytic functional, which means that the path of integration can be deformed without altering the integral. A standard trick to solve such integrals, the method of steepest descent (Carrier et al. 1966), is to deform the path from the imaginary axis to one that passes through a point where

$$\frac{\mathcal{D}F[W]}{\mathcal{D}W(\mathbf{r})} = 0 \tag{1.147}$$

in a direction such that the imaginary part of $F[W]$ remains constant. At such a point, the real part of $F[W]$ has a saddle shape, and consequently it is denoted as a *saddle* point . Changing the path of integration in this way concentrates the non-zero contribution of the integral to the neighborhood of the saddle point, allowing for a convenient expansion of which the first term gives

$$Z \approx \exp\left(-\frac{F[w]}{k_B T}\right) \tag{1.148}$$

where $w(\mathbf{r})$ is the solution to Eq. (1.147). Thus, $F[w]$ becomes the SCFT approximation to the free energy of the system. It follows from the functional differentiation in Eq. (1.147), that $w(\mathbf{r})$ must be chosen such that

$$\phi(\mathbf{r}) = 1 \tag{1.149}$$

where

$$\phi(\mathbf{r}) \equiv -\mathcal{V}\frac{\mathcal{D}\ln(\mathcal{Q}[w])}{\mathcal{D}w(\mathbf{r})} \tag{1.150}$$

is the segment concentration of n polymers in the external field, $w(\mathbf{r})$; see Eq. (1.32).

The quantity, $\phi(\mathbf{r})$, can also be identified as the SCFT approximation for $\left\langle \hat{\phi}(\mathbf{r}) \right\rangle$, but the explanation for this is often glossed over. It is justified by starting with the formal definition,

$$\left\langle \hat{\phi}(\mathbf{r}) \right\rangle \equiv \frac{1}{Z}\int \left(\prod_{\alpha=1}^{n} \tilde{\mathcal{D}}\mathbf{r}_\alpha \delta(z_\alpha(1) - \epsilon) \right) \hat{\phi}(\mathbf{r}) \delta[1 - \hat{\phi}] \tag{1.151}$$

where here Z is evaluated with the missing proportionality constant set to one. Of course, the Dirac delta functional implies that $\left\langle \hat{\phi}(\mathbf{r}) \right\rangle = 1$, but let us instead evaluate it in the manner of SCFT. With steps equivalent to those that lead to Eq. (1.145), we arrive at

$$\left\langle \hat{\phi}(\mathbf{r}) \right\rangle = \frac{1}{Z} \int \mathcal{D}W \phi(\mathbf{r}) \exp\left(-\frac{F[W]}{k_B T} \right) \tag{1.152}$$

Here, $\phi(\mathbf{r})$ is the concentration of n polymers subjected to the fluctuating field, $W(\mathbf{r})$, but since the integrand is dominated by $W(\mathbf{r}) \approx w(\mathbf{r})$, the concentration can be evaluated at the saddle point. This allows $\phi(\mathbf{r})$ to be moved outside the functional integration, leading immediately to our intended identity,

$$\left\langle \hat{\phi}(\mathbf{r}) \right\rangle \approx \frac{\phi(\mathbf{r})}{Z} \int \mathcal{D}W \exp\left(-\frac{F[W]}{k_B T} \right) = \phi(\mathbf{r}) \tag{1.153}$$

With the saddle-point approximation, the calculation now becomes tractable. The partition function for a chain in the field, $w(z)$, with its $s = 1$ end fixed at $z = \epsilon$ is

$$\frac{\mathcal{Q}[w]}{\mathcal{V}} = \frac{1}{L} \int_0^L dz \; q(z,s) q^\dagger(z,s) \tag{1.154}$$

where the integral can be evaluated with any $0 \leq s \leq 1$. The partial partition function, $q(z,s)$, is obtained by solving the diffusion Eq. (1.24) with the initial condition, $q(z,0) = 1$, and similarly the complementary function, $q^\dagger(z,s)$, is calculated with Eq. (1.28), subject to $q^\dagger(z,1) = aN^{1/2}\delta(z-\epsilon)$. These quantities also provide the concentration,

$$\phi(z) = \frac{\mathcal{V}}{\mathcal{Q}[w]} \int_0^1 ds \; q(z,s) q^\dagger(z,s) \tag{1.155}$$

which must be equated to one, by an appropriate adjustment of the field, $w(z)$. Once the field is determined self-consistently, the free energy of the brush, $F[w]$, can be evaluated using Eq. (1.146).

1.6.5 Boundary Conditions

In the bulk region of a melt, the long-range attractive interactions favoring a high density are balanced against short-range hard-core interactions to produce a more or less uniform segment concentration, ρ_0. The details of this mechanism are easily avoided by invoking the incompressibility assumption, $\hat{\phi}(\mathbf{r}) = 1$. This is no longer valid near the substrate ($z = 0$) nor the air interface ($z = L$). At any surface, the dimensionless concentration, $\hat{\phi}(\mathbf{r})$, must drop to zero. Although the decay in concentration is generally very sharp, it cannot occur as a true step function. Instead, there must be a continuous surface profile, $\phi_s(z)$, that switches from 1 to 0 over a narrow region next to the surface.

The calculation of $\phi_s(z)$ requires an involved treatment that takes a detailed account of the molecular interactions. (Although we will be explicitly referring to the $z = 0$ surface, everything we say applies equally to the $z = L$ surface.) In a proper treatment, the partial

partition functions would be solved under the boundary conditions, $q(0,s) = q^\dagger(0,s) = 0$, which prevents the polymers from crossing the $z = 0$ plane and ensures that $\phi_s(z) \to 0$ as $z \to 0$. For discussion purposes, we will assume that the profile is not so sharp as to invalidate our coarse-grained model. It will certainly be sharp enough for the ground-state-dominance approximation to hold, which implies that the surface field is given by

$$w_s(z) = \frac{a^2 N}{6} \frac{\nabla^2 \sqrt{\phi_s(z)}}{\sqrt{\phi_s(z)}} \tag{1.156}$$

However, one further relation between $w_s(z)$ and $\phi_s(z)$ is required in order to solve for the surface profile. This is where the details of the molecular interactions must enter.

Provided that we are not concerned with knowing the details of the surface, such as $\phi_s(z)$ and the resulting surface tension, it is possible to proceed without a full treatment of the surface profile. This involves implementing the alternative boundary conditions,

$$\frac{\partial}{\partial z} q(0,s) = \frac{\partial}{\partial z} q^\dagger(0,s) = 0 \tag{1.157}$$

and solving the SCFT for $w(z)$ ignoring the deviation from $\phi(z) = 1$ at the surface. The full solution would only differ in the narrow region next to the substrate where $\phi_s(z) < 1$. More specifically, if we were given $\phi_s(z)$, the proper solution would be obtained by making the substitutions,

$$q(z,s) \Rightarrow q(z,s)\sqrt{\phi_s(z)} \tag{1.158}$$

$$q^\dagger(z,s) \Rightarrow q^\dagger(z,s)\sqrt{\phi_s(z)} \tag{1.159}$$

$$w(z) \Rightarrow w(z) + w_s(z) \tag{1.160}$$

The added factor of $\sqrt{\phi_s(z)}$ would restore the proper boundary condition for the partial partition functions, and would transform the concentration profile from $\phi(z) = 1$ to $\phi(z) = \phi_s(z)$. One can also confirm that the transformation in the field is exactly as required for the transformed partition functions to satisfy the diffusion Eqs. (1.24) and (1.28); the proof of this requires that the pretransformed partition functions satisfy

$$\left[\frac{\partial}{\partial z} q(z,s)\right]\left[\frac{\partial}{\partial z}\sqrt{\phi_s(z)}\right] = \left[\frac{\partial}{\partial z} q^\dagger(z,s)\right]\left[\frac{\partial}{\partial z}\sqrt{\phi_s(z)}\right] = 0 \tag{1.161}$$

Indeed, it is safe to assume that the boundary conditions in Eq. (1.157) extend over the narrow region where $\phi_s(z)$ has a nonzero gradient.

For most problems such as the brush, we simply assume that there is no variation in the profile, $\phi_s(z)$, of each surface, rendering them as inert features that conveniently decouple from the behavior of the remaining system. Thus, we can continue to ignore the details of the molecular interactions and solve the field subject to the incompressibility condition, $\phi(z) = 1$, with the partial partition functions satisfying reflecting boundary conditions, Eq. (1.157), at $z = 0$ and $z = L$.

For the case of the polymer brush, there is still one more issue to deal with at the $z = 0$ substrate. The grafting of the chain ends in a perfect plane, which for the moment is at $z = \epsilon$, produces a delta function in the field (Likhtman and Semenov 2000). Our intention is to

incorporate this singularity into the boundary condition, restoring $w(z)$ to a continuous, finite function. We must, however, begin with the true field,

$$w_t(z) = \frac{\beta a^2 N}{6}\delta(z-\epsilon) + w(z) \tag{1.162}$$

containing the singularity at a small infinitesimal distance, ϵ, from the substrate. The diffusion Eq. (1.24) requires the delta function in $w_t(z)$ to be balanced by an infinity in $\nabla^2 q(\epsilon, s)$. In other words, the delta function produces a sharp kink in $\frac{\partial}{\partial z}q(z,s)$ at $z=\epsilon$, and similarly in $\frac{\partial}{\partial z}q^\dagger(z,s)$. The strength of the kink is determined by integrating the diffusion equation from $z=0$ to 2ϵ, which gives

$$\frac{a^2 N}{6}\left[\frac{\partial}{\partial z}q(2\epsilon,s) - \frac{\partial}{\partial z}q(0,s)\right] - \frac{\beta a^2 N}{6}q(\epsilon,s) \approx 0 \tag{1.163}$$

Our original reflecting boundary condition implies that $\frac{\partial}{\partial z}q_z(0,s) = 0$. Dropping this term from Eq. (1.163) and then taking the limit $\epsilon \to 0$ yields the new boundary condition,

$$\frac{\partial}{\partial z}q(0,s) = \beta q(0,s) \tag{1.164}$$

Naturally, the complementary partition function, $q^\dagger(z,s)$, satisfies the same boundary condition at $z=0$. The constant β is determined by the requirement that $w(z)$ does not develop a delta function at $z=0$.

1.6.6 Spectral Solution to SCFT

There are two main ways to solve the SCFT; one is a direct real-space method (Matsen 2004), where the diffusion equations are solved using finite differences for the derivatives (the Crank-Nicolson algorithm), and the other involves a spectral method (Matsen and Schick 1994a) much like that discussed in Section 1.5.1. The spectral method is particularly efficient for lower grafting densities, while the real-space one is better suited to thick brushes. Note that there are also semi-spectral algorithms (Rasmussen and Kalosakas 2002) that combine the advantages of the two methods. Here, we demonstrate the spectral method.

Since the field is unknown, the functional expansions will be performed in terms of Laplacian eigenfunctions, $f_i(z)$, defined by

$$\nabla^2 f_i(z) = -\frac{\lambda_i}{L^2}f_i(z) \tag{1.165}$$

subject to the boundary conditions, $f_i'(0) = \beta f_i(0)$ and $f_i'(L) = 0$. Note that the L^2 in Eq. (1.165) has been included so that λ_i becomes dimensionless. The solution to this eigenvalue problem is

$$f_i(z) = C_i \cos\left(\sqrt{\lambda_i}(1-z/L)\right) \tag{1.166}$$

where the boundary conditions require

$$\sqrt{\lambda_i}\tan\left(\sqrt{\lambda_i}\right) = \beta L \tag{1.167}$$

With the normalization constant set to

$$C_i = \sqrt{\frac{4\sqrt{\lambda_i}}{2\sqrt{\lambda_i} + \sin\left(2\sqrt{\lambda_i}\right)}} \tag{1.168}$$

the basis functions obey the orthonormal condition in Eq. (1.60). Once the basis functions are determined, there are a couple of useful quantities to calculate. The first is the symmetric tensor,

$$\Gamma_{ijk} \equiv \frac{1}{L}\int dz f_i(z) f_j(z) f_k(z) \tag{1.169}$$

and the second is the set of coefficients for the identity function,

$$\mathcal{I}_i \equiv \frac{1}{L}\int_0^L dz f_i(z) = C_i \frac{\sin\left(\sqrt{\lambda_i}\right)}{\sqrt{\lambda_i}} \tag{1.170}$$

defined such that $\sum_i \mathcal{I}_i f_i(z) = 1$.

With the preamble complete, we are now ready to solve for the partial partition function. The procedure is slightly more involved than in Section 1.5.1, because the field is now omitted from Eq. (1.165), but that is the price we pay to have simple basis functions. Nevertheless, the procedure is much the same. The expansions, $q(z,s) = \sum_i q_i(s) f_i(z)$ and $w(z) = \sum_k w_k f_k(z)$, are first inserted into the diffusion Eq. (1.24), giving

$$\sum_i \frac{dq_i(s)}{ds} f_i(z) = -\frac{a^2 N}{6L^2}\sum_i \lambda_i q_i(s) f_i(z) - \sum_{ik} w_k q_i(s) f_i(z) f_k(z) \tag{1.171}$$

By multiplying through by $f_j(z)$, integrating over $\mathbf{r}$, and using the orthonormal condition, this can be rewritten as a system of first-order linear ordinary differential equations,

$$\frac{d}{ds} q_i(s) = \sum_j A_{ij} q_j(s) \tag{1.172}$$

subject to the initial conditions, $q_i(0) = \mathcal{I}_i$. The coefficients of the matrix, $\mathbf{A}$, are given by

$$A_{ij} \equiv -\frac{\lambda_i a^2 N}{6L^2}\delta_{ij} - \sum_k w_k \Gamma_{ijk} \tag{1.173}$$

Note that the boundary conditions on $q(z,s)$ are already accounted for by those on $f_i(z)$.

The solution to Eq. (1.172) is simply

$$q_i(s) = \sum_j T_{ij}(s) q_j(0) \tag{1.174}$$

where $\mathbf{T}(s) \equiv \exp(\mathbf{A}s)$ is referred to as a transfer matrix. To evaluate it, we perform a matrix diagonalization

$$\mathbf{A} = \mathbf{U}\mathbf{D}\mathbf{U}^{-1} \tag{1.175}$$

where the elements of the diagonal matrix, $d_k \equiv D_{kk}$, are the eigenvalues of $\mathbf{A}$ and the respective columns of $\mathbf{U}$ are the corresponding normalized eigenvectors. Since $\mathbf{A}$ is symmetric, all the eigenvalues will be real and $\mathbf{U}^{-1} = \mathbf{U}^T$. We can then express $\mathbf{T}(s) = \mathbf{U}\exp(\mathbf{D}s)\mathbf{U}^T$, from which it follows that

$$T_{ij}(s) = \sum_k \exp(sd_k)U_{ik}U_{jk} \tag{1.176}$$

Similarly, the solution for the complementary function, $q^\dagger(z,s) \equiv \sum_i q_i^\dagger(s)f_i(z)$, is given by

$$q_i^\dagger(s) = \sum_j T_{ij}(1-s)q_j^\dagger(1) \tag{1.177}$$

where

$$q_i^\dagger(1) = \frac{1}{L}\int_0^L dz q^\dagger(z,1)f_i(z) = C_i\cos\left(\sqrt{\lambda_i}\right)\frac{aN^{1/2}}{L} \tag{1.178}$$

This result is obtained by first integrating with $q^\dagger(z,1) = aN^{1/2}\delta(z-\epsilon)$, and then taking the limit, $\epsilon \to 0$. Once the partial partition functions are evaluated, the partition function for the entire chain is obtained by

$$\frac{\mathcal{Q}[w]}{\mathcal{V}} = \sum_i q_i(s)q_i^\dagger(s) = \sum_i \exp(d_i)\bar{q}_i(0)\bar{q}_i^\dagger(1) \tag{1.179}$$

where we have made the convenient definitions, $\bar{q}_i(0) \equiv \sum_j q_j(0)U_{ji}$ and $\bar{q}_i^\dagger(1) \equiv \sum_j q_j^\dagger(1)U_{ji}$.

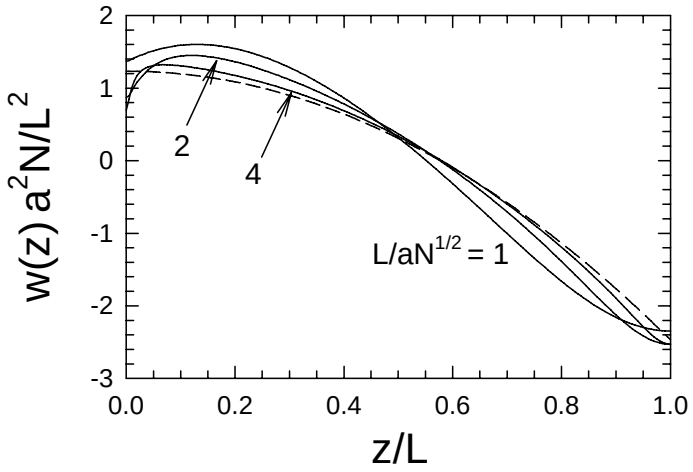

Figure 1.7: Self-consistent field, $w(z)$, plotted for several brush thicknesses, L. The dashed curve denotes the SST prediction in Eq. (1.113), shifted vertically such that its average is zero.

The coefficients of the average polymer concentration can be expressed as

$$\phi_i = \frac{\mathcal{V}}{\mathcal{Q}[w]} \sum_{jk} I_{jk} \Gamma_{ijk} \tag{1.180}$$

where the components of the matrix, **I**, are defined as

$$I_{jk} \equiv \int_0^1 ds\, q_j(s) q_k^\dagger(s) \tag{1.181}$$

$$= \sum_{m,n} \left[\frac{\exp(d_m) - \exp(d_n)}{d_m - d_n} \right] U_{jm} U_{kn} \bar{q}_m(0) \bar{q}_n^\dagger(1) \tag{1.182}$$

Note that in the instances where $d_m = d_n$, the factor in the square brackets reduces to $\exp(d_m)$.

Given the formula to evaluate the segment concentration, the coefficients of the field, w_i, can now be adjusted to satisfy the incompressibility condition, $\phi(z) = 1$, which is expressed in terms of coefficients as

$$\phi_i = \mathcal{I}_i \tag{1.183}$$

In practice, the functional expansion has to be truncated at some value $i = M$, where M is chosen based on an acceptable error tolerance. In principle, the first $(M+1)$ components, w_i, would be adjusted to satisfy the first $(M+1)$ conditions for ϕ_i. However, Eqs. (1.183) are not completely independent, due to the fact that SCFT is not affected by an additive constant to $w(z)$; see the discussion at the end of Section 1.2. To rectify this problem, the first condition, $\phi_0 = \mathcal{I}_0$, can be replaced by

$$\sum_i \mathcal{I}_i w_i = 0 \tag{1.184}$$

which sets the spatial average of $w(z)$ to zero. Now the set of equations are independent, and they can be solved by standard numerical techniques. There are various techniques that can be used (Thompson et al. 2004); we generally use the Broyden algorithm, which is a quasi-Newton-Raphson method. This requires a reasonable initial guess for $w(z)$, but that can be provided by the SST estimate in Eq. (1.113). Figure 1.7 shows the field, $w(z)$, obtained from SCFT (solid curves) for several different brush thicknesses compared against the SST result (dashed curve) from Eq. (1.113). As expected, the SST prediction becomes increasingly accurate as $L \to \infty$.

We have glossed over the fact that β was introduced in order to prevent a delta function from developing in $w(z)$ at $z = 0$. The signature of a delta function is that the field coefficients, w_i, fail to converge to zero in the limit of large i. To prevent this, we could include the extra condition, $w_M = 0$, in our Broyden iterations and use it to determine β. The estimate, $\beta \approx 3L/a^2N$, by Likhtman and Semenov (2000) provides a suitable initial guess. In reality, this initial guess turns out to be very accurate, and since the spectral method can cope with a small delta function, we simply use the initial guess provided by Likhtman and Semenov (2000).

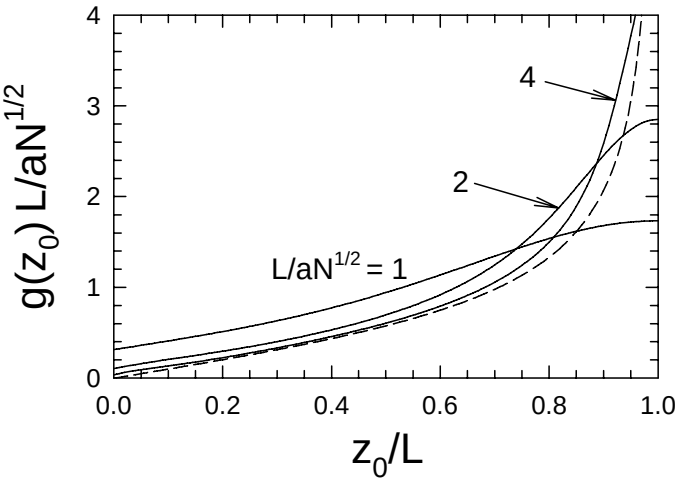

Figure 1.8: End-segment distribution, $g_0(z_0)$, calculated by SCFT for several brush thicknesses, L. The dashed curve denotes the SST prediction from Eq. (1.119).

Although the end-segment distribution function, $g(z_0)$, is not a direct by-product of SCFT, it is easily evaluated. The formula for it,

$$g(z_0) = \frac{\mathcal{V}}{\mathcal{Q}[w]} q^\dagger(z_0, 0) \tag{1.185}$$

is derived in the same manner as Eq. (1.155) for $\phi(z)$. Figure 1.8 shows the SCFT prediction for $g(z_0)$ (solid curves) calculated for several different brush thicknesses compared against the SST prediction (dashed curve) from Eq. (1.119). As with the field, SST becomes increasingly accurate as $L \to \infty$.

The free energy of the brush is given by

$$\frac{F}{nk_BT} = -\ln\left(\frac{\mathcal{Q}[w]}{\mathcal{A}aN^{1/2}}\right) - \frac{\beta a^2 N}{6L} \tag{1.186}$$

The second term comes from the delta function contribution to the true potential, $w_t(z)$, in Eq. (1.162), which was removed from $w(z)$ by the use of the boundary condition in Eq. (1.164). The resulting energy is plotted in Fig. 1.9. Included with a dotted curve is an approximation,

$$\frac{F}{nk_BT} \approx \frac{\pi^2 L^2}{8a^2 N} - \ln\left(\frac{\sqrt{3}L}{2aN^{1/2}}\right) + 0.1544 - 0.64\left(\frac{L}{aN^{1/2}}\right)^{-2/3} - 0.09\left(\frac{L}{aN^{1/2}}\right)^{-4/3} \tag{1.187}$$

based on a theoretical expansion by Likhtman and Semenov (2000). The two coefficients of 0.64 and 0.09 were obtained by a previous fit to SCFT (Matsen 2004) at $L/aN^{1/2} \gg 1$, but as Fig. 1.9 clearly shows, the fit remains accurate down to reasonably low values of L. Notice that the dominant term in Eq. (1.187) is precisely the SST prediction from Eq. (1.121).

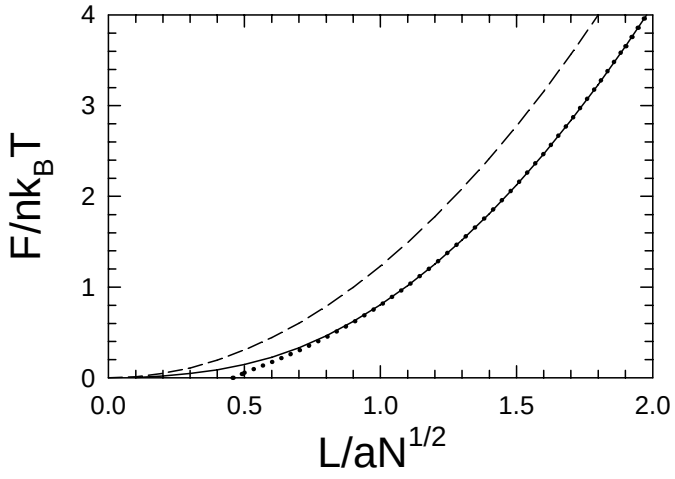

Figure 1.9: Free energy, F, per chain versus brush thickness, L, calculated by SCFT. The dashed curve shows the SST prediction from Eq. (1.121), and the dotted curve denotes the improved approximation in Eq. (1.187), which on this scale is indistinguishable from SCFT for $L/aN^{1/2} \gtrsim 1$.

1.7 Polymer Blends

The polymer brush treated in the previous section provided a good illustration of how SCFT works. The procedure began with an expression for the partition function of the system, Z, expressed in terms of functional integrals over the path of each molecule. An integral representation was used to replace a Dirac delta functional, so that the functional integrations over each polymer could be performed. However, this left a functional integral over a field, which could not be evaluated and required a saddle-point approximation. Although these basic steps remain common to all SCFT calculations, the simple brush misses out some common features of the more elaborate systems. Most notably, the brush contained only a single molecular species, which in turn was composed of only one monomer type. This section demonstrates the natural extension to multi-component systems.

Let us now consider a blend of n_A A-type homopolymers with n_B B-type homopolymers, and for simplicity assume that both species have the same degree of polymerization, N, and the same statistical segment length, a. The volume of the system is therefore $\mathcal{V} = nN/\rho_0$, where $n = n_A + n_B$ is the total number of molecules in the blend. (For convenience, we follow the standard convention of defining the A and B coarse-grained segments such that they each occupy the same volume, ρ_0^{-1}.) The volume fraction of A-type segments (i.e., composition of the blend) will be denoted by $\phi \equiv n_A N/\mathcal{V}\rho_0$. Again, all polymers are parameterized by s running from 0 to 1, and the configurations of A- and B-type polymers are specified by $\mathbf{r}_{A,\alpha}(s)$ and $\mathbf{r}_{B,\alpha}(s)$, respectively. Given this, the overall A-segment concentration can be

expressed as

$$\hat{\phi}_A(\mathbf{r}) = \frac{N}{\rho_0} \sum_{\alpha=1}^{n_A} \int_0^1 ds\ \delta(\mathbf{r} - \mathbf{r}_{A,\alpha}(s)) \tag{1.188}$$

with an analogous expression specifying the B-segment concentration, $\hat{\phi}_B(\mathbf{r})$.

With the inclusion of two chemically distinct segments, it is no longer possible to sidestep the issue of monomer-monomer interactions. For discussion purposes, assume that the interaction between two monomers, i and j, obeys a simple Lennard-Jones potential,

$$u(r_{ij}) = \epsilon \left[\left(\frac{\sigma}{r_{ij}} \right)^{12} - 2 \left(\frac{\sigma}{r_{ij}} \right)^{6} \right] \tag{1.189}$$

where r_{ij} is their separation. The incompressibility assumption

$$\hat{\phi}_A(\mathbf{r}) + \hat{\phi}_B(\mathbf{r}) = 1 \tag{1.190}$$

acts to maintain the spacing between neighboring monomers at the minimum of the potential energy, $r_{ij} = \sigma$. The detailed shape of the potential is therefore no longer needed; we can simply assume that the interaction energy is $-\epsilon$ between neighboring monomers and zero otherwise. In the brush system, all the interactions were the same and thus they added up to a constant energy that could be ignored, assuming the total number of monomer contacts remained more or less fixed. In the blend, however, we must account for the fact that the depth of the potential will differ between the A-A, A-B, and B-B contacts. Noting that the range of the monomer-monomer interactions, σ, is negligible on the coarse-grained scale, the interactions can be treated as contact energies and thus the internal energy can be expressed as

$$\begin{aligned} U \equiv & -\frac{N^2 \epsilon_{AA}}{2\rho_0^2} \sum_{\alpha,\beta} \int ds\ dt\ \delta(\mathbf{r}_{A,\alpha}(s) - \mathbf{r}_{A,\beta}(t)) - \\ & \frac{N^2 \epsilon_{AB}}{\rho_0^2} \sum_{\alpha,\beta} \int ds\ dt\ \delta(\mathbf{r}_{A,\alpha}(s) - \mathbf{r}_{B,\beta}(t)) - \\ & \frac{N^2 \epsilon_{BB}}{2\rho_0^2} \sum_{\alpha,\beta} \int ds\ dt\ \delta(\mathbf{r}_{B,\alpha}(s) - \mathbf{r}_{B,\beta}(t)) \end{aligned} \tag{1.191}$$

Using the incompressibility assumption, $\hat{\phi}_A(\mathbf{r}) + \hat{\phi}_B(\mathbf{r}) = 1$, this simplifies to

$$\frac{U[\hat{\phi}_A, \hat{\phi}_B]}{k_B T} = \chi \rho_0 \int d\mathbf{r}\ \hat{\phi}_A(\mathbf{r}) \hat{\phi}_B(\mathbf{r}) \tag{1.192}$$

where the interaction strengths are grouped together into a single dimensionless parameter,

$$\chi \equiv \frac{\epsilon_{AA} - 2\epsilon_{AB} + \epsilon_{BB}}{2 k_B T \rho_0} \tag{1.193}$$

Note that the value of χ is inversely proportional to the segment density, ρ_0, and thus is not an invariant quantity; one must be careful of this fact when referring to literature values of χ. Equation (1.192) is the simplest and by far most common expression for the interactions, but SCFT is perfectly capable of accommodating more elaborate treatments (Matsen 2002a), if so desired.

1.7.1 SCFT for a Polymer Blend

The partition function for a polymer blend is hardly any more involved than that for the polymer brush in Section 1.6.4. In this case, it becomes

$$Z \propto \frac{1}{n_A! n_B!} \int \prod_{\alpha=1}^{n_A} \tilde{\mathcal{D}}\mathbf{r}_{A,\alpha} \prod_{\beta=1}^{n_B} \tilde{\mathcal{D}}\mathbf{r}_{B,\beta} \exp\left(-\frac{U[\hat{\phi}_A, \hat{\phi}_B]}{k_B T}\right) \delta[1 - \hat{\phi}_A - \hat{\phi}_B] \quad (1.194)$$

As before, there is a functional integration over the configuration of each polymer and a Dirac delta functional is used to enforce the incompressibility condition. Of course, the delta functions constraining the chain ends are gone, and there is now a Boltzmann weight accounting for the energy of the segment interactions. Also present are factors of $n_A!$ and $n_B!$ to account for the indistinguishability of the A- and B-polymers, respectively.

This time, we start by inserting a functional integral over $\delta[\Phi_A - \hat{\phi}_A]$, allowing the operator, $\hat{\phi}_A(\mathbf{r})$, to be swapped with the ordinary function, $\Phi_A(\mathbf{r})$. This transforms $\delta[1 - \hat{\phi}_A - \hat{\phi}_B]$ into $\delta[1 - \Phi_A - \hat{\phi}_B]$, which, in turn, allows the exchange of $\hat{\phi}_B(\mathbf{r})$ with $1 - \Phi_A(\mathbf{r})$. The result of this manipulation is

$$Z \propto \frac{1}{n_A! n_B!} \int \mathcal{D}\Phi_A \prod_{\alpha=1}^{n_A} \tilde{\mathcal{D}}\mathbf{r}_{A,\alpha} \prod_{\beta=1}^{n_B} \tilde{\mathcal{D}}\mathbf{r}_{B,\beta} \exp\left(-\frac{U[\Phi_A, 1 - \Phi_A]}{k_B T}\right) \times$$
$$\delta[\Phi_A - \hat{\phi}_A] \delta[1 - \Phi_A - \hat{\phi}_B] \quad (1.195)$$

As with the brush, the two delta functionals are replaced with integral representations analogous to that in Eq. (1.142), which allows us to complete the integrals over the polymer configurations, leading to the result,

$$Z \propto \frac{1}{n_A! n_B!} \int \mathcal{D}\Phi_A \mathcal{D}W_A \mathcal{D}W_B \left(\frac{\rho_0}{N} \mathcal{Q}_A[W_A]\right)^{n_A} \left(\frac{\rho_0}{N} \mathcal{Q}_B[W_B]\right)^{n_B} \times$$
$$\exp\left(-\frac{U[\Phi_A, 1 - \Phi_A]}{k_B T} + \frac{\rho_0}{N} \int d\mathbf{r} [W_A \Phi_A + W_B (1 - \Phi_A)]\right) \quad (1.196)$$

where

$$\mathcal{Q}_\gamma[W_\gamma] \propto \int \tilde{\mathcal{D}}\mathbf{r}_{\gamma,\alpha} \exp\left(-\int_0^1 ds\, W_\gamma(\mathbf{r}_{\gamma,\alpha}(s))\right) \quad (1.197)$$

is the partition function of a single γ-type polymer in the external field, $W_\gamma(\mathbf{r})$. (For the purpose of future simplification, a factor of $(\rho_0/N)^n$ has been extracted from the unspecified proportionality constant in Eq. (1.196).) Next, the factorials are replaced by the usual Stirling approximations (e.g., $\ln(n_\gamma!) \approx n_\gamma \ln(n_\gamma) - n_\gamma$), giving

$$Z \propto \int \mathcal{D}\Phi_A \mathcal{D}W_A \mathcal{D}W_B \exp\left(-\frac{F[\Phi_A, W_A, W_B]}{k_B T}\right) \quad (1.198)$$

where

$$\frac{F}{nk_BT} = \phi\left[\ln\left(\frac{\phi\mathcal{V}}{\mathcal{Q}_A[W_A]}\right) - 1\right] + (1-\phi)\left[\ln\left(\frac{(1-\phi)\mathcal{V}}{\mathcal{Q}_B[W_B]}\right) - 1\right] + \frac{1}{\mathcal{V}}\int d\mathbf{r}[\chi N\Phi_A(1-\Phi_A) - W_A\Phi_A - W_B(1-\Phi_A)] \tag{1.199}$$

As before with the brush, all the steps above are exact. The partition functions, $\mathcal{Q}_A[W_A]$ and $\mathcal{Q}_B[W_B]$, can still be calculated by the method outlined in Section 1.2, and thus $F[\Phi_A, W_A, W_B]$ can be evaluated without difficulty. It is the functional integration of $\exp(-F/k_BT)$ in Eq. (1.198) that poses a problem. So once again, the saddle-point approximation is implemented, which requires us to locate the extremum denoted by the lower-case functions, ϕ_A, w_A, and w_B. Setting to zero the functional derivative of $F[\Phi_A, W_A, W_B]$ with respect to W_A gives the condition,

$$\phi_A(\mathbf{r}) = -\mathcal{V}\phi\frac{\mathcal{D}\ln(\mathcal{Q}_A[w_A])}{\mathcal{D}w_A(\mathbf{r})} \tag{1.200}$$

Equation (1.32) identifies $\phi_A(\mathbf{r})$ as the average concentration of n_A polymers in the external field, $w_A(\mathbf{r})$, which is evaluated by

$$\phi_A(\mathbf{r}) = -\frac{\mathcal{V}\phi}{\mathcal{Q}_A[w_A]}\int_0^1 ds\; q_A(\mathbf{r},s)q_A^\dagger(\mathbf{r},s) \tag{1.201}$$

where

$$\mathcal{Q}_A[w_A] = \int d\mathbf{r}\; q_A(\mathbf{r},s)q_A^\dagger(\mathbf{r},s) \tag{1.202}$$

Here, the partial partition functions, $q_A(\mathbf{r},s)$ and $q_A^\dagger(\mathbf{r},s)$, obey the previous diffusion Eqs. (1.24) and (1.28), but with the field, $w_A(\mathbf{r})$. Differentiation of $F[\Phi_A, W_A, W_B]$ with respect to W_B leads to the incompressibility requirement,

$$\phi_A(\mathbf{r}) + \phi_B(\mathbf{r}) = 1 \tag{1.203}$$

where

$$\phi_B(\mathbf{r}) \equiv -\mathcal{V}\phi\frac{\mathcal{D}\ln(\mathcal{Q}_B[w_B])}{\mathcal{D}w_B(\mathbf{r})} \tag{1.204}$$

is the average concentration of n_B polymers in the external field, $w_B(\mathbf{r})$, evaluated in the same manner as $\phi_A(\mathbf{r})$. Following arguments already presented in Section 1.6.4, $\phi_A(\mathbf{r})$ and $\phi_B(\mathbf{r})$ are the SCFT approximations for $\left\langle\hat{\phi}_A(\mathbf{r})\right\rangle$ and $\left\langle\hat{\phi}_B(\mathbf{r})\right\rangle$, respectively. The last remaining differentiation of $F[\Phi_A, W_A, W_B]$ with respect to Φ_A gives the self-consistent field condition,

$$w_A(\mathbf{r}) - w_B(\mathbf{r}) = \chi N(1 - 2\phi_A(\mathbf{r})) \tag{1.205}$$

In principle, the two Eqs. (1.203) and (1.205) should be enough to determine the two functions, $w_A(\mathbf{r})$ and $w_B(\mathbf{r})$, but this is not exactly the case. With similar arguments to those

at the end of Section 1.2, one can show that $F[\phi_A, w_A, w_B]$ is unaffected by an added constant to either $w_A(\mathbf{r})$ or $w_B(\mathbf{r})$. These degrees of freedom can be removed by fixing their spatial averages to $\bar{w}_A = \bar{w}_B = 0$, and adding an appropriate constant to Eq. (1.205) such that

$$w_A(\mathbf{r}) - w_B(\mathbf{r}) = 2\chi N(\phi - \phi_A(\mathbf{r})) \tag{1.206}$$

With this revised field equation, the SCFT approximation of the free energy, $F[\phi_A, w_A, w_B]$, given by Eq. (1.199) can be reexpressed as

$$\frac{F}{nk_BT} = \frac{F_h}{nk_BT} - \phi \ln\left(\frac{\mathcal{Q}_A[w_A]}{\mathcal{V}}\right) - (1-\phi)\ln\left(\frac{\mathcal{Q}_B[w_B]}{\mathcal{V}}\right) - \frac{\chi N}{\mathcal{V}}\int d\mathbf{r}(\phi_A(\mathbf{r}) - \phi)(\phi_B(\mathbf{r}) - 1 + \phi) \tag{1.207}$$

where

$$\frac{F_h}{nk_BT} = \phi[\ln\phi - 1] + (1-\phi)[\ln(1-\phi) - 1] + \chi N\phi(1-\phi) \tag{1.208}$$

1.7.2 Homogeneous Phases and Macrophase Separation

The simplest solution to the self-consistent field equations is that for uniform fields, $w_A(\mathbf{r}) = w_B(\mathbf{r}) = 0$, corresponding to a homogeneous mixture. In this case, the partition functions reduce to $\mathcal{Q}_A[w_A] = \mathcal{Q}_B[w_B] = \mathcal{V}$, and the segment concentrations simplify to $\phi_A(\mathbf{r}) = \phi$ and $\phi_B(\mathbf{r}) = 1 - \phi$. Inserting these results into Eq. (1.207), we find that $F = F_h$. Indeed, Eq. (1.208) is the well-known Flory-Huggins expression for the free energy of a homogeneous blend of composition, ϕ. Figure 1.10(a) shows the free energy curve for $\chi N = 3$. Notice that there is a region, between the two inflection points denoted by diamond symbols, where the free energy has negative curvature. This property implies that the system is unstable towards macrophase separation, where the melt splits into A- and B-rich phases occupying separate regions of the volume, $\mathcal{V}$.

To determine whether or not the blend will macrophase separate, we need an expression for the combined energy free, $F_s = F_h^{(1)} + F_h^{(2)}$, of two distinct phases of compositions, $\phi^{(1)}$ and $\phi^{(2)}$, respectively. If the blend is to macrophase separate, it has to obey some basic conservation rules. First, the number of molecules in the two phases, $n^{(1)}$ and $n^{(2)}$, must satisfy

$$n^{(1)} + n^{(2)} = n \tag{1.209}$$

and second, the number of A-type polymers in each phase must comply with

$$n^{(1)}\phi^{(1)} + n^{(2)}\phi^{(2)} = n\phi \tag{1.210}$$

These conservation laws imply that the fraction of molecules in phase (1) will be

$$\frac{n^{(1)}}{n} = \frac{\phi^{(2)} - \phi}{\phi^{(2)} - \phi^{(1)}} \tag{1.211}$$

Now we can rewrite the total energy, F_s, of a macrophase separated system as

$$\frac{F_s}{nk_BT} = \frac{F_h^{(2)}}{n^{(2)}k_BT} + \left(\frac{F_h^{(1)}}{n^{(1)}k_BT} - \frac{F_h^{(2)}}{n^{(2)}k_BT} \right) \frac{n^{(1)}}{n} \tag{1.212}$$

which is plotted in Fig. 1.10(a) for the example where $\phi^{(1)} = 0.3$ and $\phi^{(2)} = 0.6$. It is clear from the form of Eqs. (1.211) and (1.212) that F_s versus ϕ is simply a straight line extending from $F_s = F_h^{(1)}$ and $\phi = \phi^{(1)}$ to $F_s = F_h^{(2)}$ and $\phi = \phi^{(2)}$. Naturally, the line must terminate at $\phi^{(1)}$ and $\phi^{(2)}$ since the overall composition, ϕ, is a volume-average over two individual phases (i.e., $\phi^{(1)} \leq \phi \leq \phi^{(2)}$). In this particular example, the entire line, F_s, lies below the curve, F_h, and thus macrophase separation is preferred at all compositions, $0.3 < \phi < 0.6$. The volumes occupied by the two resulting phases would occur in the ratio,

$$\frac{n^{(1)}}{n^{(2)}} = \frac{\phi^{(2)} - \phi}{\phi - \phi^{(1)}} \tag{1.213}$$

which is known as the *lever rule*, on account of its graphical interpretation in terms of the two portions, $(\phi^{(2)} - \phi)$ and $(\phi - \phi^{(1)})$, of the straight line. Of course, the particular compositions, $\phi^{(1)} = 0.3$ and $\phi^{(2)} = 0.6$, do not represent the global free energy minimum.

The lowest possible energy that can be achieved by macrophase separation is determined by the double-tangent construction denoted with a dotted line in Fig. 1.10(a). At any ϕ along this line, the blend will ultimately macrophase separate into the compositions at the two ends of the line marked by solid triangles and referred to as *binodal* points. Near these binodal compositions, however, the system is metastable against macrophase separation and can exist in the single mixed state for a considerable time. This is because the positive curvature in F_h causes the free energy to initially increase as $\phi^{(1)}$ and $\phi^{(2)}$ depart from the average composition, ϕ. Only when $\phi^{(1)}$ and $\phi^{(2)}$ are sufficiently far apart does the system benefit from a reduction in free energy. The presence of this energy barrier requires the phase separation to proceed by the slow process of nucleation and growth. In contrast, there is no energy barrier at compositions between the *spinodal* points denoted by the solid diamonds, due to the fact that the curvature in the free energy is negative. In this instance, phase separation is relatively fast and occurs by a process referred to as spinodal decomposition.

In this symmetric case where both polymers are the same size, the double-tangent line is horizontal and thus the binodals occur at zero slope in the free energy, which works out to be

$$\chi N = \frac{1}{2\phi - 1} \ln \left(\frac{\phi}{1 - \phi} \right) \tag{1.214}$$

The spinodals occur when the second derivative is zero, which corresponds to

$$\chi N = \frac{1}{2\phi(1 - \phi)} \tag{1.215}$$

The phase diagram in Fig. 1.10(b) shows the binodals (solid curves) between which the system favors macrophase separation, and the spinodals (dotted curves) between which the separation is more or less immediate. Both sets of curves terminate at a critical point ($\chi N = 2$), below which the interaction strength is too weak to induce phase separation, regardless of the composition.

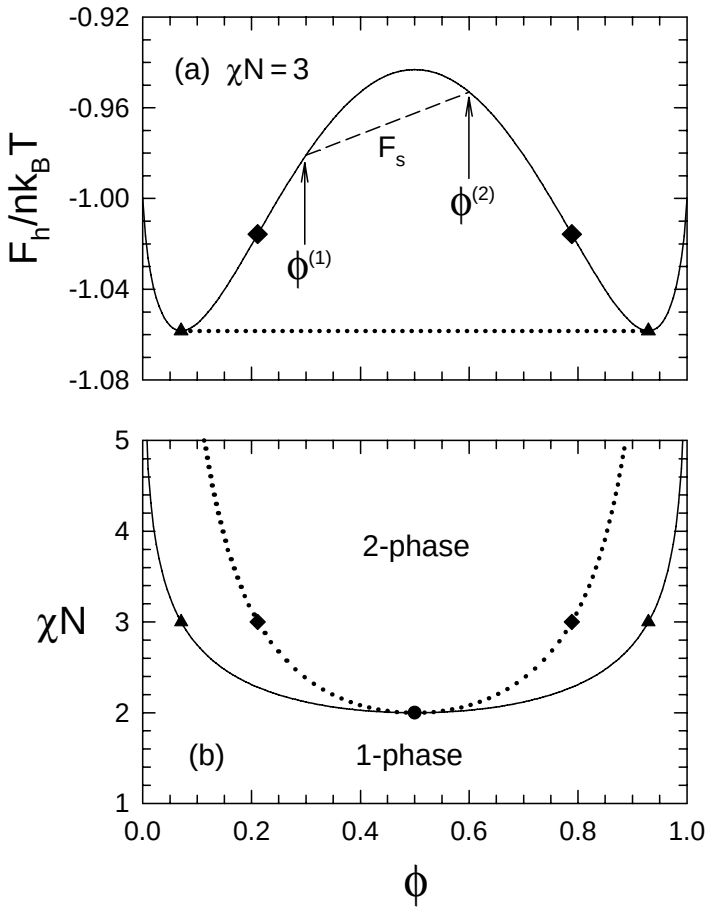

Figure 1.10: (a) Free energy, F_h, of a homogeneous blend as a function of composition, ϕ, calculated for $\chi N = 3$. The dashed line denotes the free energy, F_s, for a macrophase-separated blend with compositions, $\phi^{(1)} = 0.3$ and $\phi^{(2)} = 0.6$, and the dotted line is the double-tangent construction locating the binodal points denoted by triangles. The two diamonds denote spinodal points, where the curvature of the free energy curve switches sign. (b) Phase diagram showing the binodal (solid) and spinodal (dotted) curves as a function of χN. The triangular and diamond symbols correspond to those in (a), and the solid dot denotes a critical point.

1.7.3 Scattering Function for a Homogeneous Blend

A beam of radiation (e.g., x-rays or neutrons) will pass undeflected through a perfectly homogeneous blend, $\hat{\phi}_A(\mathbf{r}) = \phi$, assuming the wavelength, λ, is above the atomic resolution and that absorption is negligible. However, there are always thermal functuations that disturb the uniform composition, which in turn scatter the radiation by various angles, θ. To predict the

resulting pattern of radiation, $I(\theta)$, we must first calculate the free energy cost, $F[\Phi_A]$, of producing a specified composition fluctuation, $\hat{\phi}_A(\mathbf{r}) = \Phi_A(\mathbf{r})$. The fact that we will continue to implement mean-field theory implies that, in reality, the free energy we calculate will be for a fixed $\phi_A(\mathbf{r}) \equiv \left\langle \hat{\phi}_A(\mathbf{r}) \right\rangle$ as opposed to a fixed $\hat{\phi}_A(\mathbf{r})$; this limitation will be discussed further in Section 1.10.

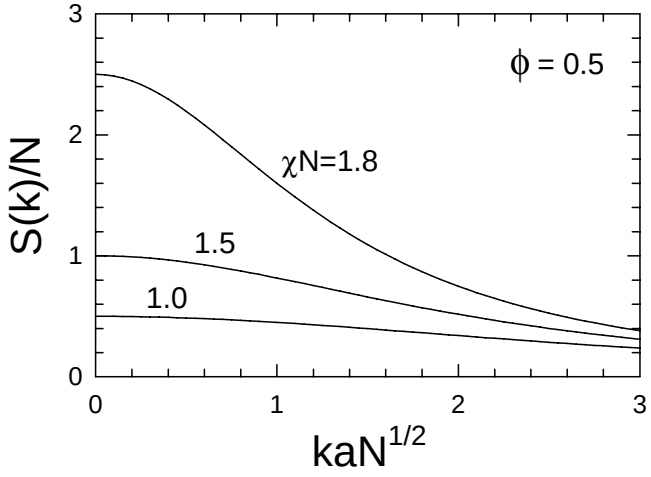

Figure 1.11: Scattering function, $S(\mathbf{k})$, for binary blends of symmetric composition, $\phi = 0.5$, plotted for several degrees of segregation, χN.

To perform the calculation, we use the Fourier representation developed in Section 1.5.4. In terms of the Fourier transforms of the composition, $\phi_A(\mathbf{k})$ and $\phi_B(\mathbf{k})$, the free energy is approximated by

$$\frac{F}{nk_BT} = \frac{F_h}{nk_BT} + \frac{1}{2\phi(2\pi)^3\mathcal{V}} \int_{\mathbf{k}\neq 0} d\mathbf{k} \frac{\phi_A(-\mathbf{k})\phi_A(\mathbf{k})}{g(x,1)} + \frac{1}{2(1-\phi)(2\pi)^3\mathcal{V}} \int_{\mathbf{k}\neq 0} d\mathbf{k} \frac{\phi_B(-\mathbf{k})\phi_B(\mathbf{k})}{g(x,1)} + \frac{\chi N}{(2\pi)^3\mathcal{V}} \int_{\mathbf{k}\neq 0} d\mathbf{k}\phi_A(-\mathbf{k})\phi_B(\mathbf{k}) \tag{1.216}$$

The first term is the free energy of a perfectly homogeneous state, Eq. (1.208), the following two integrals represent the loss in configurational entropy, Eq. (1.105), experienced by the A- and B-type polymers, and the final integral accounts for the increased number of A-B contacts, Eq. (1.192) transformed by Eq. (1.82). The incompressibility condition is enforced by setting, $\phi_B(\mathbf{k}) = -\phi_A(\mathbf{k})$, which simplifies the free energy to

$$\frac{F}{nk_BT} = \frac{F_h}{nk_BT} + \frac{N}{2(2\pi)^3\mathcal{V}} \int_{\mathbf{k}\neq 0} d\mathbf{k} S^{-1}(\mathbf{k})\phi_A(-\mathbf{k})\phi_A(\mathbf{k}) \tag{1.217}$$

where $S(\mathbf{k})$, referred to as the scattering function, is defined by

$$S^{-1}(\mathbf{k}) = \frac{1}{N\phi(1-\phi)g(k^2a^2N/6,1)} - 2\chi \tag{1.218}$$

The scattering function for a 50-50 blend is plotted in Fig. 1.11 at several values of χN within the one-phase region of the phase diagram in Fig. 1.10(b). The inverse of $S(\mathbf{k})$ determines the free energy cost of producing a compositional fluctuation of wavelength, $D = 2\pi/k$. In the one-phase region, $S^{-1}(\mathbf{k}) > 0$ for all $\mathbf{k}$, implying that all fluctuations cost energy and are thus suppressed. However, as the two-phase region is entered, $S^{-1}(\mathbf{k})$ becomes negative, starting with the longest wavelengths. For small $\mathbf{k}$,

$$S^{-1}(\mathbf{k}) \approx \frac{1 + \frac{1}{18}k^2a^2N}{N\phi(1-\phi)} - 2\chi \tag{1.219}$$

which implies that the blend becomes unstable to long-wavelength fluctuations at

$$\chi N = \frac{1}{2\phi(1-\phi)} \tag{1.220}$$

This is precisely the spinodal line, Eq. (1.215), calculated in the preceding section.

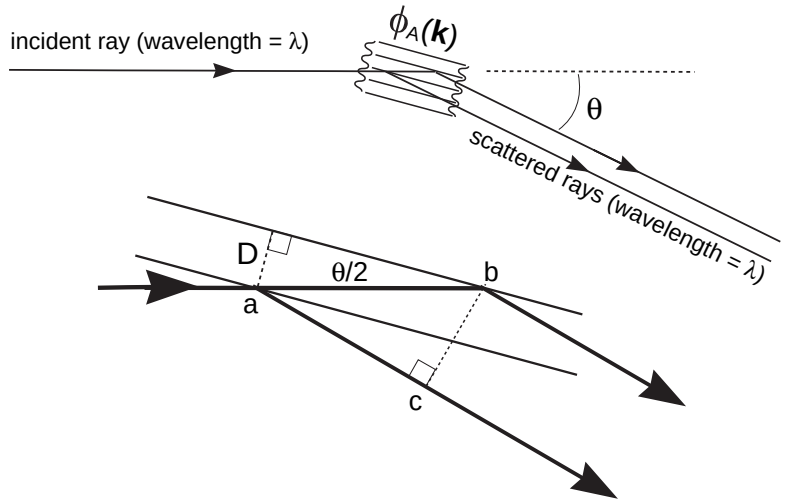

Figure 1.12: Diagram showing scattered rays of wavelength, λ, due to a composition fluctuation, $\phi_A(\mathbf{k})$, of period, $D \equiv 2\pi/k$. The sketch at the bottom shows the condition for a first-order Bragg reflection, where the path difference, $\overline{ab} - \overline{ac}$, equals one wavelength, λ.

The quantity, $S(\mathbf{k})$, is called the scattering function because of its direct relevance to the pattern, $I(\theta)$, produced by the scattering of radiation. First of all, there is a one-to-one

correspondence between k and θ due to the fact that a periodic compositional fluctuation of wavevector, $\mathbf{k}$, predominantly scatters radiation by a particular angle, θ, determined by the Bragg condition outlined in Fig. 1.12. First-order constructive interference requires that the path difference, $\overline{ab} - \overline{ac}$, equals one wavelength, λ, of the incident radiation. By simple trigonometry, the path-length between points a and b is $\overline{ab} = D/\sin(\theta/2)$, where $D = 2\pi/k$ is the period of the composition fluctuation. The alternative path-length between a and c is $\overline{ac} = \overline{ab}\cos(\theta) = \overline{ab}[1 - 2\sin^2(\theta/2)]$. Thus, the Bragg condition relating k and θ is

$$\theta = 2\sin^{-1}\left(\frac{\lambda k}{4\pi}\right) \tag{1.221}$$

Second of all, the intensity of the scattered radiation, $I(\theta)$, is proportional to the ensemble average of $|\phi_A(\mathbf{k})|^2$, where the orientation of $\mathbf{k}$ fulfils the Bragg condition. Since the probability of a harmonic fluctuation is given by the Boltzmann factor, $\exp(-cS^{-1}(\mathbf{k})|\phi_A(\mathbf{k})|^2)$, where c is independent of $\mathbf{k}$ and $\phi_A(\mathbf{k})$, it follows that $\left\langle|\phi_A(\mathbf{k})|^2\right\rangle \propto S(\mathbf{k})$. This, in turn, implies $I(\theta) \propto S(\mathbf{k})$, and hence the name, scattering function.

1.7.4 SCFT for a Homopolymer Interface

When a blend macrophase separates, there is inevitably an interface between the two phases as illustrated in Fig 1.3(b). Here, we calculate its properties and determine the resulting excess free energy per area, referred to as the interfacial tension, γ_I. Since the interface is unfavorable, it tends to be flat so as to minimize its total area, $\mathcal{A}$. Therefore, we set up a Cartesian coordinate system with the z axis perpendicular to the interface, and we consider a volume, $\mathcal{V} = L\mathcal{A}$, where L is sufficiently large that the system attains the properties of the bulk A- and B-rich phases at $z = -L/2$ and $z = L/2$, respectively. Because of the translational symmetry parallel to the interface, there will be no spatial variation in the x and y directions. These facts allow us to impose reflecting boundary conditions at the edges of $\mathcal{V}$.

As for the brush in Section 1.6.6, we again solve this problem using the spectral method. For the symmetry of our current problem, the appropriate basis functions are

$$f_i(z) = \begin{cases} 1\,, & \text{if } i = 0 \\ \sqrt{2}\cos(i\pi(1 + 2z/L))\,, & \text{if } i > 0 \end{cases} \tag{1.222}$$

This is, in fact, the same set of functions used for the polymer brush in Eq. (1.166), but with $\beta = 0$. In this case, the eigenvalues of the Laplacian become

$$\lambda_i = 4\pi^2 i^2 \tag{1.223}$$

and the symmetric tensor simplifies to

$$\Gamma_{ijk} = (\delta_{i+j,k} + \delta_{|i-j|,k})/\sqrt{2} \tag{1.224}$$

when all the indices are nonzero. If one or more of the indices are zero, then it reduces to a single delta function (e.g. $\Gamma_{ij0} = \delta_{ij}$ when $k = 0$).

The SCFT calculation for this system proceeds remarkably like that of the polymer brush, with only a couple of key differences. The first difference occurs because there are now two

distinct fields, $w_A(z)$ and $w_B(z)$, acting on the A and B segments, respectively. This results in two different transfer matrices, $\mathbf{T}_A(s) \equiv \exp(\mathbf{A}s)$ and $\mathbf{T}_B(s) \equiv \exp(\mathbf{B}s)$, where the coefficients of $\mathbf{A}$ and $\mathbf{B}$ are

$$A_{ij} \equiv -\frac{2\pi^2 i^2 a^2 N}{3L^2}\delta_{ij} - \frac{w_{A,(i+j)} + w_{A,|i-j|}}{\sqrt{2}} \tag{1.225}$$

$$B_{ij} \equiv -\frac{2\pi^2 i^2 a^2 N}{3L^2}\delta_{ij} - \frac{w_{B,(i+j)} + w_{B,|i-j|}}{\sqrt{2}} \tag{1.226}$$

These matrices are equivalent to that in Eq. (1.173), but with the simplified expressions for λ_i and Γ_{ijk} explicitly inserted. We have also assumed that the spatial averages of $w_A(z)$ and $w_B(z)$ are both zero, which, for the current set of basis functions, implies $w_{A,0} = w_{B,0} = 0$.

The fact that all chain ends are now free is accounted for by the conditions, $q_\gamma(\mathbf{r}, 0) = 1$ and $q^\dagger_\gamma(\mathbf{r}, 1) = 1$, where γ denotes either an A- or B-type polymer. In terms of the coefficients, $q_{\gamma,i}(s)$ and $q^\dagger_{\gamma,i}(s)$, these conditions become

$$q_{\gamma,i}(0) = \delta_{i0} \tag{1.227}$$

$$q^\dagger_{\gamma,i}(1) = \delta_{i0} \tag{1.228}$$

Other than this one minor difference, the calculation of the concentrations coefficients, $\phi_{\gamma,i}$, proceeds exactly as before in Eqs. (1.180) and (1.181).

The procedure for solving the self-consistent field Eqs. (1.203) and (1.206) changes ever so slightly from the case of the polymeric brush. The summations are still truncated at $i = M$, where M is large enough that the resulting inaccuracy is negligible. This time, however, there is no β to worry about, and the arbitrary constant to the fields have already been taken care of by setting $w_{A,0} = w_{B,0} = 0$. The remaining $2M$ field coefficients are determined by requiring

$$\phi_{A,i} + \phi_{B,i} = 0 \tag{1.229}$$

$$w_{A,i} - w_{B,i} = -2\chi N \phi_{A,i} \tag{1.230}$$

for $i = 1, 2, 3, ..., M$. Once these equations are satisfied, the free energy is given by Eq. (1.207), which simplifies to

$$\frac{F}{nk_BT} = \frac{F_h}{nk_BT} - \phi \ln(q_{A,0}(1)) - (1-\phi)\ln(q_{B,0}(1)) - \chi N \sum_{i=1}^{M} \phi_{A,i}\phi_{B,i} \tag{1.231}$$

This expression is arrived at by the fact that $\mathcal{Q}_\gamma = \mathcal{V} q_{\gamma,0}(1)$, $\phi_{A,0} = \phi$, and $\phi_{B,0} = 1 - \phi$.

Figure 1.13(a) shows the segment profiles calculated at several degrees of segregation within the two-phase region of Fig. 1.10(b). The interface appears in the center of the system at $z = 0$, because a symmetric blend composition of $\phi = 0.5$ was chosen. A convenient definition for the width over which the profile switches between the A- and B-rich phases is

$$w_I \equiv \frac{\phi_A(L/2) - \phi_A(-L/2)}{\phi'_A(0)} \tag{1.232}$$

As χN increases, the interface becomes narrower as illustrated in Fig. 1.13(b) so as to reduce the overlap between the A- and B-segment profiles. The interfacial tension, γ_I, associated

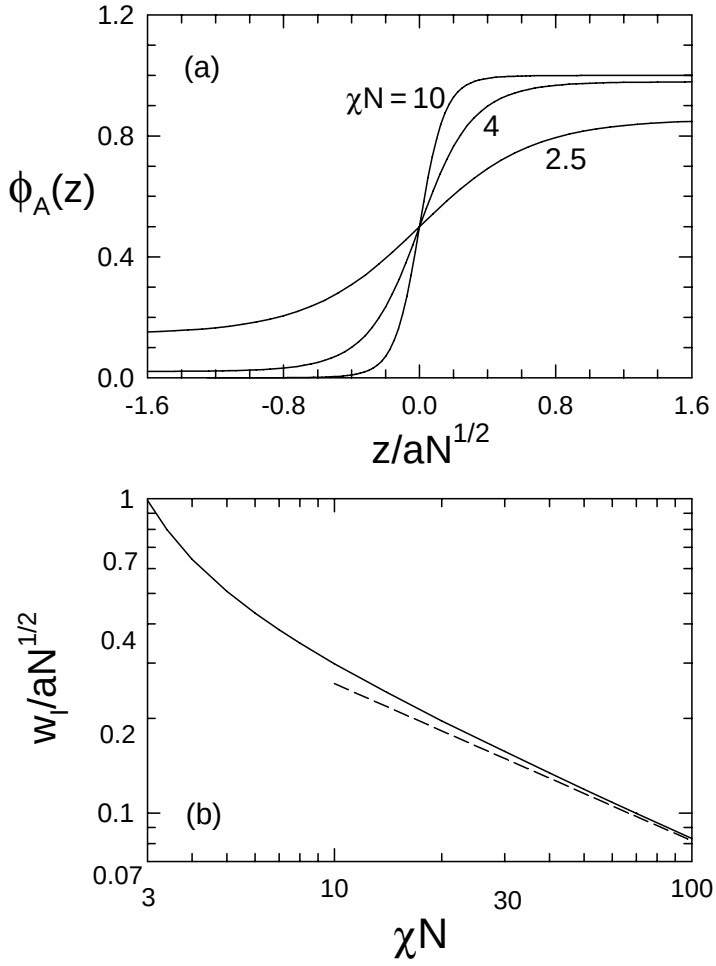

Figure 1.13: (a) Segment profile, $\phi_A(z)$, of an A/B interface at $z = 0$ calculated for several different levels of segregation, χN. (b) Interfacial width, w_I, plotted logarithmically as a function of segregation. The dashed line denotes the strong-segregation prediction in Eq. (1.239).

with the interface is given by the excess free energy per unit area of interface,

$$\gamma_I \equiv \frac{F - F_s}{\mathcal{A}} = \left(\frac{F - F_s}{nk_BT}\right)\left(\frac{L}{aN^{1/2}}\right)\rho_0 a N^{-1/2} k_B T \tag{1.233}$$

As χN increases beyond 2, γ_I grows monotonically from zero as shown in Fig. 1.14. These calculations can also be extended to curved interfaces (Matsen 1999), if one also wishes to evaluate the bending moduli of the interface.

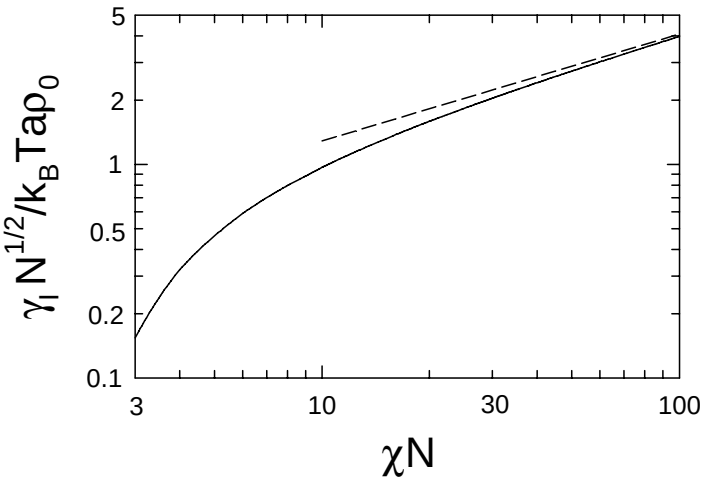

Figure 1.14: Interfacial tension, γ_I, plotted logarithmically as a function of segregation, χN. The dashed line denotes the strong-segregation prediction in Eq. (1.244).

1.7.5 Interface in a Strongly-Segregated Blend

In the limit of large χN, it becomes possible to derive analytical predictions for the interface between the A- and B-rich homopolymer phases. The strong field gradients that develop at the interface cause the ground-state-dominance approximation from Section 1.5.2 to become increasingly accurate. This allows the free energy of the blend to be expressed as

$$\frac{F}{nk_BT} = \frac{a^2N}{24L}\int dz \left(\frac{[\phi_A'(z)]^2}{\phi_A(z)} + \frac{[\phi_B'(z)]^2}{\phi_B(z)} \right) + \frac{\chi N}{L}\int dz\, \phi_A(z)\phi_B(z) \qquad (1.234)$$

where the configurational entropy of the polymers has been approximated by Eq. (1.78). The dependence on the B-polymer concentration is easily eliminated using the incompressibility condition, $\phi_B(z) = 1 - \phi_A(z)$. This leaves one unknown concentration, $\phi_A(z)$, which is determined by minimizing F subject to the boundary conditions, $\phi_A(-L/2) = 0$ and $\phi_A(L/2) = 1$. Note that we will ultimately extend L to infinity.

The functional minimization is facilitated by invoking the substitution

$$\phi_A(z) = \sin^2(\Theta(z)) \qquad (1.235)$$

which recasts the free energy expression as

$$\frac{F}{nk_BT} = \frac{1}{L}\int dz \left(\frac{a^2N}{6}[\Theta'(z)]^2 + \chi N \sin^2(\Theta(z))\cos^2(\Theta(z)) \right) \qquad (1.236)$$

with the new boundary conditions, $\Theta(-L/2) = 0$ and $\Theta(L/2) = \pi/2$. This functional has the identical form to that encountered in Section 1.3, where the classical trajectory was calculated

for an arbitrary field, $w(\mathbf{r})$. Applying the equivalent steps here to the Euler-Lagrange equation leads to

$$\frac{a^2 N}{6}[\Theta'(z)]^2 - \chi N \sin^2(\Theta(z))\cos^2(\Theta(z)) = \text{constant} \tag{1.237}$$

The boundary conditions on $\Theta(z)$ coupled with the fact that the profile must become flat in the limit, $z \to \pm\infty$, implies that the constant of integration must be zero, and thus

$$w_I \Theta'(z) = 2\sin(\Theta(z))\cos(\Theta(z)) \tag{1.238}$$

where

$$w_I \equiv \frac{2a}{\sqrt{6\chi}} \tag{1.239}$$

Returning to the original function, $\phi_A(z)$, Eq. (1.238) becomes

$$w_I \phi_A'(z) = 4\phi_A(z)[1 - \phi_A(z)] \tag{1.240}$$

which can be rearranged as

$$\frac{d\phi_A}{\phi_A(1-\phi_A)} = \frac{4dz}{w_I} \tag{1.241}$$

Integrating this equation, using the method of partial fractions on the right-hand side, and setting the constant of integration such that $\phi_A(0) = 1/2$ results in the predicted profile,

$$\phi_A(z) = \frac{1}{2}\left[1 + \tanh\left(\frac{2z}{w_I}\right)\right] \tag{1.242}$$

Referring to the definition in Eq. (1.232), the constant, w_I, can now be interpreted as the interfacial width. This approximate width is plotted as a dashed line in Fig. 1.13(b) along side the SCFT prediction, and indeed it is reasonably accurate for $\chi N \gtrsim 10$.

Inserting the calculated profile into the free energy expression, Eq. (1.234), gives

$$\frac{F}{nk_BT} = \frac{aN}{L}\sqrt{\frac{\chi}{6}} \tag{1.243}$$

where the integral, $\int dx \cosh^{-2}(x) = 2$, has been used. Given that the free energy of the two bulk phases is $F_s = 0$ in the strong-segregation limit, it follows from Eq. (1.233) that the interfacial tension is

$$\gamma_I = k_B T a \rho_0 \sqrt{\frac{\chi}{6}} \tag{1.244}$$

Figure 1.14 demonstrates that this well-known estimate becomes reasonably good once $\chi N \gtrsim 10$.

1.7.6 Grand-Canonical Ensemble

Up to this point, the polymer blend has been treated in the canonical ensemble (Hong and Noolandi 1981), where the numbers of A- and B-type polymers are fixed. However, the statistical mechanics of multicomponent blends can be equally well performed in the grand-canonical ensemble (Matsen 1995a), where n_A and n_B are permitted to fluctuate with chemical potentials, μ_A and μ_B, controlling their respective averages. The grand-canonical partition function, Z_g, is related to the canonical one, Z, by the expression,

$$Z_g = \sum_{n_A=0}^{\infty} \sum_{n_B=0}^{\infty} z_A^{n_A} z_B^{n_B} Z \tag{1.245}$$

where $z_A = \exp(\mu_A/k_BT)$ and $z_B = \exp(\mu_B/k_BT)$. When the melt is treated as incompressible such that $n_A + n_B = n$, one of the chemical potentials becomes redundant and the definition can be simplified to

$$Z_g = \sum_{n_A=0}^{\infty} \sum_{n_B=0}^{\infty} z^{n_A} Z \tag{1.246}$$

with $z = \exp(\mu/k_BT)$. This is evaluated by inserting the expression for Z from Eq. (1.196) and summing over n_A and n_B. The sum over n_A is carried out using the Taylor series expansion,

$$\sum_{n_A=0}^{\infty} \frac{1}{n_A!} \left(\frac{\rho_0}{N} z \mathcal{Q}_A[W_A]\right)^{n_A} = \exp\left(\frac{\rho_0}{N} z \mathcal{Q}_A[W_A]\right) \tag{1.247}$$

with an equivalent expansion for the sum over n_B. With the summations completed, the partition function reduces to

$$Z_g \propto \int \mathcal{D}\Phi_A \mathcal{D}W_A \mathcal{D}W_B \exp\left(-\frac{F_g[\Phi_A, W_A, W_B]}{k_BT}\right) \tag{1.248}$$

where

$$\frac{F_g}{nk_BT} = -z\frac{\mathcal{Q}_A[W_A]}{\mathcal{V}} - \frac{\mathcal{Q}_B[W_B]}{\mathcal{V}} + \frac{1}{\mathcal{V}} \int d\mathbf{r}[\chi N \Phi_A(1-\Phi_A) - W_A\Phi_A - W_B(1-\Phi_A)] \tag{1.249}$$

Just as before, $F_g[\Phi_A, W_A, W_B]$ can be readily evaluated but the functional integration in Eq. (1.248) cannot. The saddle-point approximation is therefore once again applied, producing the identical self-consistent conditions,

$$\phi_A(\mathbf{r}) + \phi_B(\mathbf{r}) = 1 \tag{1.250}$$

$$w_A(\mathbf{r}) - w_B(\mathbf{r}) = \chi N(1 - 2\phi_A(\mathbf{r})) \tag{1.251}$$

derived in the canonical ensemble. However, $\phi_A(\mathbf{r})$ and $\phi_B(\mathbf{r})$ are now defined by

$$\phi_A(\mathbf{r}) \equiv -\frac{z}{\mathcal{V}} \frac{\mathcal{D}\mathcal{Q}_A[w_A]}{\mathcal{D}w_A(\mathbf{r})} = z \int_0^1 ds\, q_A(\mathbf{r}, s) q_A^\dagger(\mathbf{r}, s) \tag{1.252}$$

$$\phi_B(\mathbf{r}) \equiv -\frac{1}{\mathcal{V}} \frac{\mathcal{D}\mathcal{Q}_B[w_B]}{\mathcal{D}w_B(\mathbf{r})} = \int_0^1 ds\, q_B(\mathbf{r}, s) q_B^\dagger(\mathbf{r}, s) \tag{1.253}$$

but they are still identified, using an analogous argument to that in Section 1.6.4, as the SCFT approximations for $\left\langle \hat{\phi}_A(\mathbf{r}) \right\rangle$ and $\left\langle \hat{\phi}_B(\mathbf{r}) \right\rangle$, respectively. The solution to the self-consistent field equations are solved as before in the canonical ensemble, but this time additive constants to the fields do affect F_g. Therefore, we are no longer free to select the spatial averages for $\bar{w}_A$ and $\bar{w}_B$, and thus Eq. (1.251) is used as is. Once the fields are determined, the grand-canonical free energy is given by $F_g[\phi_A, w_A, w_B]$ from Eq. (1.249).

The advantages of the grand-canonical ensemble come into play when dealing with macrophase separation and coexisting phases. Rather than having to perform a double-tangent construction like that in Fig. 1.10(a), coexistence is determined by simply equating the grand-canonical free energies of the two phases. Here we demonstrate the procedure for the binary homopolymer blends treated in Section 1.7.2. Since the A- and B-rich phases are homogeneous, the fields are constant and therefore the diffusion equations for the partial partition functions are easily solved. From their solutions, it follows that

$$\phi_A(\mathbf{r}) = z \exp(-w_A) \tag{1.254}$$

$$\phi_B(\mathbf{r}) = \exp(-w_B) \tag{1.255}$$

$$\mathcal{Q}_A[w_A] = \mathcal{V} \exp(-w_A) \tag{1.256}$$

$$\mathcal{Q}_B[w_B] = \mathcal{V} \exp(-w_B) \tag{1.257}$$

The incompressibility condition, Eq. (1.250), is enforced by setting $\phi \equiv \phi_A(\mathbf{r}) = 1 - \phi_B(\mathbf{r})$, which allows the four equations to be rewritten as

$$w_A = -\ln \phi + \frac{\mu}{k_B T} \tag{1.258}$$

$$w_B = -\ln(1-\phi) \tag{1.259}$$

$$\mathcal{Q}_A[w_A] = \mathcal{V}\phi/z \tag{1.260}$$

$$\mathcal{Q}_B[w_B] = \mathcal{V}(1-\phi) \tag{1.261}$$

The remaining self-consistent field condition, Eq. (1.251), requires that ϕ satisfy

$$\frac{\mu}{k_B T} = \ln \phi - \ln(1-\phi) + \chi N(1-2\phi) \tag{1.262}$$

In general, there will be one solution, $\phi = \phi^{(1)}$, corresponding to a B-rich phase and another, $\phi = \phi^{(2)}$, for an A-rich phase. Their grand-canonical free energies are then given by Eq. (1.249), which, for homogeneous phases, becomes

$$\frac{F_{g,h}}{n k_B T} = \phi[\ln \phi - 1] + (1-\phi)[\ln(1-\phi) - 1] + \chi N \phi(1-\phi) - \frac{\mu\phi}{k_B T} \tag{1.263}$$

Notice that $F_{g,h} = F_h - \mu n_A$, which is the standard relation between the grand-canonical and canonical free energies.

Figure 1.15 plots the grand-canonical free energies, $F_{g,h}^{(1)}$ and $F_{g,h}^{(2)}$, of the two phases as a function of chemical potential, μ. For purposes of comparison, this is done for the same degree of segregation, $\chi N = 3$, used in Fig. 1.10(a), where the canonical free energy, F_h, was plotted as a function of composition, ϕ. In the grand-canonical ensemble, the coexistence is associated with the crossing of $F_{g,h}^{(1)}$ and $F_{g,h}^{(2)}$, which, due to symmetry, occurs at $\mu = 0$. It is reasonably

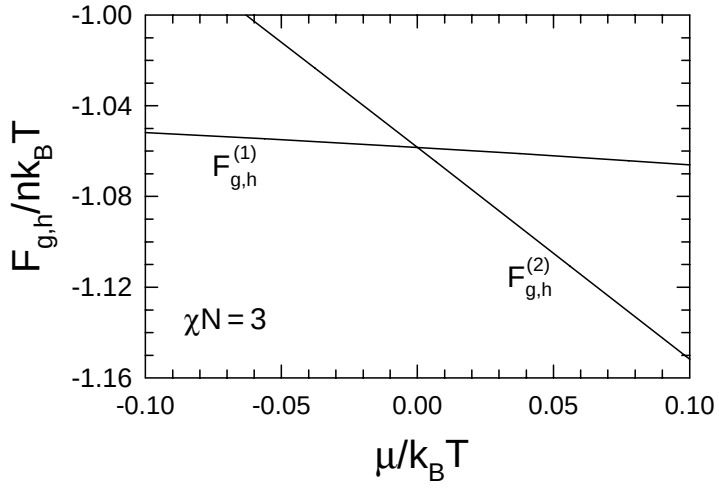

Figure 1.15: Grand-canonical free energy, $F_{g,h}$, of homogeneous blends as a function of chemical potential, μ, calculated for $\chi N = 3$. The two curves, $F^{(1)}_{g,h}$ and $F^{(2)}_{g,h}$, correspond to separate B- and A-rich phases, respectively. The B-rich phase is stable at $\mu < 0$ and the A-rich one is favored for $\mu > 0$; they coexist at $\mu = 0$.

straightforward to show that the negative slope of the curves in Fig. 1.15 is equal to the composition of the blend, which confirms that the more horizontal curve, $F^{(1)}_{g,h}$, corresponds to a B-rich phase, while the steeper one, $F^{(2)}_{g,h}$, represents an A-rich phase. According to Eq. (1.262), the compositions of the coexisting phases at $\mu = 0$ satisfy

$$\chi N = \frac{1}{1-2\phi} \ln\left(\frac{1-\phi}{\phi}\right) \tag{1.264}$$

which is precisely the same condition derived in Section 1.7.2 using the canonical ensemble. Indeed, the two ensembles always provide equivalent results and therefore either one can, in principle, do the job. However, there can be significant computational advantages of using them in conjunction with each other (Matsen 2003a).

1.8 Block Copolymer Melts

One way of preventing the macrophase separation of A- and B-type homopolymers is to covalently bond them together into a single AB diblock copolymer as depicted in Fig. 1.1. In this architecture, the first fN segments ($0 \leq f \leq 1$) of the polymer are type A, and the remaining $(1-f)N$ segments are type B. The A and B segments still segregate at large χN, but the domains remain microscopic in size, and thus the process is referred to as microphase separation. Not only that, the domains within the resulting microstructures take on periodically ordered geometries, such as the lamellar phase depicted in Fig. 1.3(c).

In this section, we consider a melt of n identical diblock copolymer molecules, occupying a fixed volume of $\mathcal{V} = nN/\rho_0$. This time, there is only a single molecular species, and thus one set of functions, $\mathbf{r}_\alpha(s)$ with α = 1,2,...,n, is sufficient to specify the configuration of the system. In terms of these trajectories, the dimensionless A-segment concentration is expressed as

$$\hat{\phi}_A(\mathbf{r}) = \frac{N}{\rho_0} \sum_{\alpha=1}^{n} \int_0^f ds\, \delta(\mathbf{r} - \mathbf{r}_\alpha(s)) \tag{1.265}$$

and that of the B segments is the same, but with the integration extending from $s = f$ to $s = 1$. As before with the homopolymer blend, the segment interactions are described by the same $U[\hat{\phi}_A, \hat{\phi}_B]$ defined in Eq. (1.192).

1.8.1 SCFT for a Diblock Copolymer Melt

The SCFT for diblock copolymers (Helfand 1975) is remarkably similar to that for the homopolymer blend considered in Section 1.7.1. The partition function for a block copolymer melt,

$$Z \propto \frac{1}{n!} \int \prod_{\alpha=1}^{n} \tilde{\mathcal{D}}\mathbf{r}_\alpha \exp\left(-\frac{U[\hat{\phi}_A, \hat{\phi}_B]}{k_B T}\right) \delta[1 - \hat{\phi}_A - \hat{\phi}_B] \tag{1.266}$$

is virtually the same, except that there are now only functional integrals over one molecular type. Proceeding as before, the partition function is converted to the same form as Eq. (1.198) for the polymer blend, but with

$$\frac{F}{nk_BT} = -\ln\left(\frac{\mathcal{Q}[W_A, W_B]}{\mathcal{V}}\right) + \frac{1}{\mathcal{V}} \int d\mathbf{r}[\chi N \Phi_A(1 - \Phi_A) - W_A\Phi_A - W_B(1 - \Phi_A)] \tag{1.267}$$

where

$$\mathcal{Q}[W_A, W_B] \propto \int \tilde{\mathcal{D}}\mathbf{r}_\alpha \exp\left(-\int_0^f ds\, W_A(\mathbf{r}_\alpha(s)) - \int_f^1 ds\, W_B(\mathbf{r}_\alpha(s))\right) \tag{1.268}$$

is identified as the partition function for a single diblock copolymer with its A and B blocks subjected to the fields, $W_A(\mathbf{r})$ and $W_B(\mathbf{r})$, respectively. Note that an irrelevant constant of one has been dropped from Eq. (1.267).

As always in SCFT, the free energy of the melt is approximated by $F[\phi_A, w_A, w_B]$, where the functions, ϕ_A, w_A, and w_B, correspond to a saddle point obtained by equating the functional derivatives of Eq. (1.267) to zero. The derivative of $F[\Phi_A, W_A, W_B]$ with respect to W_A leads to the condition,

$$\phi_A(\mathbf{r}) = -\mathcal{V}\frac{\mathcal{D}\ln(\mathcal{Q}[w_A, w_B])}{\mathcal{D}w_A(\mathbf{r})} \tag{1.269}$$

which identifies $\phi_A(\mathbf{r})$ as the average A-segment concentration from n diblock copolymers in the fields, $w_A(\mathbf{r})$ and $w_B(\mathbf{r})$. Differentiation with respect to W_B leads to the incompressibility constraint,

$$\phi_A(\mathbf{r}) + \phi_B(\mathbf{r}) = 1 \tag{1.270}$$

where

$$\phi_B(\mathbf{r}) \equiv -\mathcal{V}\frac{\mathcal{D}\ln(\mathcal{Q}[w_A, w_B])}{\mathcal{D}w_B(\mathbf{r})} \tag{1.271}$$

is the analogous B-segment concentration. The remaining functional derivative with respect to Φ_A provides the self-consistent field condition,

$$w_A(\mathbf{r}) - w_B(\mathbf{r}) = 2\chi N(f - \phi_A(\mathbf{r})) \tag{1.272}$$

where again an appropriate constant has been added to allow for $\bar{w}_A = \bar{w}_B = 0$. With that, the free energy reduces to

$$\frac{F}{nk_BT} = \chi N f(1-f) - \ln\left(\frac{\mathcal{Q}[w_A, w_B]}{\mathcal{V}}\right) - \frac{\chi N}{\mathcal{V}}\int d\mathbf{r}(\phi_A(\mathbf{r}) - f)(\phi_B(\mathbf{r}) - 1 + f) \tag{1.273}$$

where the first term, $\chi N f(1-f)$, gives the free energy of the disordered state in which all the A and B blocks are homogeneously mixed.

The statistical mechanics for a diblock copolymer in fields, $w_A(\mathbf{r})$ and $w_B(\mathbf{r})$, differs ever so slightly from that of the homopolymer considered in Section 1.2. The full single-polymer partition function is still expressed as

$$\mathcal{Q}[w_A, w_B] = \int d\mathbf{r}\; q(\mathbf{r}, s)q^\dagger(\mathbf{r}, s) \tag{1.274}$$

and the partial partition functions still satisfy the same diffusion equations with $q(\mathbf{r}, 0) = q^\dagger(\mathbf{r}, 1) = 1$. The diblock architecture enters simply by the fact that the field, $w(\mathbf{r})$, in Eqs. (1.24) and (1.28) is substituted by $w_A(\mathbf{r})$ for $0 < s < f$ and by $w_B(\mathbf{r})$ for $f < s < 1$. Once the partial partition functions are evaluated, the average A-segment concentration is given by

$$\phi_A(\mathbf{r}) = \frac{\mathcal{V}}{\mathcal{Q}[w_A, w_B]}\int_0^f ds\; q(\mathbf{r}, s)q^\dagger(\mathbf{r}, s) \tag{1.275}$$

and $\phi_B(\mathbf{r})$ is given by the same integral, but with an appropriate change of limits.

1.8.2 Scattering Function for the Disordered Phase

Here a Landau-Ginzburg free energy functional (Leibler 1980) is calculated for small variations in the A-segment profile, $\phi_A(\mathbf{r})$, about the average value of $\bar{\phi}_A = f$, following analogous steps to those in Section 1.7.3 for polymer blends. As before, we assume that the variations in

$w_A(\mathbf{r})$ and $w_B(\mathbf{r})$ are sufficiently small such that $q(\mathbf{r}, f)$ is well described by Eq. (1.99) with the field $w_A(\mathbf{r})$ and similarly such that $q^\dagger(\mathbf{r}, f)$ is given by Eq. (1.100) with the field $w_B(\mathbf{r})$. These approximations are then inserted into Eq. (1.274) to give

$$\frac{\mathcal{Q}[w_A, w_B]}{\mathcal{V}} \approx 1 + \frac{1}{2(2\pi)^3\mathcal{V}} \int d\mathbf{k}[S_{11}w_A(-\mathbf{k})w_A(\mathbf{k}) + S_{22}w_B(-\mathbf{k})w_B(\mathbf{k}) + 2S_{12}w_A(-\mathbf{k})w_B(\mathbf{k})] \tag{1.276}$$

where $S_{11} \equiv g(x, f)$, $S_{22} \equiv g(x, 1-f)$, and $S_{12} \equiv h(x, f)h(x, 1-f)$. Differentiating $\mathcal{Q}[w_A, w_B]$ with respect to the Fourier transforms of the fields, as we did in Section 1.7.3, gives the Fourier transforms of the concentrations,

$$\phi_A(\mathbf{k}) = -S_{11}w_A(\mathbf{k}) - S_{12}w_B(\mathbf{k}) \tag{1.277}$$

$$\phi_B(\mathbf{k}) = -S_{22}w_B(\mathbf{k}) - S_{12}w_A(\mathbf{k}) \tag{1.278}$$

for all $\mathbf{k} \neq 0$. These equations are then inverted to obtain the expressions,

$$w_A(\mathbf{k}) = \frac{-S_{22}\phi_A(\mathbf{k}) + S_{12}\phi_B(\mathbf{k})}{\det(S)} \tag{1.279}$$

$$w_B(\mathbf{k}) = \frac{S_{12}\phi_A(\mathbf{k}) - S_{11}\phi_B(\mathbf{k})}{\det(S)} \tag{1.280}$$

for the fields, where $\det(S) \equiv S_{11}S_{22} - S_{12}^2$. At this point, the incompressibility condition can be used to set $\phi_B(\mathbf{k}) = -\phi_A(\mathbf{k})$, for all $\mathbf{k} \neq 0$. Substituting the expressions for the two fields into that for $\mathcal{Q}[w_A, w_B]$, and then inserting that into the logarithm of Eq. (1.273) gives

$$\frac{F}{nk_BT} = \chi N f(1-f) + \frac{N}{2(2\pi)^3\mathcal{V}} \int_{\mathbf{k}\neq 0} d\mathbf{k}\, S^{-1}(\mathbf{k})\phi_A(-\mathbf{k})\phi_A(\mathbf{k}) \tag{1.281}$$

to second order in $|\phi_A(\mathbf{k})|$, where

$$S^{-1}(\mathbf{k}) = \frac{g(x,1)}{N\det(S)} - 2\chi \tag{1.282}$$

is the inverse of the scattering function for a disordered melt. In a somewhat analogous but considerably more complicated procedure, the scattering functions can also be evaluated for periodically ordered phases (Yeung et al. 1996; Shi et al. 1996). It involves a very elegant method akin to band-structure calculations in solid-state physics, providing yet another example of where SCFT draws upon existing techniques from quantum mechanics.

Figure 1.16 shows the disordered-state $S(\mathbf{k})$ for diblock copolymers of symmetric composition, $f = 0.5$, plotted for a series of χN values. As the interaction strength increases, $S(\mathbf{k})$ develops a peak over a sphere of wavevectors at radius, $kaN^{1/2} = 4.77$, which corresponds to composition fluctuations of wavelength, $D/aN^{1/2} = 1.318$. The peak eventually diverges at $\chi N = 10.495$, at which point the disordered state becomes unstable and switches by a continuous transition to the ordered lamellar phase. With the exception of $f = 0.5$, the spinodal point is preempted by a discontinuous transition to the ordered phase, but an approximate treatment of this requires, at the very least, fourth-order terms in the free energy expansion of Eq. (1.281) (Leibler 1980). Better yet, the next section will show how to calculate the exact mean-field phase boundaries.

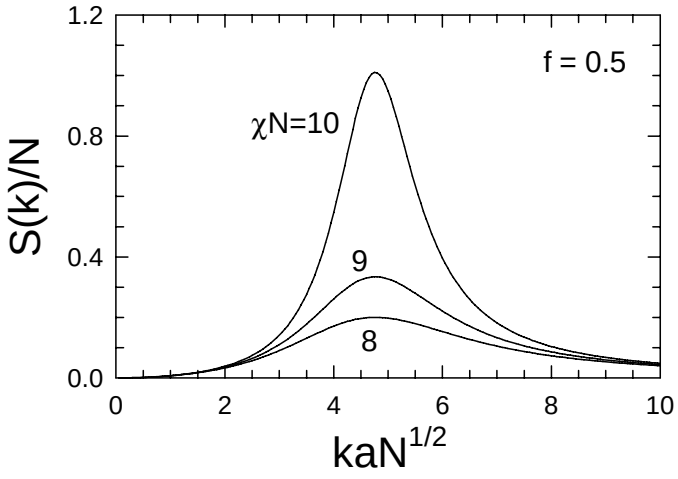

Figure 1.16: Scattering function, $S(\mathbf{k})$, for a disordered diblock copolymer melt of symmetric composition, $f = 0.5$, plotted for several degrees of segregation, χN.

1.8.3 Spectral Method for the Ordered Phases

Now we turn our attention to the ordered block-copolymer phases. Due to the periodicity of their domain structures, the spectral method is by far the most efficient method for solving the SCFT. Here, the method is illustrated starting with the simplest microstructure, the one-dimensional lamellar phase pictured in Fig. 1.3(c). Our chosen coordinate system orients the z axis perpendicular to the interfaces, so that there is translational symmetry in the x and y directions. This allows for the relatively simple basis functions,

$$f_i(z) = \begin{cases} 1\,, & \text{if } i = 0 \\ \sqrt{2}\cos(i\pi(1+2z/D))\,, & \text{if } i > 0 \end{cases} \tag{1.283}$$

where D corresponds to the lamellar period. In fact, these are the precise functions used in Section 1.7.4 for the interface of a binary homopolymer blend, but with L replaced by D. Consequently, the eigenvalues, λ_i, and the tensor, Γ_{ijk}, are given by the exact same Eqs. (1.223) and (1.224). Again, these quantities are used to construct the transfer matrices, $\mathbf{T}_A(s) \equiv \exp(\mathbf{A}s)$ and $\mathbf{T}_B(s) \equiv \exp(\mathbf{B}s)$, where

$$A_{ij} = -\frac{\lambda_i a^2 N}{6D^2}\delta_{ij} - \sum_k w_{A,k}\Gamma_{ijk} \tag{1.284}$$

$$B_{ij} = -\frac{\lambda_i a^2 N}{6D^2}\delta_{ij} - \sum_k w_{B,k}\Gamma_{ijk} \tag{1.285}$$

The evaluation of the transfer matrices is performed by the same diagonalization procedure detailed in Section 1.6.6. Just as before, the coefficients for the partial partition functions are

expressed in terms of the transfer matrices as

$$q_i(s) = \begin{cases} T_{A,i0}(s)\,, & \text{if } s \le f \\ \sum_j T_{B,ij}(s-f)q_j(f)\,, & \text{if } s > f \end{cases} \tag{1.286}$$

$$q_i^\dagger(s) = \begin{cases} \sum_j T_{A,ij}(f-s)q_j^\dagger(f)\,, & \text{if } s < f \\ T_{B,i0}(1-s)\,, & \text{if } s \ge f \end{cases} \tag{1.287}$$

although there are now separate expressions for $s < f$ and $s > f$ due to the field switching from $w_A(\mathbf{r})$ to $w_B(\mathbf{r})$. The coefficients for the average polymer concentration continue to be expressed as

$$\phi_{\gamma,i} = \frac{1}{q_0(1)} \sum_{jk} I_{\gamma,jk}\Gamma_{ijk} \tag{1.288}$$

in terms of matrices, $\mathbf{I}_\gamma$, defined much as before in Eq. (1.181). For the A-segment concentration,

$$I_{A,jk} \equiv \int_0^f ds\; q_j(s)q_k^\dagger(s) \tag{1.289}$$

$$= \sum_{m,n} \left[\frac{\exp(fd_{A,m}) - \exp(fd_{A,n})}{d_{A,m} - d_{A,n}} \right] U_{A,jm}U_{A,kn}\bar{q}_m(0)\bar{q}_n^\dagger(f) \tag{1.290}$$

Note that for equal eigenvalues, $d_{A,m} = d_{A,n}$, the factor in the square brackets reduces to $f\exp(fd_{A,m})$. The expression for $I_{B,jk}$ is analogous, but with $d_{B,i}$ and $U_{B,ij}$ calculated from the $\mathbf{B}$ matrix, and with $s = 0$ and f switched to $s = f$ and 1, respectively.

The self-consistent field conditions for $w_{A,i}$ and $w_{B,i}$ remain exactly as in Eqs. (1.229) and (1.230) for the homopolymer blends. We still follow the same practice of setting the spatial average of the fields to zero, which implies $w_{A,0} = w_{B,0} = 0$, and the sums are still truncated at $i = M$, where M is chosen sufficiently large to meet the desired numerical accuracy. Once the field coefficients, $w_{A,i}$ and $w_{B,i}$ for $i = 1, 2, ..., M$, are determined, the free energy can be evaluated by

$$\frac{F}{nk_BT} = \chi Nf(1-f) - \ln(q_0(1)) - \chi N \sum_{i=1}^{M} \phi_{A,i}\phi_{B,i} \tag{1.291}$$

where we have exploited the fact that $\mathcal{Q}[w_A, w_B] = \mathcal{V}q_0(1)$, $\phi_{A,0} = f$, and $\phi_{B,0} = 1 - f$. In this block copolymer case, there is the one additional step of minimizing the free energy with respect to the periodicity, D, of the microstructure.

Figure 1.17(a) shows the predicted segment profile, $\phi_A(z)$, of the lamellar phase for symmetric diblocks, $f = 0.5$, at several different degrees of segregation, χN. The lamellar phase first appears at $\chi N = 10.495$ with a period of $D/aN^{1/2} = 1.318$, consistent with the divergence in $S(\mathbf{k})$ discussed in Section 1.8.2. At weak segregations such as $\chi N \approx 11$, the profile is approximately sinusoidal. By $\chi N = 20$, the center of the A and B domains become relatively pure, and by $\chi N = 50$, the A-B contacts are restricted to the relatively narrow interfacial regions. The series of profiles clearly demonstrates that the domain spacing, D, swells

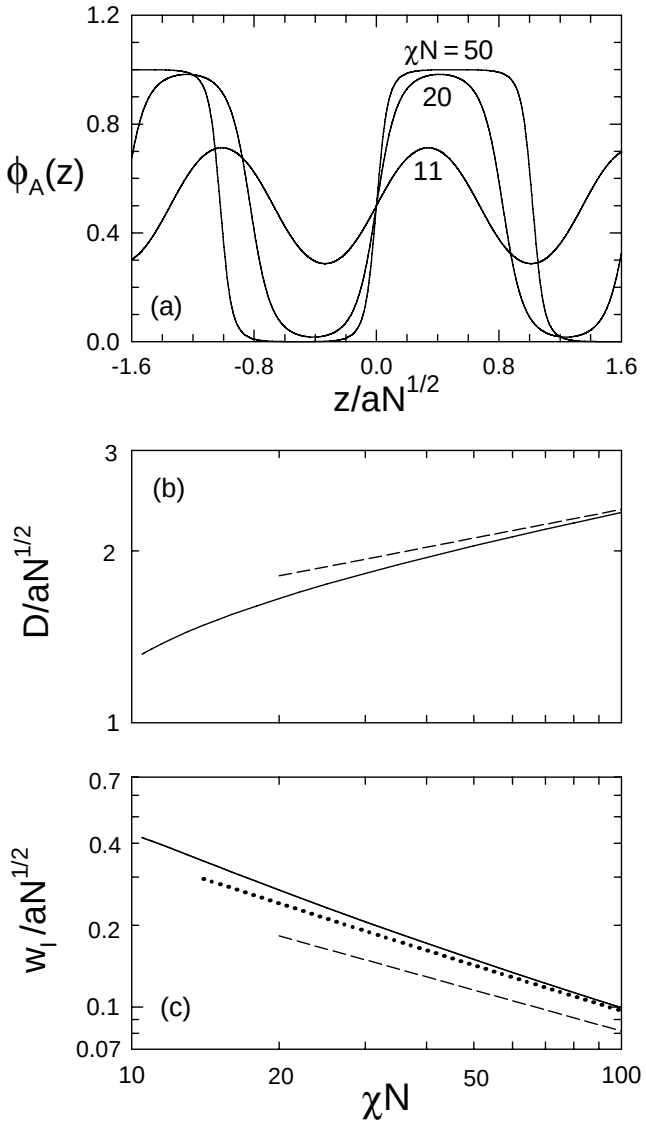

Figure 1.17: (a) Segment profiles, $\phi_A(z)$, from the lamellar phase of symmetric diblock copolymers, $f = 0.5$ plotted for three levels of segregation, χN. (b) Domain spacing, D, versus segregation plotted logarithmically; the dashed curve denotes the SST prediction from Eq. (1.302). (c) Interfacial width, w_I, versus segregation plotted logarithmically; the dashed and dotted lines correspond to the SST predictions in Eqs. (1.239) and (1.299), respectively.

and the interfacial width,

$$w_I \equiv \frac{\phi_A(D/2) - \phi_A(-D/2)}{\phi_A'(0)} \tag{1.292}$$

narrows as the segregation increases. Plots 1.17(b) and 1.17(c) show these trends on logarithmic scales so as to highlight the well-known scaling behavior that emerges for strongly-segregated microstructures. The dashed line in Fig. 1.17(b) denotes the domain scaling of $D \propto a\chi^{1/6}N^{2/3}$, where the proportionality constant will be derived in the next Section using SST. At intermediate segregations, the rate of increase is somewhat more rapid, consistent with the fact that the experimentally measured exponent for N tends to be ~ 0.8 (Almdal et al. 1990). The dashed and dotted lines in Fig. 1.17(c) show SST predictions for the interfacial width, which will be discussed in the next Section.

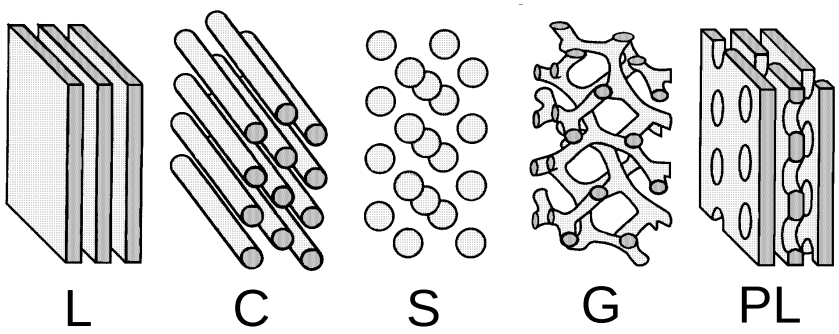

Figure 1.18: Minority domains from the periodically ordered phases observed in diblock copolymer melts. The first three, lamellar (L), cylindrical (C), and spherical (S), are referred to as the classical phases, and the latter two, gyroid (G) and perforated-lamellar (PL), are denoted as the complex phases. Although the PL phase is often observed, our best experimental evidence indicates that it is only ever metastable (Hajduk *et al.* 1997).

The lamellar phase is only observed for $f \approx 0.5$. When the diblock copolymer becomes sufficiently asymmetric, the domains transform into other periodic geometries as depicted in Fig. 1.18. In the cylindrical (C) phase, the shorter minority blocks form cylindrical domains aligned in a hexagonal packing with the longer majority blocks filling the intervening space. In the spherical (S) phase, the minority blocks form spheres that generally pack in a body-centered cubic (bcc) arrangement. Note, however, that there are occasions where the spherical (S_{cp}) phase prefers close-packed (e.g., fcc or hcp) arrangements. In addition to these *classical* phases, two *complex* phases, gyroid (G) and perforated-lamellar (PL), have also been observed. The minority domains of the G phase (Hajduk et al. 1994; Schulz et al. 1994) form two interweaving networks composed of three-fold coordinated junctions. The PL phase (Hamley et al. 1993) is much like the classical L phase, but the minority-component lamellae develop perforations through which the majority-component layers become connected. The perforations tend to be aligned hexagonally within the layers and staggered between neighboring layers.

Fortunately, the only part of the spectral method that changes when considering the non-lamellar morphologies are the basis functions, and these changes are entirely contained within the values of λ_i and Γ_{ijk}. Take the C phase for example. Its hexagonal unit cell is shown in Fig. 1.19 with a coordinated system defined such that the cylinders are aligned in the z

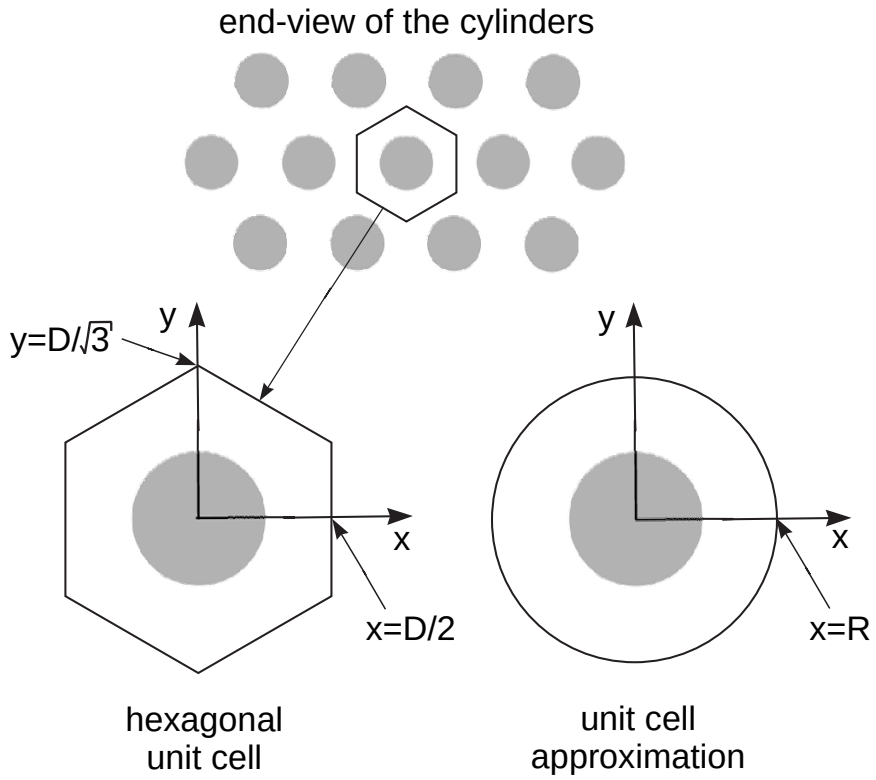

Figure 1.19: End-view showing the hexagonal arrangement of the minority domains of the cylinder (C) phase. Below to the left is the proper hexagonal unit cell, and to the right is a circular unit-cell approximation (UCA), where the radius R is set by the equal area condition, $\pi R^2 = \sqrt{3}D^2/2$.

direction. The orthonormal basis functions for this symmetry start off as

$$f_0(\mathbf{r}) = 1 \tag{1.293}$$

$$f_1(\mathbf{r}) = \sqrt{2/3}[\cos(2Y) + 2\cos(X)\cos(Y)] \tag{1.294}$$

$$f_2(\mathbf{r}) = \sqrt{2/3}[\cos(2X) + 2\cos(X)\cos(3Y)] \tag{1.295}$$

$$f_3(\mathbf{r}) = \sqrt{2/3}[\cos(4Y) + 2\cos(2X)\cos(2Y)] \tag{1.296}$$

$$f_4(\mathbf{r}) = \sqrt{4/3}[\cos(3X)\cos(Y) + \cos(2X)\cos(4Y) + \cos(X)\cos(5Y)] \tag{1.297}$$

where $X \equiv 2\pi x/D$ and $Y \equiv 2\pi y/\sqrt{3}D$. (The general formula is provided by Henry and Lonsdale (1969) under the space-group symmetry of p6mm.) The corresponding eigenvalues of the Laplacian are $\lambda_0 = 0$, $\lambda_1 = 16\pi^2/3$, $\lambda_2 = 16\pi^2$, $\lambda_3 = 64\pi^2/3$, $\lambda_4 = 112\pi^2/3$, and so on. Although there are simply too many elements of Γ_{ijk} to begin enumerating them, it is a trivial matter to generate them by computer. Once they have been evaluated and stored away

in a file, the free energy of the C phase is calculated using the exact same expressions as for the L phase. The same goes for the S and G phases, where their basis functions are catalogued by Henry and Lonsdale (1969) under the space-group symmetries, Im $\bar{3}$m and Ia$\bar{3}$d, respectively. For the S_{cp} and PL phases, there are near degeneracies (Matsen and Bates 1996a) in the arrangement of spheres and the stacking of layers, respectively. As suggested by Matsen and Bates (1996a), this is likely to result in irregular non-periodic arrangements, which is indeed consistent with recent experimental observations (Sakamoto et al. 1997; Zhu et al. 2001). Nevertheless, for the purpose of calculating phase boundaries, it is sufficient to use the symmetries Fm$\bar{3}$m (i.e., fcc packing) and R$\bar{3}$m (i.e., ABCABC... stacking), respectively. The PL phase is also different in that it has two distinct periodicities, which implies that the eigenvalue Eq. (1.165) for the basis functions must be generalized to

$$\nabla^2 f_i(\mathbf{r}) = -\left(\frac{\lambda_{\parallel,i}}{D_\parallel^2} + \frac{\lambda_{\perp,i}}{D_\perp^2}\right) f_i(\mathbf{r}) \tag{1.298}$$

where $D_\parallel$ is the in-plane spacing between perforations and $D_\perp$ is the out-of-plane lamellar spacing. However, this distinction only enters in an obvious extension to Eqs. (1.284) and (1.285), and in the need to minimize F with respect to both $D_\parallel$ and $D_\perp$.

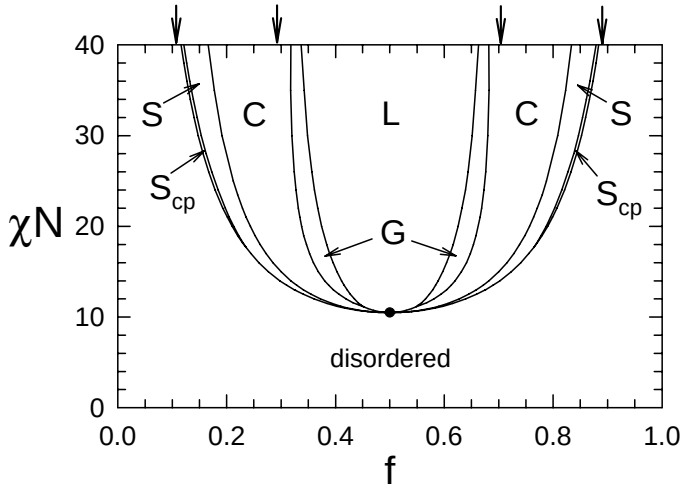

Figure 1.20: Theoretical phase diagram for diblock copolymer melts showing where the various morphologies in Fig. 1.18 are stable. All phase transitions are discontinuous except for the mean-field critical point denoted by the solid dot. Along part of the order-disorder transition (ODT) is a narrow region, S_{cp}, where spherical domains prefer a close-packed arrangement over the usual bcc one. In the strong-segregation limit, the G region pinches off at $\chi N \approx 60$, the ODT approaches the two edges of the diagram, and the C/S and L/C boundaries approach the fixed compositions estimated by the arrows at the top of the diagram.

Comparing the free energies of the disordered phase and all the ordered phases of Fig. 1.19 generates the phase diagram in Fig. 1.20, which maps the phase of lowest free energy as

a function of composition, f, and segregation, χN. This theoretical diagram is in excellent agreement with experiment (Matsen 2002a) apart from a few minor differences. Experimental phase diagrams (Bates et al. 1994) have varying degrees of asymmetry about $f = 0.5$, but this is well accounted for by conformational asymmetry (Matsen and Bates 1997a) occuring due to unequal statistical lengths of the A and B segments. Aside from that, the small remaining differences with experiment are generally attributed to fluctuation effects, which will be discussed later in Section 1.10. According to the theory, the only complex microstructure present in the equilibrium phase diagram is G, and based on extrapolations (Matsen and Bates 1996a) its region of stability pinches off at $\chi N \approx 60$. Although the PL phase never, at any point, possesses the lowest free energy, it is very close to being stable in the G region. This integrates well with recent experiments (Hajduk et al. 1997) demonstrating that occurances of PL eventually convert to G, given sufficient time. In addition to predicting a phase diagram in agreement with experiment, the theory also provides powerful intuitive explanations for the behavior in terms of spontaneous interfacial curvature and packing frustration (Matsen 2002a).

Many, particularly older, block copolymer calculations employ a unit-cell approximation (UCA), where the hexagonal cell is replaced by a circular cell of equal area as depicted in Fig. 1.19. This creates a rotational symmetry that transforms the two-dimensional diffusion equation into a simpler one-dimensional version. An equivalent approximation is also available for the spherical phase. The diblock copolymer phase diagram calculated (Vavasour and Whitmore 1992) with this UCA is very similar to that in Fig. 1.20, except that it leaves out the G phase as there are no UCA's for the complex phases. Nevertheless, the complex phase region is a small part of the diblock copolymer phase diagram, and thus its omission is not particularly serious. While there is no longer any need to invoke this approximation for simple diblock copolymer melts, there are many other systems with dauntingly large parameter spaces (e.g., blends) that are still computationally demanding. For those that are dominated by the classical phases, the omission of the complex phases is a small price to pay for the tremendous computational advantage gained by implementing the UCA. The spectral method can still be used exactly as described above, but with the expansion performed in terms of Bessel functions (Matsen 2003a).

1.8.4 SST for the Ordered Phases

The free energy of a well-segregated diblock-copolymer microstructure has three main contributions, the tension of the internal interface and the stretching energies of the A and B blocks (Matsen and Bates 1997b). In the large-χN regime, these energies can all be approximated by simple expressions, producing a very useful analytical strong-segregation theory (SST) (Semenov 1985). In fact, the interface of a block copolymer melt is the same as that of a homopolymer blend, to a first-order approximation. The derivation in Section 1.7.5 just requires sufficiently steep field gradients at the interface such that the ground-state dominance applies, and this continues to be the case. Therefore, the tension, γ_I, in Eq. (1.244) and the interfacial width, w_I, in Eq. (1.239) also apply to block copolymer melts. Indeed, the approximation for the width, shown by the dashed line in Fig. 1.17(c), is reasonable, although not nearly as

accurate as it was in Fig. 1.13(b) for the homopolymer blend. A much better approximation,

$$w_I = \frac{2a}{\sqrt{6\chi}}\left[1 + \frac{4}{\pi}\left(\frac{3}{\pi^2\chi N}\right)^{1/3}\right] \tag{1.299}$$

denoted by the dotted curve in Fig. 1.17(c), can be derived by accounting for the connectivity of the A and B blocks (Semenov 1993), but it is considerably more complicated. For simplicity, we stick with the simple first-order approximation for γ_I in Eq. (1.244).

The stretching energies of the A and B blocks are approximated by noting that, as χN increases, the junction points become strongly pinned to narrow interfaces, while the domains swell in size. Consequently, the A and B domains can be described as strongly-stretched brushes. The lamellar (L) phase consists of four brushes per period, D, and it follows from the incompressibility constraint that the thicknesses of the A and B brushes are $fD/2$ and $(1-f)D/2$, respectively. Since all the brushes are flat, their energies are given by Eq. (1.121), and thus the total free energy of the L phase, F_L, can be approximated as

$$\frac{F_L}{nk_BT} = \frac{\gamma_I\Sigma}{k_BT} + \frac{\pi^2[fD/2]^2}{8a^2[fN]} + \frac{\pi^2[(1-f)D/2]^2}{8a^2[(1-f)N]} \tag{1.300}$$

where $\Sigma = 2N/D\rho_0$ is the interfacial area per molecule. Inserting the interfacial tension from Eq. (1.244), the expression simplifies to

$$\frac{F_L}{nk_BT} = 2\sqrt{\frac{\chi N}{6}}\left(\frac{D}{aN^{1/2}}\right)^{-1} + \frac{\pi^2}{32}\left(\frac{D}{aN^{1/2}}\right)^{2} \tag{1.301}$$

The equilibrium domain spacing, obtained by minimizing F_L, is then given by

$$\frac{D}{aN^{1/2}} = 2\left(\frac{8\chi N}{3\pi^4}\right)^{1/6} \tag{1.302}$$

which is shown in Fig. 1.17(b) with a dashed line. This provides the domain-size scaling alluded to earlier. Inserting the equilibrium value of D into Eq. (1.301) provides the final expression,

$$\frac{F_L}{nk_BT} = \frac{1}{4}(9\pi^2\chi N)^{1/3} \tag{1.303}$$

for the free energy of the lamellar phase.

For non-lamellar phases, the SST becomes complicated, unless the unit-cell approximation (UCA) is implemented. First of all, this allows the interfacial shape to be determined by symmetry rather than by minimizing the free energy. For instance, the symmetry of the approximate unit cell shown in Fig. 1.19 for the cylindrical (C) phase implies a perfectly circular interface. Given this, the incompressibility condition requires the radius of the interface to be $R_I \equiv \sqrt{f}R$, from which it follows that the interfacial area per molecule is

$$\Sigma = \frac{2N\sqrt{f}}{R\rho_0} \tag{1.304}$$

Second of all, the symmetry requires that the strongly-stretched chains follow straight trajectories in the radial direction, for which Eq. (1.123) is easily generalized. The stretching energy of the γ-type blocks (γ =A or B) becomes

$$\frac{f_{\gamma,e}}{k_BT} = \frac{3\pi^2}{8a^2N_\gamma} \times \frac{1}{\mathcal{V}_\gamma} \int d\mathbf{r}\; z_d^2 \tag{1.305}$$

which involves an average of z_d^2 over the volume, $\mathcal{V}_\gamma$, of the γ domain, where z_d is the radial distance to the interface and N_γ is the number of segments in the γ-type block. For a C phase with A-type cylinders and a B-type matrix, the stretching energy of the A blocks becomes

$$\frac{f_{A,e}}{k_BT} = \frac{3\pi^2}{4a^2Nf^2R^2} \int_0^{R_I} d\rho\; \rho(\rho - R_I)^2 = \frac{\pi^2R^2}{16a^2N} \tag{1.306}$$

and that of the B blocks is

$$\frac{f_{B,e}}{k_BT} = \frac{3\pi^2}{4a^2N(1-f)^2R^2} \int_{R_I}^{R} d\rho\; \rho(\rho - R_I)^2 = \frac{\pi^2R^2}{16a^2N}\alpha_B \tag{1.307}$$

where

$$\alpha_B \equiv \frac{(1-\sqrt{f})^3(3+\sqrt{f})}{(1-f)^2} \tag{1.308}$$

Combining the three contributions, the total free energy of the C phase is written as

$$\frac{F_C}{nk_BT} = 2\sqrt{\frac{\chi Nf}{6}} \left(\frac{R}{aN^{1/2}}\right)^{-1} + \frac{\pi^2(1+\alpha_B)}{16} \left(\frac{R}{aN^{1/2}}\right)^{2} \tag{1.309}$$

Again, minimization leads to a domain size that scales as $R \sim a\chi^{1/6}N^{2/3}$, which when inserted back into Eq. (1.309), gives

$$\frac{F_C}{nk_BT} = \frac{1}{4}(18\pi^2(1+\alpha_B)\chi N)^{1/3} \tag{1.310}$$

Comparing F_L and F_C, we find that the C phase has a lower free energy than the L phase for $f < 0.2991$. The symmetry of the phase diagram implies that a C phase with B-rich cylinders becomes preferred over L when $f > 0.7009$. The analogous calculation for the spherical (S) phase (Matsen and Bates 1997b) predicts C/S boundaries at $f = 0.1172$ and $f = 0.8828$.

There is one problem that has been overlooked. Equation (1.305) provided the stretching energies while avoiding the need to work out the distribution of chain ends. However, had we evaluated the concentration of B ends, we would have encountered a negative distribution along side the interface. Of course a negative concentration is unphysical. The proper solution (Ball et al. 1991) has instead a narrow exclusion zone next to the interface that is free of chain ends, and as a consequence the SST field, $w_B(\mathbf{r})$, deviates slightly from the parabolic potential. (The classical-mechanical analogy with a simple harmonic oscillator used in Section 1.6.1 only holds if the chain ends have a finite population over the entire domain.) Fortunately, the effect is exceptionally small and can be safely ignored (Matsen and Whitmore 1996).

The only significant inaccuracy comes from the unit-cell approximation (UCA) (Matsen and Whitmore 1996). An improved SST-based calculation (Likhtman and Semenov 1994) with the proper unit cell of the C phase, but still assuming a circular interface and radial trajectories, predicts a L/C phase boundary at $f = 0.293$. Although a relatively minor problem in this instance, the assumption of straight trajectories (in general, the shortest distance to an interface (Likhtman and Semenov 1994)) minimizes the stretching energy without enforcing the connectivity of the A and B blocks. This approximation can, in fact, lead to highly erroneous predictions (Matsen 2003b). One way of enforcing the connectivity is to subdivide the A and B domains into wedges along which the diblocks follow straight paths with a kink at the interface (Olmsted and Milner 1998). Furthermore, the proper interface is not a perfect circle, but is slightly perturbed towards the six corners of the hexagonal unit cell (Matsen and Bates 1997b). Likhtman and Semenov (1997) have recently presented a method for performing SST calculations that minimize the free energy with respect to the interfacial shape while maintaining the connectivity of the blocks (the trajectory of each block is still straight and the exclusion zones are still ignored), but the method is highly computational. With this more accurate SST algorithm, they showed that the gyroid (G) phase becomes unstable in the strong-segregation limit, consistent with the SCFT extrapolations by Matsen and Bates (1996a), but unfortunately they did not calculate accurate values for the remaining L/C and C/S boundaries. At present, our best SST estimates for these boundaries are $f = 0.294$ and $f = 0.109$, respectively, obtained by adjusting the UCA predictions according to SCFT-based corrections calculated by Matsen and Whitmore (1996). These values are denoted by arrows at the top of Fig. 1.20, and indeed they correspond reasonably well with the SCFT boundaries at finite χN.

1.9 Current Track Record and Future Outlook for SCFT

Although SCFT has only been demonstrated here for three relatively simple systems, it is a fantastically versatile theory that can be applied to multi-component mixtures with any number of species (Hong and Noolandi 1981; Matsen 1995a) and to polymer architectures of virtually any complexity (Matsen and Schick 1994b; Matsen and Schick 1994c). Solvent molecules can also be included in the theory (Naughton and Matsen 2002). Interactions are easily generalized (Matsen 2002a) beyond the simple Flory-Huggins form in Eq. (1.192), and the constraint, $\hat{\phi}_A(\mathbf{r}) + \hat{\phi}_B(\mathbf{r}) = 1$, can be relaxed to allow for some degree of compressibility (Yeung et al. 1994). To include liquid-crystalline interactions (Netz and Schick 1996) or to account for chain stiffness (Morse and Fredrickson 1994; Matsen 1996), the Gaussian model for flexible polymers can be substituted by a worm-like chain model (Takahashi and Yunoki 1967), in which the flexibility can be adjusted. The possibilities are truly limitless.

Not only is SCFT highly versatile, it also has a track record to rival any and all theories in soft condensed matter physics. On the topic of polymer brushes, SCFT has recently resolved (Matsen and Gardiner 2001) a discrepancy between SST (Leibler et al. 1994) and experiment (Reiter and Khanna 2000) on the subtle effect of autophobic dewetting, where a small interfacial tension of entropic origins causes a homopolymer film to dewet from a chemically identical brush. However, to date, the majority of its triumphs have involved the subtleties of block copolymer phase behavior. Most notably, SCFT correctly predicted the

complex phase behavior of diblock copolymer melts several years in advance of experiment. At the time that SCFT predicted (Matsen and Schick 1994a) the phase diagram in Fig. 1.20, experiments had reported four stable complex phases: the double-diamond (Thomas et al. 1987), the perforated-lamellar (PL) (Hamley et al. 1993), the modulated-lamellar (Hamley et al. 1993), and the gyroid (G) (Hajduk et al. 1994; Schulz et al. 1994). The existence of the modulated-lamellar phase, based solely on scattering experiments, was the least certain, and strongly conflicted with our theoretical understanding of the complex phase behavior (Matsen 2002b; Matsen and Bates 1996b). It is now accepted and well supported by theory (Yeung et al. 1996) that the observed scattering pattern was simply a result of anisotropic fluctuations from the classical lamellar (L) phase. Secondly, it has become apparent that the double-diamond phase was nothing more than a misidentified gyroid phase (Hajduk et al. 1995), attributed to the remarkable similarities of the two microstructures, coupled with the limited resolution of scattering experiments at the time. Conversely, the perforated-lamellar phase is most definitely observed in diblock copolymer melts, but it is now accepted to be a metastable state that, given sufficient time, converts to the gyroid morphology (Hajduk et al. 1997). With that final realization, experiments are now in line with the SCFT prediction that gyroid is the only stable complex phase in diblock copolymer melts. However, in more elaborate architectures, notably ABC triblock copolymers, a zoo of complex morphologies are possible (Bates and Fredrickson 1999), and SCFT is having equal success in resolving their complex phase behavior (Matsen 1998; Shefelbine et al. 1999; Wickham and Shi 2001). Another impressive accomplishment of SCFT has been the successful treatment (Matsen 1997) of a delicate symmetry-breaking transition in the grain boundary of a lamellar morphology, where a symmetric chevron boundary switches to an asymmetric omega boundary as the angle between two lamellar grains increases (Gido and Thomas 1994). Arguably, the most impressive accomplishment up to now involves the macrophase separation of chemically-equivalent small and large diblock copolymers (Hashimoto et al. 1993). The fact that SCFT is the only theory to correctly predict (Matsen 1995b) this effect is impressive in its own right, but the truly stunning achievement emerged later when Papadakis et al. (1998) purposely synthesized diblock copolymers in order to quantitatively test one of the predicted SCFT phase diagrams. The agreement between the theoretical and experimental phase boundaries is virtually perfect, which is particularly remarkable, given the fact that the competing theories fail to predict any boundaries at all. With this level of success, SCFT has unequivocally emerged as the state-of-the-art theory for structured polymeric melts.

The superb track record of SCFT can be attributed to the sound approximations upon which it is built. Although the Gaussian chain model treats polymers as simple microscopic elastic threads, which may seem at first to be highly artificial, it is a well-grounded model for high-molecular-weight polymers as justified in Section 1.1. In this limit of high molecular weight, the separation between the atomic and molecular length scales allows for the effective treatment of the monomer-monomer interactions by the simple Flory-Huggins form, $U[\hat{\phi}_A, \hat{\phi}_B]$, in Eq. (1.192) coupled with the incompressibility constraint, $\hat{\phi}_A(\mathbf{r}) + \hat{\phi}_B(\mathbf{r}) = 1$. Beyond these approximations in the underlying model, the only other is the saddle-point approximation, which amounts to mean-field theory. Again, this approximation becomes increasingly accurate for large invariant polymerization indices, $\mathcal{N}$, where the individual polymers acquire more and more contacts with their neighboring molecules. The conventional understanding is that SCFT becomes exact in the limit of $\mathcal{N} \to \infty$. Nevertheless, real poly-

mers are of finite molecular weight, and thus there is still a need for further development.

1.10 Beyond SCFT: Fluctuation Corrections

The main shortcoming of SCFT is that it does not properly account for composition fluctuations (Matsen 2002b), where $\hat{\phi}_A(\mathbf{r})$ and $\hat{\phi}_B(\mathbf{r})$ deviate from their ensemble averages, $\left\langle \hat{\phi}_A(\mathbf{r}) \right\rangle$ and $\left\langle \hat{\phi}_B(\mathbf{r}) \right\rangle$, respectively. These fluctuations are best known for disordering the weakly-segregated phases near the mean-field critical points in Figs. 1.10(b) and 1.20, but they also have some significant effects on strongly-segregated melts. In particular, capillary-wave fluctuations broaden the internal interfaces in both polymer blends and block copolymer microstructures. Furthermore, fluctuations are responsible for disordering the lattice arrangement of the close-packed spherical (S_{cp}) phase predicted by SCFT in Fig. 1.20 for diblock copolymer melts (Matsen 2002b; Sakamoto et al. 1997; Wang et al. 2005).

Composition fluctuations are often treated with the use of Landau-Ginzburg free energy expressions like those derived in Eqs. (1.217), (1.234), and (1.281). The formal procedure involves breaking the calculation of the partition function, Z, into two separate steps. For the polymer blend considered in Section 1.7.1, the procedure begins with the calculation of

$$Z_{LG}[\Phi_A] \propto \frac{1}{n_A! n_B!} \exp\left(-\frac{U[\Phi_A, 1-\Phi_A]}{k_B T}\right) \prod_{\alpha=1}^{n_A} \tilde{\mathcal{D}}\mathbf{r}_{A,\alpha} \prod_{\beta=1}^{n_B} \tilde{\mathcal{D}}\mathbf{r}_{B,\beta} \times \delta[\Phi_A - \hat{\phi}_A]\delta[1 - \Phi_A - \hat{\phi}_B] \qquad (1.311)$$

which provides the Landau-Ginzburg free energy, $F_{LG}[\Phi_A] = -k_B T \ln(Z_{LG}[\Phi_A])$, for a fixed composition profile, $\Phi_A(\mathbf{r})$. Next, the functional integration

$$Z = \int \mathcal{D}\Phi_A Z_{LG}[\Phi_A] \qquad (1.312)$$

is performed over all possible compositions. While it is obvious that these steps reproduce the result of Eq. (1.195), $F_{LG}[\Phi_A]$ is no easier to calculate than the actual free energy, $F = -k_B T \ln Z$, of the system.

To proceed, the Landau-Ginzburg free energy can be approximated by the methods of SCFT. It may seem odd to correct the SCFT prediction for F by using the SCFT prediction for $F_{LG}[\Phi_A]$, but SCFT is better suited to the latter problem, where the composition is not permitted to fluctuate. Still, the SCFT calculation of $F_{LG}[\Phi_A]$ can run into problems, because it only constrains the average concentration of A segments [i.e., $\left\langle \hat{\phi}_A(\mathbf{r}) \right\rangle = \Phi_A(\mathbf{r})$] rather than the actual concentration [i.e., $\hat{\phi}_A(\mathbf{r}) = \Phi_A(\mathbf{r})$]. For well-segregated compositions, where $\Phi_A(\mathbf{r})$ is generally close to either zero or one, there is little distinction between constraining $\hat{\phi}_A(\mathbf{r})$ as opposed to its ensemble average, and therefore the method works well. The treatment of capillary-wave fluctuations in both polymer blends and block copolymer microstructures agrees well with experiment (Sferrazza et al. 1997; Shull et al. 1993). However, for the most widely used application (Fredrickson and Helfand 1987) on the Brazovskii fluctuations (Brazovskii 1975) of weakly-segregated block copolymer melts, this Landau-Ginzburg treatment is questionable. It predicts the ODT in Fig. 1.20 to shift upwards destroying the mean-field

critical point and opening up direct transitions between the disordered state and each of the ordered phases (Hamley and Podneks 1997). Although these qualitative predictions agree with both experiment (Bates et al. 1988) and simulation (Vassiliev and Matsen 2003), there is mounting evidence that the theoretical treatment is quantitatively inaccurate (Maurer et al. 1998). Most concerning is a recent demonstration that the treatment only produces sensible results due to an approximation of the scattering function, $S(\mathbf{k})$; when the full expression in Eq. (1.282) is used, the short-wavelength fluctuations cause a catastrophic divergence (Kudlay and Stepanow 2003).

Fortunately, new and more rigorous approaches have started to emerge. They go to the heart of the problem and attempt to improve upon the saddle-point approximation. The first by Stepanow (1995) attempts this by generating an expansion, where fluctuation corrections are represented by a series of diagrammatic graphs, much like in quantum electrodynamics (QED). However, this approach has not yet been pushed to the point of producing experimentally verifiable predictions. More promising are field-theoretic simulations (Fredrickson et al. 2002; Müller and Schmid 2005).

To help with the full evaluation of Z, we take advantage of the usual quadratic form of $U[\Phi_A, 1-\Phi_A]$ and employ a Hubbard-Stratonovich transformation (Müller and Schmid 2005)

$$\exp\left(n\chi N\int d\mathbf{r}\;\Phi_A^2\right)\propto\int\mathcal{D}W_-\exp\left(-\frac{n}{\mathcal{V}}\int d\mathbf{r}\left[\frac{W_-^2}{\chi N}+2W_-\Phi_A\right]\right)\tag{1.313}$$

to reduce the functional integrations in Eq. (1.198) from three to two. This is done by inserting the transformation into Eq. (1.198), which then allows the integration over $\Phi_A(\mathbf{r})$, producing the Dirac delta functional, $\delta[2W_- - W_A + W_B]$. This identifies

$$W_-(\mathbf{r})=\frac{W_A(\mathbf{r})-W_B(\mathbf{r})}{2}\tag{1.314}$$

and, in turn, allows the integration to be performed over $W_A(\mathbf{r})$. With the substitution of $W_B(\mathbf{r})$ for a new function $W_+(\mathbf{r})$ defined by

$$W_+(\mathbf{r})=\frac{W_A(\mathbf{r})+W_B(\mathbf{r})}{2}\tag{1.315}$$

the partition function for binary polymer blends in Eq. (1.198) becomes

$$Z\propto\int\mathcal{D}W_-\mathcal{D}W_+\exp\left(-\frac{F[W_-,W_+]}{k_BT}\right)\tag{1.316}$$

where now

$$\frac{F}{nk_BT}=\phi\ln\left(\frac{\phi\mathcal{V}}{\mathcal{Q}_A[W_++W_-]}\right)+(1-\phi)\ln\left(\frac{(1-\phi)\mathcal{V}}{\mathcal{Q}_B[W_+-W_-]}\right)+\frac{1}{\mathcal{V}}\int d\mathbf{r}\left[\frac{W_-^2}{\chi N}-W_+\right]\tag{1.317}$$

Similarly, the ensemble average of, for example, the A-segment concentration becomes

$$\left\langle\hat{\phi}_A(\mathbf{r})\right\rangle=\frac{1}{Z}\int\mathcal{D}W_-\mathcal{D}W_+\phi_A(\mathbf{r})\exp\left(-\frac{F[W_-,W_+]}{k_BT}\right)\tag{1.318}$$

where $\phi_A(\mathbf{r})$ is the concentration from n_A noninteracting A-type polymers subjected to the complex field, $W_A(\mathbf{r}) = W_+(\mathbf{r}) + W_-(\mathbf{r})$. In this case, $\phi_A(\mathbf{r})$ is a complex quantity with no physical significant. The same procedure can be adapted equally well to the partition functions of other systems such as the diblock copolymer melts considered in Section 1.8.1.

Since the integrand of Z in Eq. (1.316) involves a Boltzmann factor, $\exp(-F/k_BT)$, standard simulation techniques of statistical mechanics can be applied, where the coordinates are now the fluctuating fields, $W_-(\mathbf{r})$ and $W_+(\mathbf{r})$. Ganesan and Fredrickson (2001) have used Langevin dynamics while Düchs et al. (2003) have formulated a Monte Carlo algorithm for generating a sequence of configurations with the appropriate Boltzmann weights. The ensemble average, $\left\langle \hat{\phi}_A(\mathbf{r}) \right\rangle$, can then be approximated by averaging $\phi_A(\mathbf{r})$ over the configurations generated by the simulation. Even though $\phi_A(\mathbf{r})$ is generally complex, the imaginary part will average to zero. The need to consider two separate fluctuating fields is still computationally demanding, but in practice the functional integral over the field, $W_+(\mathbf{r})$, can be performed with the saddle-point approximation, which implies that as $W_-(\mathbf{r})$ fluctuates, $W_+(\mathbf{r})$ is continuously adjusted so that $\phi_A(\mathbf{r}) + \phi_B(\mathbf{r}) = 1$ (Düchs et al. 2003). Even with the problem reduced to a single fluctuating field, it is still an immense challenge to perform simulations in full three-dimensional space. However, with the rapid improvement in computational performance and the development of improved algorithms, it is just a matter of time before these field-theoretic simulations become viable.

1.11 Appendix: The Calculus of Functionals

SCFT is a continuum field theory that relies heavily on the calculus of functionals. For those not particularly familiar with this more obscure variant of calculus, this section reviews the essential aspects required for a comprehensive understanding of SCFT. In short, the term *functional* refers to a function of a function. A specific example of a functional is

$$\mathcal{F}[f] \equiv \int_0^1 dx \exp(f(x)) \tag{1.319}$$

This definition provides a well-defined rule for producing a scalar number from the input function, $f(x)$. For example, $\mathcal{F}[f]$ returns the value, e, for the input, $f(x) = 1$, and it returns $(e-1)$ for $f(x) = x$. Note that we follow a convention, where the arguments of a functional are enclosed in square brackets, rather than the round brackets generally used for ordinary functions.

The calculus of functionals is, in fact, very much like multi-variable calculus, where the value of $f(x)$ for each x acts as a separate variable. Take the case where $0 \leq x \leq 1$, and imagine that the x coordinate is divided into a discrete array of equally spaced points, $x_m \equiv m/M$ for $m = 0, 1, 2, ..., M$. Provided that M is large, the function, $f(x)$, is well represented by the set of values, $\{f_0, f_1, ..., f_M\}$, where $f_m \equiv f(x_m)$. In turn, the functional in Eq. (1.319) is well approximated by the multi-variable function,

$$\mathcal{F}(\{f_m\}) \equiv \frac{\exp(f_0)}{2M} + \frac{1}{M}\sum_{m=1}^{M-1} \exp(f_m) + \frac{\exp(f_M)}{2M} \tag{1.320}$$

The correspondence between calculus of functionals and multi-variable calculus is easily understood in terms of this approximation. Functional derivatives are related to partial derivatives by the correspondence,

$$\frac{\mathcal{D}}{\mathcal{D}f(x)}\mathcal{F}[f] \Leftrightarrow \frac{\partial}{\partial f_n}\mathcal{F}(\{f_m\}) \tag{1.321}$$

and functional integrals are related to ordinary multi-dimensional integrals by

$$\int \mathcal{D}f\mathcal{F}[f] \Leftrightarrow \int df_0 df_1 \cdots df_M \mathcal{F}(\{f_m\}) \tag{1.322}$$

While Eq. (1.321) offers a useful intuitive definition of a functional derivative, the more rigorous definition in terms of limits is

$$\frac{\mathcal{D}\mathcal{F}[f]}{\mathcal{D}f(y)} \equiv \lim_{\epsilon\to 0}\frac{\mathcal{F}[f+\epsilon\delta]-\mathcal{F}[f]}{\epsilon} \tag{1.323}$$

where $\mathcal{F}[f+\epsilon\delta]$ represents the functional evaluated for the input function, $f(x)+\epsilon\delta(x-y)$. There is one subtle point in that the Dirac delta function is itself defined in terms of a limit involving a set of finite functions such as

$$\delta(x) = \lim_{\sigma\to 0}\frac{\exp(-x^2/\sigma)}{\sqrt{\pi\sigma}} \tag{1.324}$$

The definition in Eq. (1.323) assumes that the limit $\epsilon \to 0$ is taken before the limit $\sigma \to 0$, so that $\epsilon\delta(x-y)$ can be treated as infinitesimally small. For the specific example in Eq. (1.319),

$$\begin{aligned}\mathcal{F}[f+\epsilon\delta] &\equiv \int_0^1 dx \exp(f(x)+\epsilon\delta(x-y)) \\ &\approx \int_0^1 dx \exp(f(x))[1+\epsilon\delta(x-y)] \\ &= \mathcal{F}[f]+\epsilon\exp(f(y))\end{aligned} \tag{1.325}$$

where terms of order O(ϵ^2) have been dropped. Inserting this into the definition of a functional derivative, Eq. (1.323), and renaming y as x, it immediately follows that

$$\frac{\mathcal{D}\mathcal{F}[f]}{\mathcal{D}f(x)} = \exp(f(x)) \tag{1.326}$$

Let us now consider a general class of functionals, which are defined as an integral,

$$\mathcal{I}[f] \equiv \int_a^b dx \mathcal{L}(x, f(x), f'(x)) \tag{1.327}$$

with an arbitrary integrand, $\mathcal{L}(x, f(x), f'(x))$, involving x, the function, $f(x)$, and its first

derivative, $f'(x)$. To calculate its functional derivative, we start with

$$\begin{aligned}\mathcal{I}[f+\epsilon\delta] &\equiv \int_a^b dx\mathcal{L}(x,f(x)+\epsilon\delta(x-y),f'(x)+\epsilon\delta'(x-y)) \\ &\approx \mathcal{I}[f]+\epsilon\int_a^b dx\,\delta(x-y)\frac{\partial}{\partial f}\mathcal{L}(x,f(x),f'(x))+ \\ &\qquad \epsilon\int_a^b dx\,\delta'(x-y)\frac{\partial}{\partial f'}\mathcal{L}(x,f(x),f'(x)) \\ &= \mathcal{I}[f]+\epsilon\frac{\partial}{\partial f}\mathcal{L}(y,f(y),f'(y))- \\ &\qquad \epsilon\frac{d}{dy}\left(\frac{\partial}{\partial f'}\mathcal{L}(y,f(y),f'(y))\right) \end{aligned} \tag{1.328}$$

In the last step, the integration involving $\delta'(x-y)$ is converted to one involving $\delta(x-y)$ by performing an integration by parts, and then both integrals are evaluated using the sifting property of the Dirac delta function,

$$\int dx\,\delta(x-y)g(x)=g(y) \tag{1.329}$$

where $g(x)$ is an arbitrary function. Inserting Eq. (1.328) into the definition of a functional derivative, we have

$$\frac{\mathcal{D}\mathcal{I}[f]}{\mathcal{D}f(x)}=\frac{\partial}{\partial f}\mathcal{L}(x,f(x),f'(x))-\frac{d}{dx}\left(\frac{\partial}{\partial f'}\mathcal{L}(x,f(x),f'(x))\right) \tag{1.330}$$

This more general result is indeed consistent with our prior example. If we choose $\mathcal{L}(x,f,f')=\exp(f)$, then $\frac{\partial}{\partial f}\mathcal{L}(x,f,f')=\exp(f)$ and $\frac{\partial}{\partial f'}\mathcal{L}(x,f,f')=0$. Substituting these into Eq. (1.330) reduces it to the specific case of Eq. (1.326).

Many problems in physics can be expressed in terms of either a minimization or maximization of an integral of the form in Eq. (1.327). One such example involves the Lagrangian formalism of classical mechanics (Goldstein 1980), where the trajectory of an object, $\mathbf{r}_p(t)$, is determined by minimizing the so-called action, S, which is an integral over time involving its position, $\mathbf{r}_p(t)$, and velocity, $\mathbf{r}'_p(t)$. The condition for an extremum of the integral, $\mathcal{I}[f]$, is simply

$$\frac{d}{dx}\left(\frac{\partial}{\partial f'}\mathcal{L}(x,f(x),f'(x))\right)-\frac{\partial}{\partial f}\mathcal{L}(x,f(x),f'(x))=0 \tag{1.331}$$

which is a differential equation referred to as the Euler-Lagrange equation. This result is used numerous times throughout the Chapter.

Of course, calculus involves integration as well as differentiation. Here we demonstrate some of the intricacies of functional integration by developing a useful expression for the Dirac delta functional, $\delta[f]$. This is a generalization of the ordinary delta functional defined in Eq. (1.324), although we now use the alternative integral representation,

$$\delta(x)=\frac{1}{2\pi}\int_{-\infty}^{\infty}dk\exp(ikx) \tag{1.332}$$

which is derived using Fourier transforms, Eqs. (1.80) and (1.81), combined with the sifting property from Eq. (1.329). It is in fact the sifting property that is the essential characteristic by which the delta function is defined. The functional version of this sifting property is

$$\int \mathcal{D}f\ \delta[f-g]\mathcal{F}[f] = \mathcal{F}[g] \tag{1.333}$$

where $\mathcal{F}[f]$ is an arbitrary functional. The generalization of Eq. (1.332) is arrived at by first constructing the approximate discrete version,

$$\begin{aligned} \delta[f] &\approx \delta(f_0)\delta(f_1)\cdots\delta(f_M) \\ &= \frac{1}{(2\pi)^{(M+1)}}\int dk_0 dk_1 \cdots dk_M \exp\left(i\sum_{m=0}^{M} k_m f_m\right) \end{aligned} \tag{1.334}$$

Then taking the limit $M \to \infty$ gives

$$\delta[f] \propto \int \mathcal{D}k\ \exp\left(i\int dx\ k(x)f(x)\right) \tag{1.335}$$

where now we have a functional integral over $k(x)$. Notice that there is a slight difficulty in taking the limit; as M increases, the proportionality constant approaches zero, although this is compensated for by the increasing number of integrations. In practice, this is not a problem, because functional integrals are always evaluated for finite M, but it does prevent us from specifying a proportionality constant in Eq. (1.335). Nevertheless, the constant is unimportant in the applications to SCFT, and so Eq. (1.335) is sufficient for our purposes.

Bibliography

Almdal, K., Rosedale, J. H., Bates, F. S., Wignall, G. D., and Fredrickson, G. H., 1990, *Phys. Rev. Lett.* **65**, 1112.

Ball, R. C., Marko, J. F., Milner, S. T., and Witten, T. A., 1991, *Macromolecules* **24**, 693.

Bates, F. S. and Fredrickson, G. H., 1999, *Phys. Today* **52**, 32.

Bates, F. S., Rosedale, J. H., Fredrickson, G. H., and Glinka, C. J., 1988, *Phys. Rev. Lett.* **61**, 2229.

Bates, F. S., Schulz, M. F., Khandpur, A. K., Förster, S., Rosedale, J. H., Almdal, K., and Mortensen, K., 1994, *Faraday Discuss.* **98**, 7.

Brazovskii, S. A., 1975, *Sov. Phys. JETP* **41**, 85.

Carrier, G. F., Krook, M., and Pearson, C. E., 1966, *Functions of a Complex Variable*. McGraw-Hill, New York, section 6-3.

de Gennes, P.-G., 1979, *Scaling Concepts in Polymer Physics*. Cornell University, Ithaca.

Düchs, D., Ganesan, V., Fredrickson, G. H., and Schmid, F., 2003, *Macromolecules* **36**, 9237.

Edwards, S. F., 1965, *Proc. Phys. Soc. London* **85**, 613.

Fetters, L. J., Lohse, D. J., Richter, D., Witten, T. A., and Zirkel, A., 1994, *Macromolecules* **27**, 4639.

Feynman, R. P. and Hibbs, A. R., 1965, *Quantum Mechanics and Path Integrals*. McGraw-Hill, New York.

Fredrickson, G. H., Ganesan, V., and Drolet, F., 2002, *Macromolecules* **35**, 16.

Fredrickson, G. H. and Helfand, E., 1987, *J. Chem. Phys.* **87**, 697.

Ganesan, V. and Fredrickson, G. H., 2001, *Europhys. Lett.* **55**, 814.

Gido, S. P. and Thomas, E. L., 1994, *Macromolecules* **27**, 6137.

Goldstein, H., 1980, *Classical Mechanics, 2nd ed.* Addison-Wesley, Reading Massachusetts.

Hajduk, D. A., Harper, P. E., Gruner, S. M., Honeker, C. C., Kim, G., Thomas, E. L., and Fetters, L. J., 1994, *Macromolecules* **27**, 4063.

Hajduk, D. A., Harper, P. E., Gruner, S. M., Honeker, C. C., Kim, G., Thomas, E. L., and Fetters, L. J., 1995, *Macromolecules* **28**, 2570.

Hajduk, D. A., Takenouchi, H., Hillmyer, M. A., Bates, F. S., Vigild, M. E., and Almdal, K., 1997, *Macromolecules* **30**, 3788.

Hamley, I. W., Koppi, K. A., Rosedale, J. H., Schulz, M. F., Bates, F. S., Almdal, K., and Mortensen, K., 1993, *Macromolecules* **26**, 5959.

Hamley, I. W. and Podneks, V. E., 1997, *Macromolecules* **30**, 3701.

Hashimoto, T., Yamasaki, K., Koizumi, S., and Hasegawa, H., 1993, *Macromolecules* **29**, 2895.

Hecht, E. and Zajac, A., 1974, *Optics*. Addison-Wesley, Reading Massachusetts.

Helfand, E., 1975, *J. Chem. Phys.* **62**, 999.

Henry, N. F. M. and Lonsdale, K. (eds.), 1969, *International Tables for X-Ray Crystallography*. Kynoch, Birmingham.

Hong, K. M. and Noolandi, J., 1981, *Macromolecules* **14**, 727.

Kudlay, A. and Stepanow, S., 2003, *J. Chem. Phys.* **118**, 4272.

Leibler, L., 1980, *Macromolecules* **13**, 1602.

Leibler, L., Ajdari, A., Mourran, A., Coulon, G., and Chatenay, D., 1994, *in OUMS Conference on Ordering in Macromolecular Systems*. edited by A. Teramoto, M. Kobayashi and T. Norisuje, p. 301, Springer-Verlag, Berlin.

Likhtman, A. E. and Semenov, A. N., 1994, *Macromolecules* **27**, 3103.

Likhtman, A. E. and Semenov, A. N., 1997, *Macromolecules* **30**, 7273.

Likhtman, A. E. and Semenov, A. N., 2000, *Europhys. Lett.* **51**, 307.

Matsen, M. W., 1995a, *Phys. Rev. Lett.* **74**, 4225.

Matsen, M. W., 1995b, *J. Chem. Phys.* **103**, 3268.

Matsen, M. W., 1996, *J. Chem. Phys.* **104**, 7758.

Matsen, M. W., 1997, *J. Chem. Phys.* **107**, 8110.

Matsen, M. W., 1998, *J. Chem. Phys.* **108**, 785.

Matsen, M. W., 1999, *J. Chem. Phys.* **110**, 4658.

Matsen, M. W., 2002a, *J. Phys.: Condens. Matter* **14**, R21.

Matsen, M. W., 2002b, *J. Chem. Phys.* **117**, 2351.

Matsen, M. W., 2003a, *Macromolecules* **36**, 9647.

Matsen, M. W., 2003b, *Phys. Rev. E* **67**, 023801.

Matsen, M. W., 2004, *J. Chem. Phys.* **121**, 1938.

Matsen, M. W. and Bates, F. S., 1996a, *Macromolecules* **29**, 1091.

Matsen, M. W. and Bates, F. S., 1996b, *Macromolecules* **29**, 7641.

Matsen, M. W. and Bates, F. S., 1997a, *J. Polym. Sci.: Part B.:Polym. Phys.* **35**, 945.

Matsen, M. W. and Bates, F. S., 1997b, *J. Chem. Phys.* **106**, 2436.

Matsen, M. W. and Gardiner, J. M., 2001, *J. Chem. Phys.* **115**, 2794.

Matsen, M. W. and Schick, M., 1994a, *Phys. Rev. Lett.* **72**, 2660.

Matsen, M. W. and Schick, M., 1994b, *Macromolecules* **27**, 6761.

Matsen, M. W. and Schick, M., 1994c, *Macromolecules* **27**, 7157.

Matsen, M. W. and Whitmore, M. D., 1996, *J. Chem. Phys.* **105**, 9698.

Maurer, W. W., Bates, F. S., Lodge, T. P., Almdal, K., Mortensen, K., and Fredrickson, G. H., 1998, *J. Chem. Phys.* **108**, 2989.

Merzbacher, E., 1970, *Quantum Mechanics*. Wiley, New York, chapter 8.

Milner, S. T., Witten, T. A., and Cates, M. E., 1988, *Macromolecules* **21**, 2610.

Morse, D. C. and Fredrickson, G. H., 1994, *Phys. Rev. Lett.* **73**, 3235.

Müller, M. and Schmid, F., 2005, *Adv. Polym. Sci.* **185**, 1.

Naughton, J. R. and Matsen, M. W., 2002, *Macromolecules* **35**, 5688.

Netz, R. R. and Schick, M., 1996, *Phys. Rev. Lett.* **77**, 302.

Netz, R. R. and Schick, M., 1998, *Macromolecules* **31**, 172201.

Olmsted, P. D. and Milner, S. T., 1998, *Macromolecules* **31**, 4011.

Papadakis, C. M., Mortensen, K., and Posselt, D., 1998, *Eur. Phys. J. B* **4**, 325.

Rasmussen, K. O. and Kalosakas, G., 2002, *J. Polym. Sci.: Part B: Polym. Phys.* **40**, 1777.

Reif, F., 1965, *Fundamentals of Statistical and Thermal Physics*. McGraw-Hill, New York.

Reiter, G. and Khanna, R., 2000, *Phys. Rev. Lett.* **85**, 5599.

Sakamoto, N., Hashimoto, T., Han, C. D., Kim, D., and Vaidya, N. Y., 1997, *Macromolecules* **30**, 1621.

Schmid, F., 1998, *J. Phys.: Condens. Matter* **10**, 8105.

Schulz, M. F., Bates, F. S., Almdal, K., and Mortensen, K., 1994, *Phys. Rev. Lett.* **73**, 86.

Semenov, A. N., 1985, *Sov. Phys. JETP* **61**, 733.

Semenov, A. N., 1993, *Macromolecules* **26**, 6617; see ref 21 within.

Sferrazza, M., Xiao, C., Jones, R. A. L., Bucknall, D. G., Webster, J., and Penfold, J., 1997, *Phys. Rev. Lett.* **78**, 1997.

Shefelbine, T. A., Vigild, M. E., Matsen, M. W., Hajduk, D. A., Hillmyer, M. A., and Bates, F. S., 1999, *J. Am. Chem. Soc.* **121**, 8457.

Shi, A.-C., Noolandi, J., and Desai, R. C., 1996, *Macromolecules* **29**, 6487.

Shull, K. R., Mayes, A. M., and Russell, T. P., 1993, *Macromolecules* **26**, 3929.

Stepanow, S., 1995, *Macromolecules* **28**, 8233.

Takahashi, K. and Yunoki, Y., 1967, *J. Phys. Soc. Japan* **22**, 219.

Thomas, E. L., Kinning, D. J., Alward, D. B., and Henkee, C. S., 1987, *Nature* **334**, 598.

Thompson, R. B., Rasmussen, K. O., and Lookman, T., 2004, *J. Chem. Phys.* **120**, 31.

Vassiliev, O. N. and Matsen, M. W., 2003, *J. Chem. Phys.* **118**, 7700.

Vavasour, J. D. and Whitmore, M. D., 1992, *Macromolecules* **25**, 2041.

Wang, J. F., Wang, Z.-G., and Yang, Y. L., 2005, *Macromolecules* **38**, 1979.

Wang, Z.-G., 1995, *Macromolecules* **28**, 570.

Whitmore, M. D. and Vavasour, J. D., 1995, *Acta. Polymerica* **46**, 341.

Wickham, R. A. and Shi, A.-C., 2001, *Macromolecules* **34**, 6487.

Yeung, C., Desai, R. C., Shi, A.-C., and Noolandi, J., 1994, *Phys. Rev. Lett.* **72**, 1834.

Yeung, C., Shi, A.-C., Noolandi, J., and Desai, R. C., 1996, *Macromol. Theory Simul.* **5**, 291.

Zhu, L., Huang, P., Cheng, S. Z. D., Ge, Q., Quirk, R. P., Thomas, E. L., Lotz, B., Wittmann, J.-C., Hsiao, B. S., Yeh, F., and Liu, L., 2001, *Phys. Rev. Lett.* **86**, 6030.

Index